

How hadron collider experiments contributed to the development of QCD: from hard-scattering to the perfect liquid

M. J. Tannenbaum^a

Physics Department, Brookhaven National Laboratory Upton, NY 11973-5000 USA

Abstract. A revolution in elementary particle physics occurred during the period from the ICHEP1968 to the ICHEP1982 with the advent of the parton model from discoveries in Deeply Inelastic electron-proton Scattering at SLAC, neutrino experiments, hard-scattering observed in p+p collisions at the CERN ISR, the development of QCD, the discovery of the J/Ψ at BNL and SLAC and the clear observation of high transverse momentum jets at the CERN SPS $\bar{p} + p$ collider. These and other discoveries in this period led to the acceptance of QCD as the theory of the strong interactions. The desire to understand nuclear physics at high density such as in neutron stars led to the application of QCD to this problem and to the prediction of a Quark-Gluon Plasma (QGP) in nuclei at high energy density and temperatures. This eventually led to the construction of the Relativistic Heavy Ion Collider (RHIC) at BNL to observe superdense nuclear matter in the laboratory. This article discusses how experimental methods and results which confirmed QCD at the first hadron collider, the CERN ISR, played an important role in experiments at the first heavy ion collider, RHIC, leading to the discovery of the QGP as a perfect liquid as well as discoveries at RHIC and the LHC which continue to the present day.

1 Introduction

The beginning of the revolution in understanding the strong interactions of elementary particles took place in the period from the 14th International Conference on High Energy Physics in Vienna, Austria in 1968 (ICHEP1968) to the 16th ICHEP at Fermilab & Chicago in 1972.

1.1 ICHEP1968

Ironically it was a result from Deeply Inelastic Scattering (DIS) that started it. This was presented at the end of Pief Panofsky's rapporteur talk in the Electromagnetic Interactions - Experimental session at ICHEP1968 [Panofsky 1968]. The preliminary results from the SLAC-MIT electron+proton scattering experiment showed two very

^a e-mail: mjt@bnl.gov

striking features, the first in the structure function and the second in the ratio of the inelastic to elastic scattering cross sections.

The inelastic scattering cross section for the case when only the outgoing electron is detected is given by the formula [Drell and Walecka 1964]

$$\frac{d^2\sigma}{dQ^2 d\nu} = \frac{4\pi\alpha^2}{Q^4} \left[W_2(Q^2, \nu) \left(1 - \frac{\nu}{E} - \frac{Q^2}{4E^2} \right) + 2W_1(Q^2, \nu) \frac{Q^2}{4E^2} \right] \quad (1)$$

where $W_2(Q^2, \nu)$ and $W_1(Q^2, \nu)$ are structure functions which each depend on the 4-momentum transfer squared, Q^2 , and the energy loss $\nu = E - E'$ of the incoming electron with energy E and outgoing energy E' . The amazing result was that although one might expect many plots of W_1 and W_2 as functions of various values of Q^2 and ν , they all collapse to one curve as suggested by Bjorken [Bjorken 1969]

$$F_2(Q^2, \nu) \equiv \nu W_2(Q^2, \nu) = F_2\left(\frac{Q^2}{\nu}\right) \quad (2)$$

and thus known as Bjorken Scaling (Fig. 1a). The other important point made by Panofsky (Fig. 1b) [Breidenbach 1969] was that the inelastic cross sections in the continuum “are very large and decrease much more slowly with Q^2 than the cross-sections for elastic-scattering and the specific resonant states.”

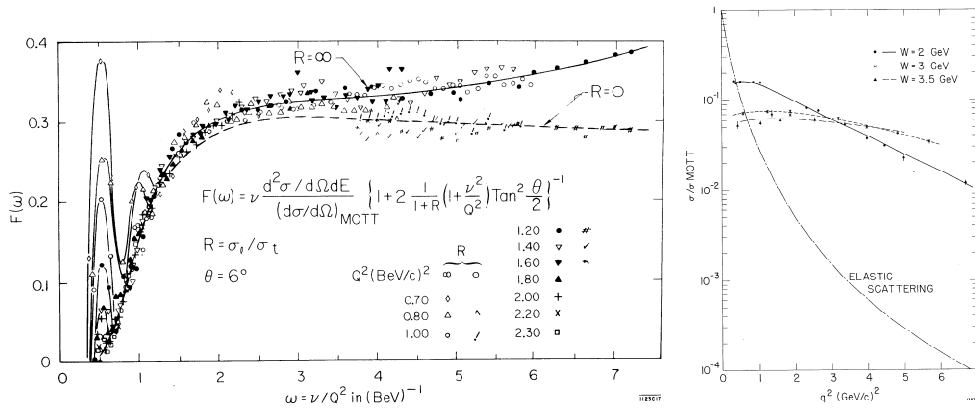


Fig. 1. a) (left) $F(\nu/Q^2)$ as a function of $\omega = \nu/Q^2$ with values of Q^2 indicated for $\theta = 6^\circ$ [Panofsky 1968] b) (right) $(d^2\sigma/d\Omega dE')/\sigma_{\text{Mott}}$ in GeV^{-1} vs q^2 for 3 values of W the invariant mass of the recoil hadron state, indicated, compared to $(d\sigma/d\Omega)_{\text{elastic}}/\sigma_{\text{Mott}}$ where $\sigma_{\text{Mott}} = (4\pi\alpha^2 \cos^2 \theta/2)/Q^4$, calculated for 10° [Breidenbach 1969].

All this led Bjorken (inspired by Feynman) [Bjorken and Paschos 1969] to the concept of a proton composed of fundamental pointlike constituents (partons) from which the electrons scatter elastically, incoherently as viewed in a frame in which the proton has infinite momentum. The free partons each have longitudinal momentum a fraction x of the proton longitudinal momentum \mathbf{P} where the probability of the parton to have the momentum $x\mathbf{P}$ is given by $F_2(x)$ where $x = Q^2/(2M\nu)$ and M is the mass of the proton. As an experimentalist, I had done muon-proton elastic scattering in the more usual frame where the proton is at rest in a liquid hydrogen target. The proton recoils with kinetic energy ν from an elastic scattering by the μ (or e) with 4-momentum-transfer² Q^2 where $\nu = Q^2/(2M)$ so that it was easy for

me to understand that DIS of an e from a proton is just quasi-elastic scattering from a parton at rest with a fraction x of the mass of the proton which would become a fraction of the momentum in any moving frame.

1.2 ICHEP1972

Frankly many physicists did not accept the idea that the proton was composed of a gigantic number of massless constituents (partons) [Friedman 1991]. In fact we used to call Manny Paschos, who worked at Brookhaven National Laboratory (BNL) in this period, “Manny Parton”. Everything changed for most people at the 16th ICHEP in 1972 at Fermilab and Chicago where three spectacular new results were presented.

1. Don Perkins in his conclusions [Perkins 1973] from new measurements of neutrino scattering cross sections and nucleon structure functions from the CERN Gargamelle collaboration emphasized: i) that both ν and $\bar{\nu}$ cross sections in the range 2-10 GeV are linear with energy, in accord with Bjorken scaling; ... iv) In terms of constituent models, the fractional charged (Gell-Mann/Zweig) quark model [Gell-Mann 1964, Zweig 2010] is the only one that fits both the neutrino and electron data ($\int F_2^{\nu N}(x) dx / \int F_2^e N(x) dx = 3.4 \pm 0.7 \approx 18/5$); v) The fractional nucleon 4-momentum carried by gluons is 50% and vi) by antiquark constituents is only $\sim 10\%$ of that carried by quarks and antiquarks together.
2. The birth of QCD where Fritzsche and Gell-Mann [Fritzsche and Gell-Mann 1973] proposed that the three distinct colors assigned to the 3 s -quarks in the $\Omega^-(sss)$ [Gell-Mann 2013] to allow them to be in the same state, avoiding simple Fermi statistics by obeying “para-Fermi statistics of rank 3” [Greenberg 1964], could also apply to gluons “which could form a color-octet of neutral vector fields obeying the Yang-Mills equations”.
3. The discovery of enhanced particle production at large transverse momentum p_T in p+p collisions at the CERN-ISR [Cool 1973] with a power-law shape, which depended on the c.m. energy of the collision, \sqrt{s} , quite distinct from the exponential e^{-6p_T} [Cocconi 1961] spectrum at low $p_T < 1$ GeV/c which depended minimally if at all on \sqrt{s} (Fig. 2a). This was proof that the partons of DIS interacted strongly with each other rather than simply scatter electromagnetically which must occur in a p+p collision since the partons are charged (Fig. 2b) [Berman 1971].

This last result changed the focus of many experimenters from the small angle, low transverse momentum region where most particles were produced, typical of fixed-target experiments in beams of high energy particles from an accelerator, to the region of large transverse momentum production, which at the CERN-ISR, the first hadron collider, was perpendicular to the axis of the colliding beams, a perfect location for the study of “high p_T physics”.

The first proposals of experiments to the ISR in early 1969 had been dominantly in the forward direction so that the ISR committee decided to divide up the angular regions for different experiments at several interaction points to three regions [Russo 1996]: small angles (up to 150 mrad); medium angles (100-300 mrad) and large angles (300 mrad to $\pi/2$ rad). The ISR did make discoveries and obtain important results on low p_T “soft” physics [Jacob 1984] so one may ask why some of the experiments wanted to run at the largest angles, where few if any particles were expected. The answer is that they were looking for W^\pm -bosons, the proposed quanta of the weak interactions [Lee and Yang 1960].

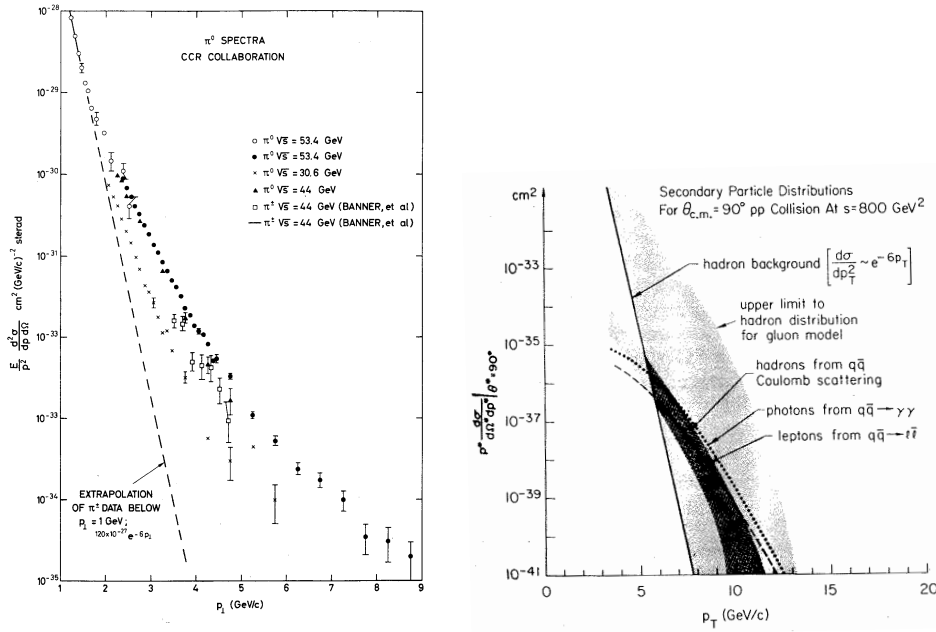


Fig. 2. a) (left) p_T spectra of invariant cross sections $E d^3\sigma/dp^3$ of π^0 and π^+ for several \sqrt{s} at the CERN-ISR [Cool 1973]. b) (right) Predicted p_T spectrum of hadrons from Coulomb scattering of partons in p+p collisions at $\sqrt{s} = 28.3 \text{ GeV}$ compared to the e^{-6p_T} [Cocconi 1961] formula background [Berman 1971].

2 Weak Bosons from strong interactions? 1960-1970

The completion of the two highest energy ($\sim 30 \text{ GeV}$) proton accelerators, the PS at CERN (November 1959) and the AGS at BNL (August 1960) opened the possibility of studying weak interactions at high energy rather than only by radioactive decay. The idea of the left-handed parity violating W^\pm bosons as the quanta of the weak interactions [Lee and Yang 1960] led to proposals for neutrino beams and experiments at the two laboratories [Pontecorvo 1959] [Schwartz 1960] to measure neutrino scattering and to discover the W which would prevent the otherwise point-like neutrino interaction cross sections from increasing monotonically with energy until they violated unitarity [Lee 1961]. Although a Nobel Prize winning discovery, the muon neutrino [Danby 1962], was made with the first accelerator neutrino experiment, the W was not observed in the early neutrino experiments. Relatively low limits were set for the mass of the W^\pm ($> 2 \text{ GeV}$) [Bernardini 1964][Burns 1965a] because of the low energy neutrino beams with small neutrino cross sections and it was realized that p+p collisions might be more favorable for producing the W , e.g. $p+p \rightarrow d + W^+$ [Bernstein 1963] [Nearing 1963] [Piccioni 1966]. This last reference is interesting for three reasons:

1. There is a comment from A. (Antonino) Zichichi [Zichichi 1966] on studies at CERN to observe the W^\pm in p+p collisions, which is so clear that it deserves a verbatim quote: "We would observe the μ 's from W -decays. By measuring the angular and momentum distribution at large angles of K and π 's, we can predict the corresponding μ -spectrum. We then see if the μ 's found at large angles agree with or exceed the expected numbers." The W^\pm would be visible above the background as a Jacobian peak at lepton transverse momentum $p_T^\mu = M_W/2$.

2. The proposed experiment was never done because the original calculation did not include the p or d form factors and thus the original cross section calculation needed be reduced by a factor of ≈ 3000 [Nearing 1964].
3. This is exactly the way that the W was discovered at the CERN $S\bar{p}pS$ collider 19 years later [Arnison 1983a, Banner 1983] as best shown in Ref. [Appel 1986].

2.1 First p+p experiments searching for the W 1965–1970

Experiments overcame the low cross section for large angle muons from the reaction $p + p \rightarrow W + \text{anything}$ by interacting the entire extracted proton beam in a well-shielded dense target where only muons could penetrate the shielding (beam dump experiments); but no signal was observed [Burns 1965b] [Lamb 1965]. This brought up the question of how to know how many W bosons should have been produced. Chilton, Saperstein and Shrauner [Chilton 1966] emphasized the need to know the time-like form factor of the proton to calculate the cross section for producing W 's and used the Conserved Vector Current (CVC) theory to estimate the W production cross section by relating it to di-muon production in the reaction $p + p \rightarrow \mu^+ + \mu^- + \text{anything}$. Yamaguchi [Yamaguchi 1966] then proposed that the time-like form factor could be found by measuring the number of $e^+ + e^-$ or $\mu^+ + \mu^-$ “massive virtual photons” of the same invariant mass as the W in the p+p reaction but warned that the individual leptons from these electromagnetically produced pairs or from real photons from the decay $\pi^0 \rightarrow \gamma + \gamma$ from the huge number of π^0 produced might mask the leptons from the W^\pm .

These developments led Leon Lederman to propose in August 1967 a more elegant beam dump di-muon experiment at the BNL-AGS (AGS 420) with a thick Uranium target and muon momentum measurement by range in a series of iron and concrete absorbers to search for W bosons, measure the time-like form factor and possibly look for ‘massive’ vector meson production. I had proposed a di-muon experiment in May 1967 (AGS 412) modifying an existing Harvard photoproduction experiment (AGS 310) so as to search for $\mu^+\mu^-$ pairs produced in a Pb target by an incident muon beam—muon tridents. With three muons in the final state, two of them identical, we could test whether muons obeyed Fermi statistics or para-statistics and whether there was a force between muons other than electromagnetic.

Leon and I had been in contact about $\mu^+\mu^-$ pairs via mail over the summer but I decided to stick with my trident experiment which did in fact measure that the muon was a Fermion [Russell 1971]. My story then loops around to Panofsky’s talk at the ICHEP1968 [Tannenbaum 2016]; but the outcome of Leon’s di-muon experiment turned out to be one of the pillars of the parton model and just missed a truly revolutionary discovery at the BNL-AGS in 1974, the J/Ψ [Aubert 1974], that cemented the parton model and belief in real quarks, which will be discussed in its chronological order below.

2.2 Drell-Yan leads to better W searches and other discoveries

Having seen Lederman’s preliminary results at an American Physical Society meeting, Sid Drell and Tung-Mow Yan at SLAC [Drell and Yan 1970] used the parton model and Bjorken scaling in m^2/s to calculate large mass timelike virtual-photon i.e. lepton pair production in hadron-hadron ‘inelastic collisions’ by parton-antiparton annihilation, or in today’s terminology $\bar{q} + q \rightarrow \mu^+ + \mu^-$. There was also another calculation described in Ref. [Drell and Yan 1970] which “employs light-cone commutators and Regge theory, yielding a relative cross section in good agreement with the shape of the experimental distribution.” [Altarelli 1971] (Fig. 3a).

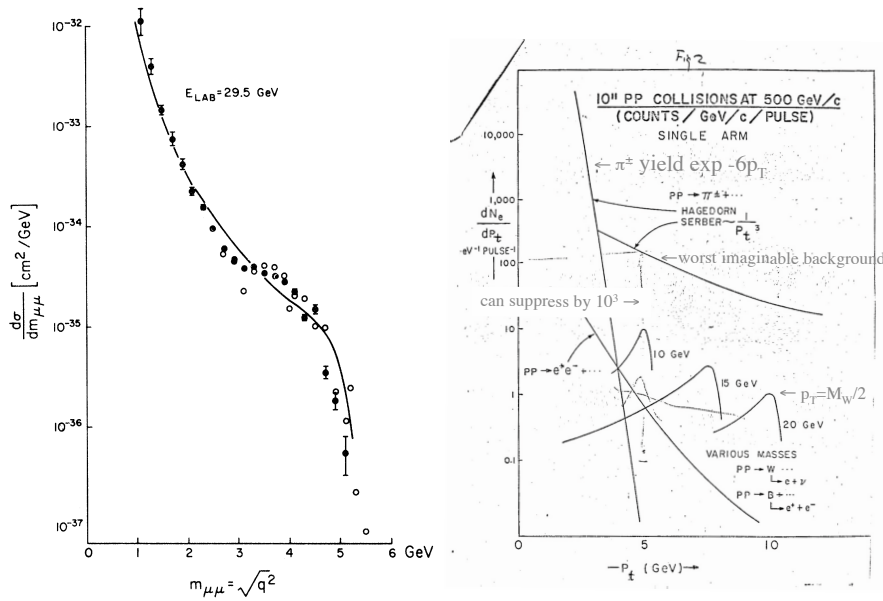


Fig. 3. a) (left) Di-muon invariant mass spectrum $d\sigma/dm_{\mu\mu}$ [Christenson 1970] with the totally incorrect theoretical prediction [Altarelli 1971] b) (right) the p_T distribution of $p+p \rightarrow \mu^+ + \mu^- + X$. The cross section was calculated with Bjorken scaling from (a) with the W cross section as $\sigma_W = 0.05 m_W^2 d\sigma/dm_{\mu\mu}$ from CVC [Chilton 1966]. The ‘Zichichi signatures’ for possible W masses are indicated [Lederman 1970]Addendum.

Lederman was very excited about this agreement with the measured $d\sigma/dm_{\mu\mu}$ distribution [Christenson 1970]. This was because with the use of the CVC theory [Chilton 1966] and Bjorken scaling he could calculate the W cross section at any \sqrt{s} and thus predict the sensitivity of his di-muon proposal (E70, which I initially joined [Lederman 1970]) at the newly opening Fermilab (Fig. 3b), as well as the di-electron proposal at the CERN ISR [Cool 1969] which became the experiment that discovered the unexpectedly large high p_T π^0 spectrum announced at ICHEP1972 [Cool 1973].

The high p_T discovery represented totally new physics, strongly interacting partons, which excited me very much. I resigned from all my Fermilab proposals, and being on the faculty of the Rockefeller University since 1971 I was able to move to Geneva to be with the Rockefeller group there and continue the work of the CERN-Columbia-Rockefeller (CCR) series of experiments which helped lead to the confirmation of QCD as the theory of the strong interactions.

Before returning to the aftermath of the high p_T discovery, a comment from the di-muon measurement paper [Christenson 1970] is worth noting. Resonances were one of the original purposes of the experiment stated in the AGS 420 proposal, and were mentioned in the di-muon publication [Christenson 1970]: “As seen in both the mass spectrum and the resultant cross section $d\sigma/dm$, there is no forcing evidence of any resonant structure” although “Indeed in the mass region near $3.5 \text{ GeV}/c^2$, the observed spectrum may be reproduced by a composite of a resonance and a steeper continuum.” A proposal was actually made in September 1970 (AGS 549) by some younger members of the Lederman group to follow up the resonance possibility; but it

never really got off the ground for various reasons.¹ As noted above the situation was finally cleared up in November 1974; but there were also many exciting developments in high p_T physics and QCD from 1971 to 1974.

3 1971-1973 QCD, Asymptotic Freedom, x_T scaling and more.

Theoretical physicists were very busy in this period inventing the theory of asymptotic freedom and QCD “from a Yang-Mills gauge model based on colored quarks and color octet gluons” [Fritzsch and Gell-Mann and Leutwyler 1973],[Politzer 1973], [Gross and Wilczek 1973], [’t Hooft 1999] A quick summary of asymptotic freedom in QCD is that the coupling constant obeys the equation [Altarelli and Parisi 1977]:

$$\alpha_s(Q^2) = \frac{12\pi}{(11N_c - 2n_f) \ln(Q^2/\Lambda^2)} = \frac{12\pi}{25 \ln(Q^2/\Lambda^2)} \quad (3)$$

for $N_c = 3$ colors and, as will turn out, $n_f = 4$ flavors of quarks. The asymptotic freedom is the decrease of $\alpha_s(Q^2)$ as Q^2 increases. However, at this point in time asymptotic freedom had minimal if any impact on experimentalists at hadron colliders who were much more interested in the scaling rules and models directly related to the high p_T measurements.

3.1 First scaling law 1971

In addition to calculating the cross sections for Coulomb scattering of partons in p+p collisions, BBK [Berman 1971] presented a scaling law for the Coulomb scattering which must exist for charged partons:

$$E \frac{d^3\sigma}{dp^3} = \frac{4\pi\alpha^2}{p_T^4} \mathcal{F}\left(\frac{-\hat{u}}{\hat{s}}, \frac{-\hat{t}}{\hat{s}}\right) \quad (4)$$

where $\alpha = e^2/\hbar c$ is the fine structure constant. The two factors are a $1/p_T^4$ term, characteristic of single photon exchange, and a form factor \mathcal{F} that scales, i.e. is only a function of the ratios of the Mandelstam variables, \hat{s} , \hat{t} and \hat{u} , the constituent-scattering invariants for scattering of a parton with 4-momentum p_1 , on another parton with 4-momentum p_2 to give an outgoing parton pair with p_3 and p_4 , i.e. $p_1 + p_2 \rightarrow p_3 + p_4$.

3.1.1 Quick kinematics review

Relativistic kinematics are important for understanding parton-parton scattering and eventually QCD so I give a brief description here with the Minkowski convention¹. The four-vector momentum p of a particle with 3-vector momentum \mathbf{P} , energy E , in a particular rest frame, and invariant mass m , in units where the speed of light c is taken as unity, is denoted such that the 4-th (time) component $\equiv iE$:

$$p = (\mathbf{P}, iE) \quad \text{or} \quad p = (P_x, P_y, P_z, iE) \quad \text{and} \quad p^2 = p \cdot p = \mathbf{P} \cdot \mathbf{P} - E^2 = -m^2 \quad . \quad (5)$$

The squared modulus of the 4-vector, p^2 , is invariant under a Lorentz transformation.

¹ See Ref. [Rak and Tannenbaum 2013] for further information about this issue and other issues raised but not discussed in full detail in this article.

The Lorentz Invariant quantities to describe two-two scattering kinematics are:

$$\begin{aligned} -\hat{s} &= (p_1 + p_2)^2 = (p_3 + p_4)^2 \\ -\hat{t} &= (p_1 - p_3)^2 = (p_4 - p_2)^2 \\ -\hat{u} &= (p_1 - p_4)^2 = (p_3 - p_2)^2 \\ \hat{s} + \hat{t} + \hat{u} &= m_1^2 + m_2^2 + m_3^2 + m_4^2 \end{aligned} \quad . \quad (6)$$

where \hat{s} is the parton-parton center of mass energy squared, $Q^2 = -\hat{t}$ is the 4-momentum-transfer-squared in the parton-parton elastic scattering. See appendix 14.2 for a full discussion of parton-parton scattering kinematics.

3.2 A better scaling rule, x_T scaling, 1972

Inspired by “The recent measurements at CERN ISR of single-particle inclusive scattering at 90° and large transverse momentum” which “revealed several dramatic features of pion inclusive reactions”, Blankenbecler, Brodsky and Gunion (BBG) proposed a new general scaling formula, x_T scaling [Blankenbecler 1972]:

$$E \frac{d^3\sigma}{dp^3} = \frac{1}{p_T^{n_{\text{eff}}}} F(x_T) \quad \text{where} \quad x_T \equiv \frac{2p_T}{\sqrt{s}} \quad . \quad (7)$$

The power n_{eff} is determined by the force-law between constituents, the quantum-exchange governing the reaction. Thus, $n_{\text{eff}} = 4$ for QED or “Vector Gluon Exchange”. However, BBG also included a new model of their own, the “constituent interchange model (CIM)” which predicted that the “proton beam at the ISR behaved like a meson beam of much lower energy” so that high p_T pions were produced by “quark-meson scattering by the exchange of a quark” which gave $n_{\text{eff}} = 8$ in their model “which does give an excellent account of the data” [Büsser 1973].

3.3 The 3 ISR experiments publish, 1973

Three ISR experiments published observation of enhanced high p_T production at 90° in the c.m. system in 1973. The first publication, from the British-Scandinavian ISR Collaboration [Alper 1973] measured non-identified charged hadrons with $1.5 \leq p_T \leq 4.5$ GeV/c at $\sqrt{s} = 44$ and 53 GeV, with the comment “no strong energy dependence is observed for these transverse momenta”. The second publication by the Saclay-Strasbourg group [Banner 1973] used a Cerenkov counter to identify π^\pm with $3.5 \leq p_T \leq 5$ GeV/c and noted an $e^{-2.4p_T}$ dependence for the invariant cross section in this range “in sharp contrast with the” e^{-6p_T} shape of the spectrum below 1 GeV/c. More importantly, they also measured π^0 by conversion of the $\pi^0 \rightarrow \gamma + \gamma$ decay photons in the ISR vacuum pipe but found no single e^\pm with $p_T > 3$ GeV/c so set a limit for single electron production.

The best and most influential measurement was the final publication of the preliminary data (Fig. 2a) shown at ICHEP1972 by the CERN Columbia Rockefeller (CCR) group (Fig. 4a) [Büsser 1973]. The π^0 were detected in two identical Pb Glass electromagnetic calorimeters preceded by tracking chambers located at 90° on both sides of the colliding proton beams. The π^0 spectrum was measured in the range $2.4 \leq p_T \leq 9$ GeV/c at 5 c.m. energies $\sqrt{s} = 23.5, 30.6, 44.8, 52.7$ and 62.4 GeV. A very large \sqrt{s} dependence was observed for the cross sections, which were all “orders of magnitude” higher than an extrapolation of the “well known exponential”, e^{-6p_\perp} . The break in the cross-section due to parton-parton electromagnetic scattering anticipated by BBK

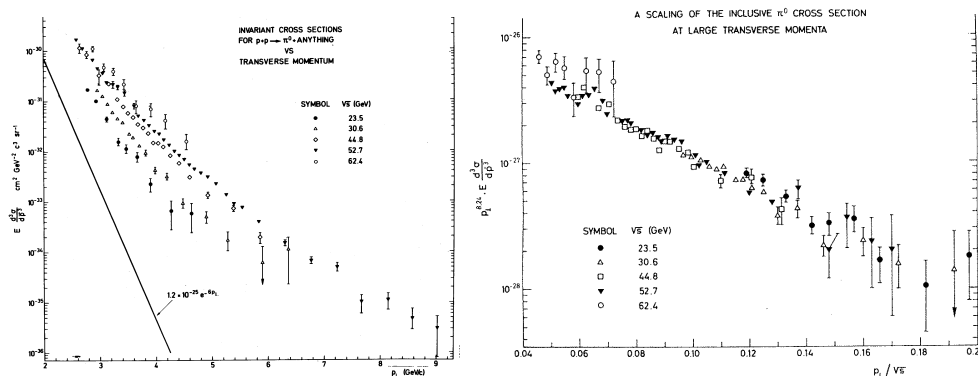


Fig. 4. [Büsser 1973] a) (left) The invariant cross section $E d^3 \sigma / dp^3$ for $p+p \rightarrow \pi^0 + X$ vs. p_{\perp} for 5 c.m. energies. b) (right) The function $F(x_T) = p_{\perp}^{n_{\text{eff}}} E d^3 \sigma / dp^3$ deduced from the measurements in (a) using the best fit value, $n = 8.24$. The errors are statistical only.

(Fig. 2b) [Berman 1971] was observed but did not agree with magnitude or the form of their Coulomb prediction, $E d^3 \sigma / dp^3 \propto p_{\perp}^{-4} F(x_T)$. However, as noted above, the data for all \sqrt{s} could be well fit by the BBG x_T scaling form (Eq. 7) with the value $n_{\text{eff}} = 8.24 \pm 0.05(\text{stat}) \pm 0.70(\text{sys})$ with $F(x_T) = A \exp(-bx_T)$, in agreement with the CIM prediction [Blankenbecler 1972], as illustrated by a plot of the data in the form $p_{\perp}^{8.24} \times E d^3 \sigma / dp^3$ (Fig. 4b).

4 1974-1976 a charming period.

4.1 The discovery of charm particles by direct $e^{+/-}$ production at the CERN ISR

This discovery [Büsser 1974] is not generally credited to the ISR, nor even mentioned in many articles about charm physics [Tavernier 1987] or the ISR [Darriulat 2012] because charm quarks (c) were only a theoretical idea [Bjorken 1964],[Glashow 1970] at that time. The discovery came about because two of the experiments, CCR [Büsser 1973] and Saclay-Strasbourg [Banner 1973], whose searches for W bosons by detecting single electrons at large p_T were overwhelmed by the high p_T pion discovery, decided to combine.

The combined experiment, the CERN, Columbia, Rockefeller, Saclay (CCRS) collaboration [CCRS 1973], had two spectrometer arms located around 90° on opposite sides of ISR intersection region II with vastly improved e^{\pm} , $e^+ + e^-$, π^{\pm} and π^0 detection as well as outstanding features to eliminate the background in this difficult measurement:

1. $\geq 10^5$ charged hadron rejection from electron identification in gas Cerenkov counters combined with matching the momentum and energy of an electron candidate in the magnetic spectrometer and the PbGlass Electromagnetic Calorimeter;
2. precision measurement of $\pi^0 \rightarrow \gamma + \gamma$ and $\eta \rightarrow \gamma + \gamma$ decays, the predominant background source;²
3. a minimum of material in the aperture to avoid external conversions of photons;
4. zero magnetic field on the axis to avoid de-correlating conversion pairs;

² This was better in ‘arm2’ with the CCR PbGlass than in ‘arm1’ with the Saclay 3X₀ shower counters.

5. rejection of conversions in the vacuum pipe (and small opening angle internal conversions) by requiring single-particle ionization in a hodoscope (H) of scintillation counters close to the vacuum pipe, preceded by a thin track chamber to avoid conversions in the hodoscope;
6. precision background determination in the direct-single- e^\pm signal channel by adding external converter—to distinguish direct single- e^\pm from e^\pm from photon conversion.

Preliminary results on “the observation of leptons at large p_T ” from 6 experiments were presented at the ICHEP in London in July 1974: one for e^\pm by CCRS [Segler 1974], [Büsser 1974]; one for both e^\pm and μ^\pm channels by Lederman’s E70 [Appel 1974] at Fermilab; and four for μ^\pm : one by Cronin and collaborators, E100 at Fermilab [Boymond 1974]; one from Serpukhov [Lebedev 1973] that had previously claimed that the observed ratio $\mu/\pi = 2.5 \times 10^{-5}$ at $\sqrt{s} = 12$ GeV was from “electromagnetic production of muon pairs” (later improved [Abramov 1976]); and two others that were upper limits on $W^\pm \rightarrow \mu^\pm + X$ production. CCRS and the Fermilab experiments all found that the ratio $e, \mu/\pi \approx 10^{-4}$. There were no clear ideas about the source of these direct leptons at this time, as well summarized by Lederman at ICHEP1974 [Lederman 1974].

Following these results, many experiments that were not originally designed for these measurements, which are extremely difficult, also attempted to look for direct single leptons. This only added confusion to the situation because they mostly found results that were incorrect. A beautiful summary of all these experiments and their difficulty was again presented by Leon Lederman at the 1975 Lepton Photon Symposium [Lederman 1975] [Lederman 1976] paraphrased succinctly as:

- μ^\pm : Muon detection requires an understanding of the trivial but devastating background of pion and kaon decay.
 e^\pm : Electron detection suffers from problems of conversions of photons (principally from π^0 decay) in any residual material, from Dalitz pairs, from electron decay of long-lived sources (K, Λ , Σ , ...)

Here I point out that Leon left out $\eta \rightarrow \gamma + \mu^+ + \mu^-$ (Dalitz) decay as a background for muons. In fact, in 1977 at the Lepton Photon Symposium, Jim Cronin [Cronin 1977] made a strong claim in his talk from which I quote the abstract: “A review of direct production of leptons and photons in hadron-hadron collisions is presented. Production of lepton pairs with large mass is well accounted for by the Drell-Yan process. The origin of direct single leptons is principally due to the production of lepton pairs. A dominant source of lepton pairs is at low effective mass, $m < 600$ MeV.” I strenuously disagreed with him for the CCRS result in a comment [Tannenbaum 1977]. Here is why.

4.2 The CCRS measurement

We made an extraordinary effort to measure all the possible backgrounds, the primary one being external conversions of decay photons or internal conversions (Dalitz pairs) from the decay $\pi^0 \rightarrow \gamma + e^+ + e^-$ and $\eta \rightarrow \gamma + e^+ + e^-$. We did this by adding material of a few percent of a radiation length X_o in addition to the $0.016 X_o$ thickness of the stainless steel corrugated vacuum pipe (Fig. 5a) [Büsser 1976b]. Measurements were made for the accepted single e^\pm events and also for selected conversions by requiring double (or more) ionization in the H hodoscope. The data are normalized to the normal running conditions with only the ISR vacuum pipe of $0.016 X_o$.

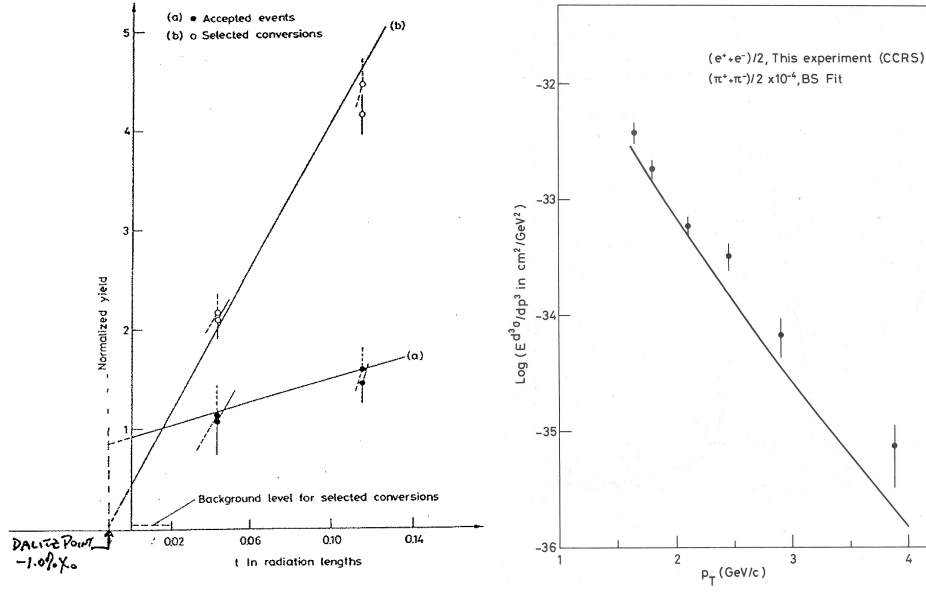


Fig. 5. a) (left) Yield of inclusive e^\pm vs. total external material t in radiation lengths for accepted prompt e^\pm events (●) and selected conversions (○) [Büsser 1976b]. b) (right) Charged averaged cross section of $(e^+ + e^-)/2$ at $\sqrt{s} = 52.7$ GeV as a function of p_T (●) [Büsser 1974]. Solid line is fit to British-Scandinavian $(\pi^+ + \pi^-)/2$ cross section multiplied by 10^{-4} [Alper 1974].

4.2.1 Dalitz pairs—Internal conversion

The converter method to determine the external and internal conversions, $\gamma \rightarrow e^+ + e^-$ from $\pi^0 \rightarrow \gamma + \gamma$ and $\eta \rightarrow \gamma + \gamma$ decay is straightforward to understand with a few equations. The total Dalitz (internal conversion) probability is [Kroll and Wada]:

$$\delta = \frac{\Gamma_{ee\gamma}}{\Gamma_{\gamma\gamma}} = \frac{2\alpha}{3\pi} \left(\ln \frac{M^2}{m_e^2} - \frac{7}{2} \right) = \begin{array}{l} 1.19\% \text{ for } \pi^0 \\ 1.62\% \text{ for } \eta \end{array}, \quad (8)$$

where M is the mass of the π^0 or η . With additional external converter present the probability of internal and external conversion per γ is

$$\frac{e^-|_\gamma}{\gamma} = \frac{e^+|_\gamma}{\gamma} = \frac{\delta_2}{2} + \frac{t}{\frac{9}{7}X_0} \equiv \delta_{eff} \quad (9)$$

where: t/X_0 , is the total external converter thickness in radiation lengths; $\delta_2/2$ is the Dalitz (internal conversion) branching ratio per photon = 0.6% for $\pi^0 \rightarrow \gamma\gamma$, 0.8% for $\eta \rightarrow \gamma\gamma$; and the factor $9/7$ comes from the ratio of conversion length to radiation length. For π^0 and η decays, the yield extrapolates to zero at the “Dalitz point” $-\frac{9}{14}\delta_2 \sim -1\%$ —actually -0.8% for π^0 and -1.0% for η —so the method has the added advantage that it depends very little on the η/π^0 ratio. In Fig. 5a, the extrapolation for the e^\pm from selected conversions (○) extrapolates nicely to zero at the Dalitz point, indicating a photonic source, while the accepted prompt e^\pm events (●) show only a small decrease from the normal thickness used for data-collecting ($t/X_0 = 1.6\%$) to the Dalitz point: the value at the Dalitz point is the normalized yield of the prompt single e^\pm with the photonic background subtracted.

The same method doesn't work at all for the single μ^\pm which have the 'devastating background' from meson decay. Furthermore the $\eta \rightarrow \gamma + \mu^+ + \mu^-$ decay which would fit Cronin's description of the source of his single muons is not given correctly by Eq. 8 when m_μ is substituted for m_e because it is valid only to leading order in m^2/M^2 [Jarlskog and Pilkuhn 1967]. The correct answer is $\delta_{\eta\mu\mu\gamma} = (0.08 \pm 0.01)\%$ [Landsberg 1985] [Djhelyadin 1980]. Furthermore, the converter method can not be used because a radiation length for muons is $(m_\mu/m_e)^2 = 42727$ times as large as X_o , the radiation length for e^\pm and γ . In fact, what I used to say in the 1970's is still valid today "all those who try to measure direct leptons become the world's experts on η Dalitz decay" [Jane 1975].

4.2.2 A final obstacle, then publication.

The last possible background source was the decay of the vector meson $\phi \rightarrow e^+e^-$ with the cross section $\sigma_\phi = 1.1\sigma_{\pi^0}$. Such copious ϕ production should be easy to detect via the principal decay mode K^+K^- , so we removed the Cerenkov counter from the trigger in 'arm2' and made a short run looking for charged hadron $h^+ + h^-$ pairs with $p_T > 1.6$ GeV/c. We didn't find any and set a limit $\sigma_\phi \leq 0.4\sigma_{\pi^0}$ to 90% confidence which implied that the possible ϕ contribution was less than 0.25 to 0.5 the observed single e^\pm signal. The result was that the direct single e^\pm cross section in the range $1.6 < p_T < 4.7$ GeV/c at $\sqrt{s} = 52.7$ GeV is $(1.2 \pm 0.2) \times 10^{-4}$ that of the π^\pm cross section (Fig. 5b) [Büsser 1974]. We submitted the publication on 28 October 1974 but of course we had spent the time since the ICHEP in July 1974 trying to find the e^\pm that was balancing the p_T of the observed e^\pm spectrum in the opposite spectrometer 'arm1', but didn't find anything. However, we did find out the answer two weeks later with the 'November revolution' in particle physics caused by the discovery of a new "heavy particle J with mass $m = 3.1$ GeV/ c^2 and width approximately zero" [Aubert 1974] in p+Be collisions at the BNL-AGS (Fig. 6a) simultaneously with the same particle except called Ψ in $e^+ + e^- \rightarrow$ hadrons in the storage ring (SPEAR) at SLAC [Augustin 1974].

4.3 Charmonia—the November Revolution that made everybody believe in partons

4.3.1 First: new proposals, new results

CERN went into a frenzy over the J/Ψ discovery [Russo 1996a] as did the individual experiments. Within another 2 weeks, just in time for a "second narrow resonance" the Ψ' with $m = 3.7$ GeV/ c^2 to be discovered at SLAC [Abrams 1974], two proposals for new e^+e^- measurements from members of CCRS were submitted to the ISRC. Also in this interval CCRS found the reason why we didn't find anything balancing our single e^\pm in the opposite spectrometer: a computer bug in 'arm1' that rejected tracks in the entire H hodoscope rather than just near the spaces between counters. In fact in the CCOR proposal [CCOR 1974] there were 7 e^+e^- events shown of which 4 clustered near $m_{ee} = 3$ GeV/ c^2 . The issue of why there were two proposals from CCRS members is also interesting.

In May 1973, the CCR part of CCRS had made a proposal [CCOR 1973]³ for a totally new detector with much larger solid angle than either the original CCR or CCRS experiments, which was approved in March 1974. It consisted of a solenoid magnet

³ Joined by Oxford in January 1974 (CERN/ISRC/73-13 Add. 2).

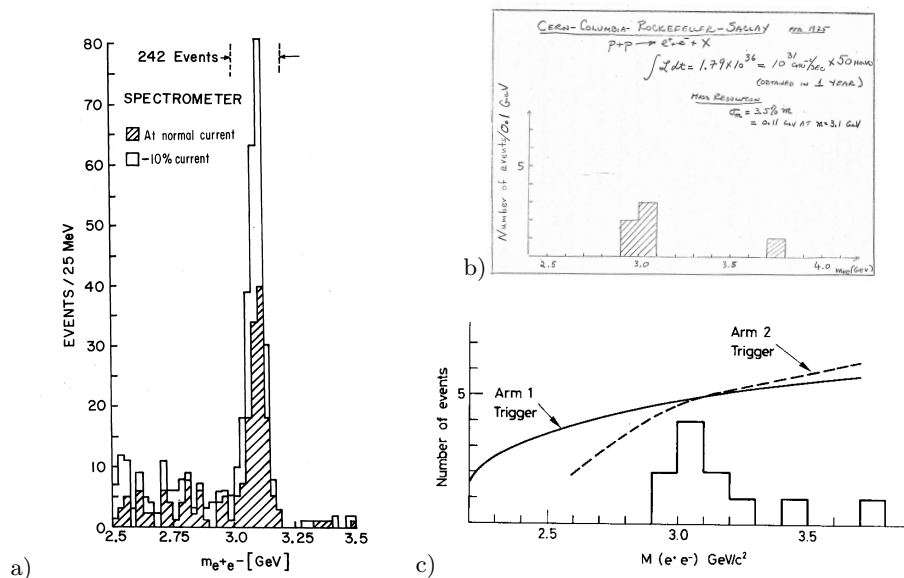


Fig. 6. a) AGS J discovery [Aubert 1974]: the mass remains the same with two different spectrometer settings. b) CCRS plot shown by Amaldi. c) First J/Ψ at CERN [Büsser 1975a].

with a thin aluminum-stabilized superconducting coil, only $1.0 X_0$ thick, outside of which were two PbGlass EMcalorimeters, opposite in azimuth, each covering a polar angle $\theta = \pm 30^\circ$ around 90° and azimuthal angle $\phi = \pm 20^\circ$ around the median plane. Tracking and momentum measurement of charged particles was accomplished by a set of cylindrical drift chambers inside the solenoid which covered the full azimuth in a polar angle range $\theta = \pm 37^\circ$ around 90° . Ironically, the day that the J/Ψ discovery was announced, November 11, 1974, was the same day that removal of the CCRS experiment from the ISR intersection region II began in order to start building the CCOR detector.

Immediately after the J/Ψ announcement, the CCRS group together with Pierre Darriulat's group started discussing a "mini" experiment to look for the single e^\pm and e^+e^- pairs; but quickly couldn't agree. Thus, CCOR [CCOR 1974] and the new Darriulat+Saclay group [CERN-Saclay 1974] quickly submitted new proposals to the ISRC. The CCOR proposal [CCOR 1974] was basically the CCR experiment with Cherenkov counters added for e^\pm identification and triggering, so was orthogonal to the approved CCOR experiment [CCOR 1973] and was wisely rejected by the ISRC. The CERN-Saclay proposal, which was basically CCRS with larger acceptance and PbGlass EMcalorimeters in both arms, was approved on December 11 and eventually became the CERN-Saclay-Zurich (CSZ) experiment with a small muon spectrometer added perpendicular to the e^\pm spectrometers.

4.3.2 Then more work, discussions and publications

Work continued on looking for more e^+e^- events in CCRS eventually ending in 11 total events. Meanwhile the rest of the CERN physicists were not idle and a series of Discussion Meetings was held in the CERN auditorium, the most memorable for me being the one on February 21, 1975: "The new particles: what are CERN experimentalists doing?" We in CCRS had the only J/Ψ data and I had collected the events we had found up to that time and submitted a plot to the ISR coordinator, Ugo

Amaldi, who gave the ISR presentation. I was sitting in the front row. Carlo Rubbia (my boss when I was a CERN post-doc in 1965-66) was seated in the second row, one seat to my left. When Ugo showed the plot (Fig. 6b), Carlo got very excited and pointed at the event at 3.7 GeV/c² and asked loudly repeatedly “What is that event at 3.7, what is that event at 3.7?” We couldn’t really claim that it was the Ψ' , so I turned to Carlo and said, “Oh Carlo, you are the expert in one-event experiments.” It was amazing: laughter filled the auditorium, moving up the rows in a wave until everybody in the audience (except Carlo) was laughing—very memorable! The CCRS result was submitted for publication on 22 April 1975 [Büsser 1975a] (Fig. 6c).

4.3.3 OK so we found the J/Ψ (a bit late): was it the source of the single e^\pm ?

In addition to the observation of the ‘new particle’ there was an important issue to address: was the J/Ψ the source of the single e^\pm ? The answer was NO as shown in the final CCRS paper on “Electrons at the ISR” (Fig. 7b) [Büsser 1976b] and also shown for charged hadron decays in Lederman’s talk [Lederman 1975] (Fig. 7a).

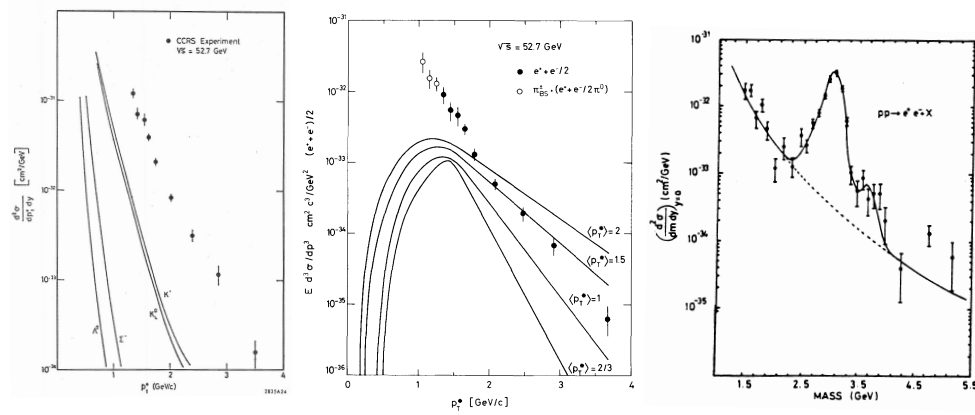


Fig. 7. CCRS direct single e^\pm p_T spectrum at $\sqrt{s} = 52.7$ GeV with background from a)(left) charged hadron decays [Lederman 1975] and b)(center) calculated e^\pm spectrum from J/Ψ decay with several values of $\langle p_T \rangle$ [Büsser 1976b]. c)(right) Best measurement of the J/Ψ $d^2\sigma/dm_{ee}dy|_{y=0}$ at the CERN ISR [Clark 1978].

Another important issue addressed by CCRS [Büsser 1975a] was the measurement of the cross section for the reaction:

$$p + p \rightarrow J(3.1) + X \rightarrow e^+ + e^- + X \quad (10)$$

with result

$$B_{ee} \times \frac{d\sigma}{dy}(p + p \rightarrow J + X) = (7.5 \pm 2.5) \times 10^{-33} \text{cm}^2 \quad (11)$$

averaged over the rapidity acceptance $|y| \leq 0.30$. This result at $\sqrt{s} \approx 50$ GeV is two-orders of magnitude larger than the value for the BNL discovery [Aubert 1974] at $\sqrt{s} \approx 7.5$ GeV. The reason that CCRS [Büsser 1975a] was able to measure the cross section was that thanks to Cerenkov counters together with the EMcalorimeter that allowed a trigger on e^\pm in the range $1.0 \leq p_T \leq 4.7$ GeV/c, the cross section

could be measured for $J/\psi \rightarrow e^+e^-$ for all $p_{T_{e_e}} > 0$. This was the first of three such measurements at the CERN ISR [Büsser 1975a, Clark 1978, Kourkouvelis 1980a] with similar e^\pm triggers and not repeated at a hadron collider until RHIC [Adcox 2002a] and eventually CDF at the Fermilab Tevatron [Acosta 2005]. The best measurement of the J/ψ at the ISR [Clark 1978] is shown in Fig. 7c.

4.3.4 What are the J/Ψ and Ψ' ?

In less than a month, the J/Ψ was understood to be a narrow bound state of the ‘heavy’ $c\bar{c}$ charm quarks [Glashow 1970, De Rujula 1975] and was given the name charmonium [Appelquist 1975]. The quarks were proposed to be bound with a simple potential (the Cornell potential [Eichten 1975, Eichten 1977]) that incorporated both the Coulomb and confining forces:

$$V(r) = -\frac{4}{3} \frac{\alpha_s}{r} + \sigma r \quad (12)$$

where α_s is the QCD coupling constant (Eq. 3) and σ represents the string-tension in a string-like confining potential. Also predictions were made for heavier quarks Q with stronger binding of $Q\bar{Q}$ leading to ‘a rich assortment of rather narrow resonances’ [Eichten 1977].

4.3.5 The Upsilon; and the ISR recognition problem

It is worth noting that in early 1976 a measurement of $p + Be \rightarrow e^+ + e^- + \text{anything}$ using a 400 GeV proton beam at Fermilab [Hom 1976a] claimed that a “statistically significant clustering near 6 GeV suggests the existence of a narrow resonance”. This was made by the Lederman group who suggested that “the name Υ (Upsilon) be given either to the resonance at 6 GeV if confirmed or to the onset of high-mass dilepton physics.” This later became known as the oopsLeon when, in a measurement of high mass $\mu^+ + \mu^-$ pairs which allowed a higher data taking rate made possible by the filtering of most hadrons, the same group [Hom 1976b] observed that “the dimuon mass spectrum provides no evidence for fine structure above 5 GeV”.

The situation was again reversed following a major redesign of the dimuon experiment, when the real $\Upsilon \rightarrow \mu^+ + \mu^-$, a narrow resonance at 9.5 GeV, was discovered [Herb 1977] (Fig. 8a). This was a narrow bound state of heavier quarks as predicted [Eichten 1977] and turned out to be the discovery of the bottom quark b , a member of a third family of quarks much heavier than the first two families.

This discovery cemented a negative view of the ISR by many CERN physicists [Russo 1996] for missing the discoveries of the c quark (actually quarkonia) and now the b quark in dilepton production by lower energy but much larger luminosity conventional fixed target accelerators. They were drawn instead to the new 400 GeV Super proton Synchrotron (SpS) which started physics operation at the end of 1976 and which ironically made its greatest contributions by being turned into a proton-antiproton collider in mid 1981. Unfortunately this negative pervasive attitude totally missed the most important physics contributions of the ISR which were in hadron physics and which made major contributions to the development of QCD.

Measurements of the Upsilon were also made at the ISR [Angelis 1979b], [Cobb 1977], [Kourkouvelis 1980a] but the best measurement (Fig. 8b) [Kourkouvelis 1980b] was more concerned about Drell-Yan production.⁴ However, the Upsilon measurement

⁴ Drell-Yan production, or $\bar{q} + q \rightarrow \mu^+ + \mu^- + X$ is predominantly an electromagnetic process which measures the \bar{q} composition of a proton. It is mainly a parton model reaction. QCD enters only in the next to leading order.

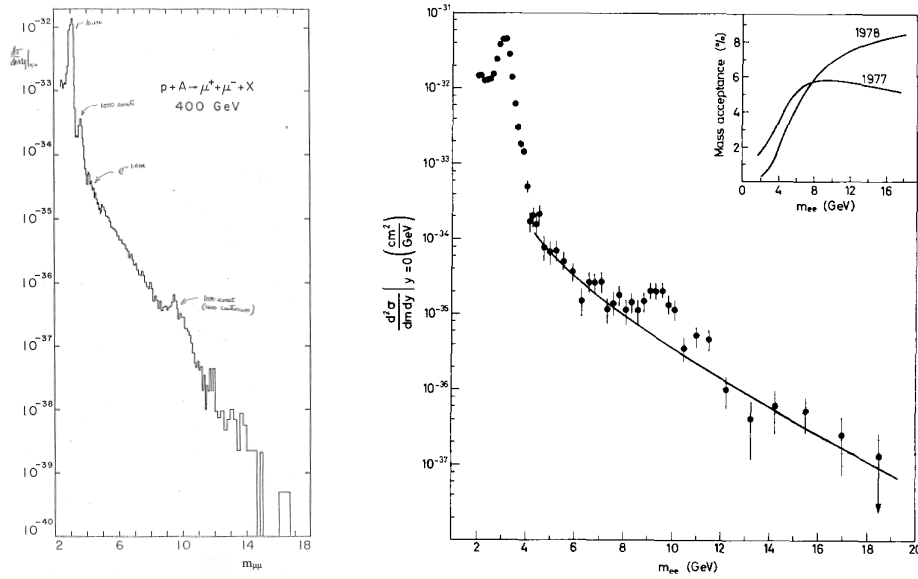


Fig. 8. a) (left) CFS dimuon spectrum [Herb 1977] with Ψ , Ψ' , Drell-Yan exponential and Υ indicated. b) (right) ABCSY $d^2\sigma/dm_{ee}dy|_{y=0}$ averaged for $\sqrt{s} = 53$ and 63 GeV [Kourkouvelis 1980b]

[Kourkouvelis 1980a] did correct an anomalously large value of the cross section claimed in their previous publication [Cobb 1977].

4.4 The direct single e^\pm are from the semi-leptonic decay of charm particles.

With the J/Ψ issue out of the way, the comprehensive CCRS single e^\pm measurements [Büsser 1976b] remained a very interesting challenge (Fig. 9). The direct-single e^\pm spectra in the range $1.3 < p_T < 3.2$ GeV/c were roughly constant at a level of 10^{-4} of charged pion production at all 5 c.m. energies measured. However, in detail, the ratio of e/π increased systematically by a factor of ~ 1.8 from $\sqrt{s} = 30$ to 60 GeV [Büsser 1976b] (Fig. 10).

4.4.1 The theorists rise to the occasion.

Although discovered in 1974, it was not until 1976 that the direct single e^\pm were shown to be from the semi-leptonic decay of charm particles. Of course without the intervening J/Ψ charmonium discovery, it is unlikely that charm particles would have been considered. In fact, the first attempt of explaining the CCRS measurements was by Farrar and Frautschi [Farrar 1976] who proposed that the direct-single- e^\pm were due to the internal conversion of direct photons with a ratio $\gamma/\pi^0 \sim 10\text{-}20\%$. However CCRS was able to cleanly detect (and reject) both external and internal conversions, since there was zero magnetic field on the axis, so was able to set limits excluding this explanation to less than 6.6% of the observed signal [Büsser 1976b].

The first correct explanation of the CCRS direct-single- e^\pm (prompt leptons) was given by Hinchliffe and Llewellyn-Smith [Hinchliffe 1976a] as due to semi-leptonic

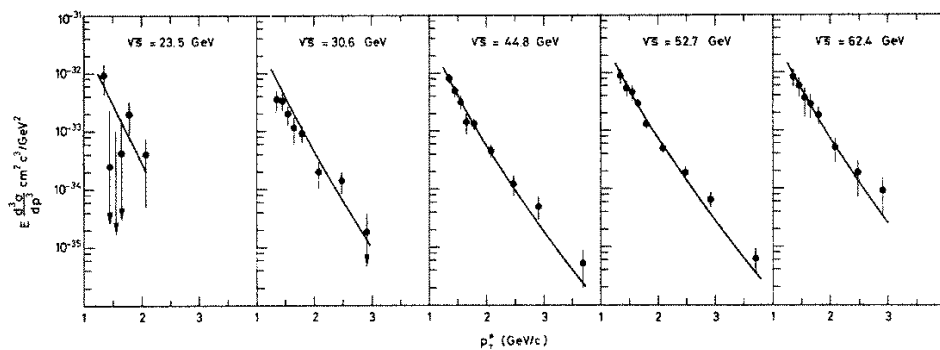


Fig. 9. Invariant cross sections of $(e^+ + e^-)/2$ (points) at mid-rapidity for 5 values of \sqrt{s} in p+p collisions at the CERN-ISR [Büsser 1976b]. Lines represent a fit of the $(\pi^+ + \pi^-)/2$ British-Scandinavian data [Alper 1975a], multiplied by 10^{-4}

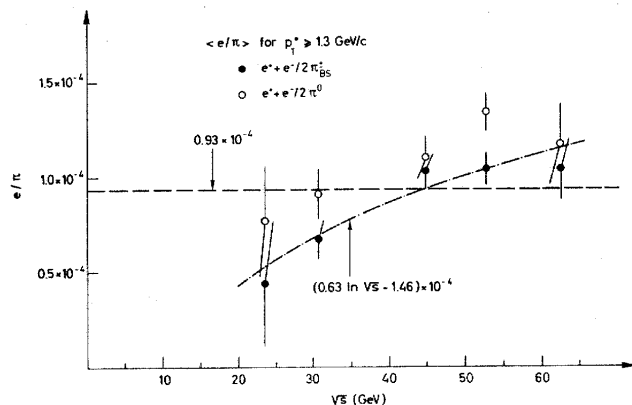


Fig. 10. The ratios $(e^+ + e^-)/(\pi^+ + \pi^-)$ and $(e^+ + e^-)/2\pi^0$ for $p_T \geq 1.3$ GeV/c as a function of c.m. energy \sqrt{s} from CCRS [Büsser 1976b]. The π^0 data were obtained from the measured spectra of selected conversions and the π^\pm from the British-Scandinavian data [Alper 1975a] (solid points). The two curves shown are fits to the solid points.

decay of charm particles. The predictions from charm decay [Hinchliffe 1976a] are in excellent agreement with the CCRS data [Büsser 1975b] submitted to the SLAC conference as shown in Fig. 11a. A similar explanation was published by Maurice Bourquin and Jean-Marc Gaillard [Bourquin 1976], two experimentalists, who compared the measured e/π ratios to a cocktail of all known leptonic decays including “Possible contributions from the conjectured charm meson...” (Fig. 11b). It is interesting to note the usage of “conjectured” because it seems that this was the notation for D^+ and D^0 charm mesons from the first SLAC paper which failed to find open charm [Boyarski 1975] a year before it was actually discovered at SLAC in August 1976 [Goldhaber 1976].

Something important to note about the charm calculations [Hinchliffe 1976b], [Bourquin 1976] and clearly shown in Fig. 11b is that neither calculation could fit the data points for $p_T < 1$ GeV/c at 30° from the CHORMN experiment [Baum 1976] at the ISR. The important issue from a historical perspective is that many experiments not designed for the purpose wanted to get into the prompt-lepton act, which resulted in questionable (i.e. incorrect) results, and this is only one example. See

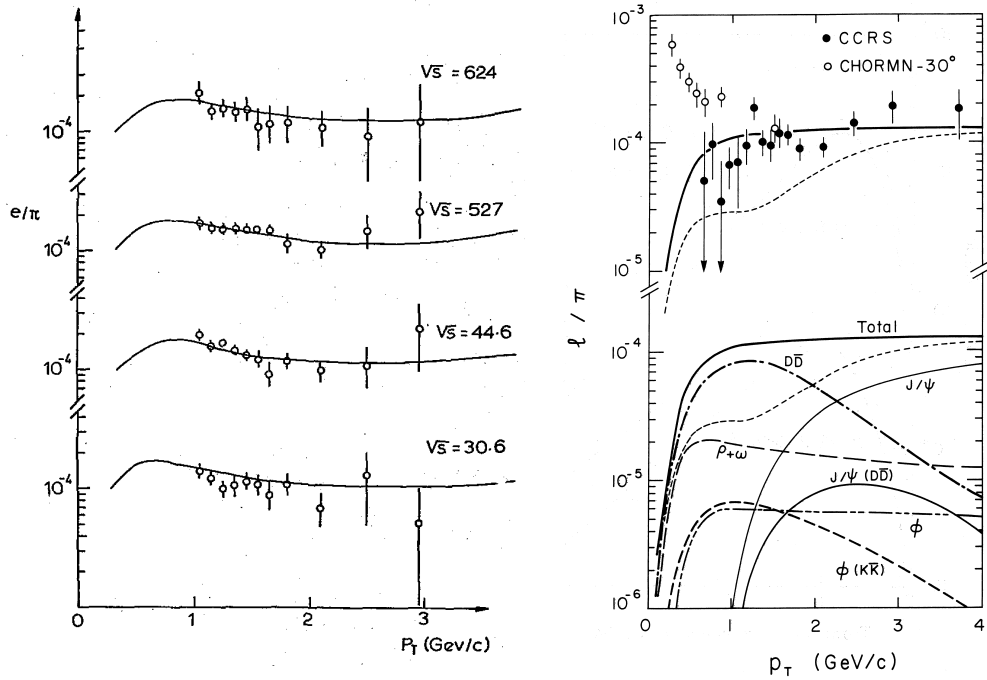


Fig. 11. a) (left) CCRS e/π in two spectrometer arms at two values of \sqrt{s} [Büsser 1975b] with prediction, see Ref. [Hinchliffe 1976a] for details. b) (right) Bourquin-Gaillard [Bourquin 1976] calculation of a cocktail of decays to the e/π ratio.

Ref. [Bourquin 1976] for more details. This led to the unfortunate situation that later papers about charm ignored the many disagreeing ISR measurements of the direct-single- e^\pm from charm, which were essentially ridiculed, or in the case of the original CCRS discovery [Büsser 1976b] downplayed in review articles [Fabjan 2004]; or ignored [Tavernier 1987] because it was published before either charm or the J/ψ were discovered so there is no reference to the word “charm” in the publication.

Later experiments at the CERN-ISR using the upgraded Split Field Magnet were designed for a program of heavy flavor searches. The CCRS direct e^\pm measurement at $\sqrt{s} = 62.4$ GeV was confirmed by a well designed single e^\pm experiment performed by the Zichichi group [Basile 1981]. Also the first direct evidence of charm hadron production in hadron interactions was the observation at the CERN-ISR of the charm D^+ meson via its $D^+ \rightarrow K^+\pi^+\pi^-$ decay by the CCHK experiment [Drijard 1979].

4.4.2 Why do I dwell on charm at the CERN-ISR?

One reason is the lack of recognition in the charm literature as noted. However the main reason is that the measurement of charm by direct single e^\pm in p+p and Au+Au collisions [Adare 2007a] 30 years later at the Relativistic Heavy Ion Collider (RHIC) at Brookhaven National Laboratory (BNL) was one of the principal observations that led to the discovery of the Quark Gluon Plasma and the conclusion that it was a perfect liquid with a viscosity to entropy density ratio “intriguingly close to the conjectured quantum lower bound” $1/4\pi$ [Kovtun, Son and Starinets 2005].

5 QCD meets high p_T 1977-1979

It wasn't until 1977 that QCD was applied to hard-scattering with the first theoretical calculations of the basic equations for the elementary QCD subprocesses at leading order [Combridge 1977] [Cutler 1978] [Fritzsch 1977]. However the first application of “asymptotic freedom (AF)” to “wide-angle hadronic collisions” was in 1975 in a publication [Cahalan 1975] with an incorrect conclusion; but with an improved x_T scaling formula, that experimenters liked, which included the evolution effects of “AF” and is still in use at present.

5.1 Improved x_T scaling.

The incorrect conclusion of Ref. [Cahalan 1975] was that “single vector gluon exchange contributes insignificantly to wide angle hadronic collisions”; but, in my humble opinion, they may have been overly influenced by at least one author of the original (BBG) x_T scaling [Blankenbecler 1972]. This is based on an acknowledgement in Ref. [Cahalan 1975]: “Two of us (J. K. and L. S.) also thank S. Brodsky for emphasizing to us repeatedly that the present data on wide-angle hadron scattering show no evidence for vector exchange”.

Nevertheless the new x_T scaling formula, which introduced the “effective index” $n_{\text{eff}}(x_T, \sqrt{s})$ to account for ‘scale breaking’ (i.e. QCD evolution):

$$E \frac{d^3\sigma}{dp^3} = \frac{1}{p_T^{n_{\text{eff}}(x_T, \sqrt{s})}} F(x_T) = \frac{1}{\sqrt{s}^{n_{\text{eff}}(x_T, \sqrt{s})}} G(x_T) \quad \text{where} \quad x_T \equiv \frac{2p_T}{\sqrt{s}} \quad (13)$$

was very useful in understanding the next round of high p_T measurements.

5.2 Second generation high p_T measurements

The second generation of high p_T experiments at the CERN-ISR straightened out the $n = 8$ issue of the first round of experiments (recall Fig. 4) and made good use of Eq. 13. The CCOR experiment presented their first results (Fig. 12) [Angelis 1978] together with data and a fit from a previous CCRS measurement [Büsser 1976a] that had an order of magnitude more data than the original CCR and Saclay-Strasbourg measurements. Thanks to further increased integrated luminosity and acceptance, the CCOR data [Angelis 1978] extended another 4 orders of magnitude in cross section to $p_T \approx 14$ GeV/c. The CCRS fit, Ae^{-bx_T}/p_T^n , to their data at all three \sqrt{s} with $n = 8.6$ and $b = 12.5$ (shown as dashed lines on Fig. 12) works in the CCRS p_T range but fails badly for $p_T > 7$ GeV/c and remains well below the CCOR data out to $p_T \approx 14$ GeV/c.

5.2.1 x_T scaling with $n_{\text{eff}}(x_T, \sqrt{s})$

x_T scaling fits to the CCOR data in Fig. 12 for $\sqrt{s} = 53.1$ and 62.4 GeV [Angelis 1978] confirmed the validity of the idea that n_{eff} is a function of x_T and \sqrt{s} with results $n_{\text{eff}} = 8.0 \pm 0.4$ for the p_T interval $3.7 < p_T < 7.0$ GeV/c and $n_{\text{eff}} = 5.13 \pm 0.14$ for $7.5 < p_T < 14.0$ GeV/c. The variation of n_{eff} with x_T and \sqrt{s} is easier to observe with a log-log plot of the invariant cross section $\sigma^{\text{inv}} = Ed^3\sigma/dp^3$ vs x_T (Fig. 13a) where n_{eff} can be read off by inspection:

$$n_{\text{eff}}(x_T, \sqrt{s_1}, \sqrt{s_2}) = \frac{\ln [\sigma^{\text{inv}}(x_T, \sqrt{s_1}) / \sigma^{\text{inv}}(x_T, \sqrt{s_2})]}{\ln [\sqrt{s_2} / \sqrt{s_1}]} \quad . \quad (14)$$

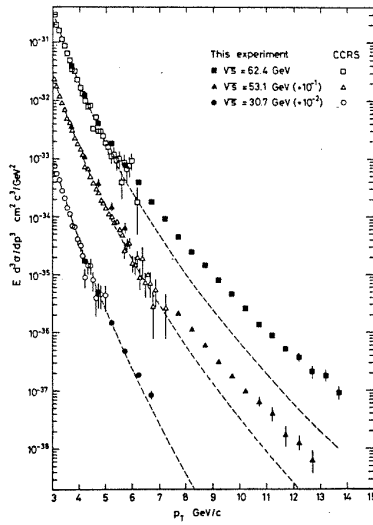


Fig. 12. Invariant π^0 cross sections $Ed^3\sigma/dp^3$ vs p_T for \sqrt{s} indicated [Angelis 1978]. Open points and dashed lines are data and fit are from a previous measurement [Büster 1976a]

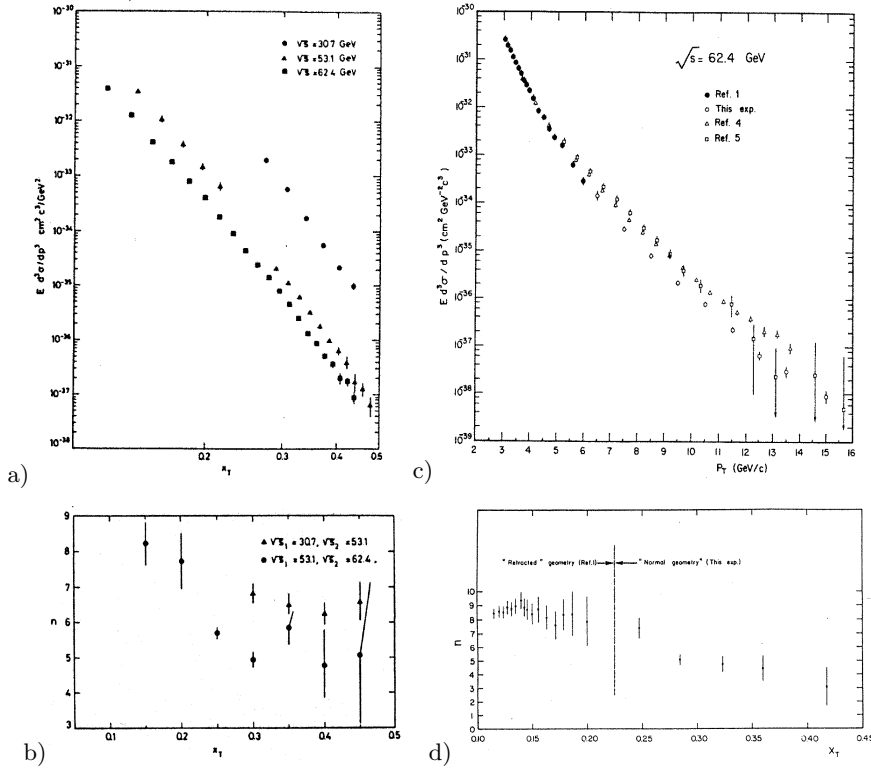


Fig. 13. [Angelis 1978] a) log-log plot of CCROR π^0 invariant cross section $Ed^3\sigma/dp^3$ vs x_T for 3 values of \sqrt{s} ; (b) $n_{\text{eff}}(x_T, \sqrt{s_1}, \sqrt{s_2})$ from (a). [Kourkoumelis 1979a] c) π^0 cross section vs p_T from ABCS at $\sqrt{s} = 62.4$ GeV with some other π^0 measurements from the ISR; d) $n_{\text{eff}}(x_T, 52.7, 62.4)$ from ABCS data. Only statistical errors are shown. There are additional common systematic uncertainties in n_{eff} of ± 0.33 in (b) and ± 0.7 in (d).

The fact that the data for $\sqrt{s} = 53.1$ and 62.4 GeV are essentially parallel for $x_T \geq 0.3$ in Fig. 13a indicates that $n_{\text{eff}} \approx 5$ is roughly constant in this range as shown in Fig. 13b, where all the point by point calculated $n_{\text{eff}}(x_T, \sqrt{s_1}, \sqrt{s_2})$ are plotted. Also the increase in the spacing in Fig. 13a for $x_T \leq 0.2$ compared to $x_T \geq 0.3$ indicates the region where $n_{\text{eff}}(x_T, 53.1, 62.4) \approx 8$. An interesting observation about the fact that $n_{\text{eff}} \approx 5$ for $x_T \geq 0.3$ is that this value is now close to the value $n_{\text{eff}} = 4$, originally expected by BBG [Blankenbecler 1972] for QED or vector gluon exchange (Section 3.2), but modified by the scale breaking from QCD evolution as suggested by Ref. [Cahalan 1975].

Another nice feature of x_T scaling for experimentalists is that in the calculation of $n_{\text{eff}}(x_T, \sqrt{s_1}, \sqrt{s_2})$ from Eq. 14 the systematic uncertainty in the absolute value of the p_T scale cancels, which eliminates the dominant source of experimental systematic uncertainty. This is nicely illustrated by the π^0 measurements from another ‘second generation’ ISR experiment [Kourkoumelis 1979a] based on liquid-argon–Pb plate calorimeters of high spatial resolution and large solid angle acceptance (Fig. 13c). Notably, the π^0 cross-sections from ‘this experiment’ and ‘Ref.4’ (CCOR) [Angelis 1978] disagree by a large factor ≈ 3 for $p_T \geq 7$ GeV/c but the values of $n_{\text{eff}}(x_T, 53.1, 62.4)$ (Fig. 13d) are in excellent agreement with the CCOR values (Fig. 13b).

5.3 First theoretical calculations of pion p_T spectra using QCD: 1978

The first calculations of inclusive high p_T pion cross sections using QCD were performed by Owens, Reya and Glück [Owens 1978a] (Fig. 14a) and Feynman, Field and Fox (FFF) [Feynman 1978] (Fig. 14b). Figure 14a shows all the QCD subprocesses

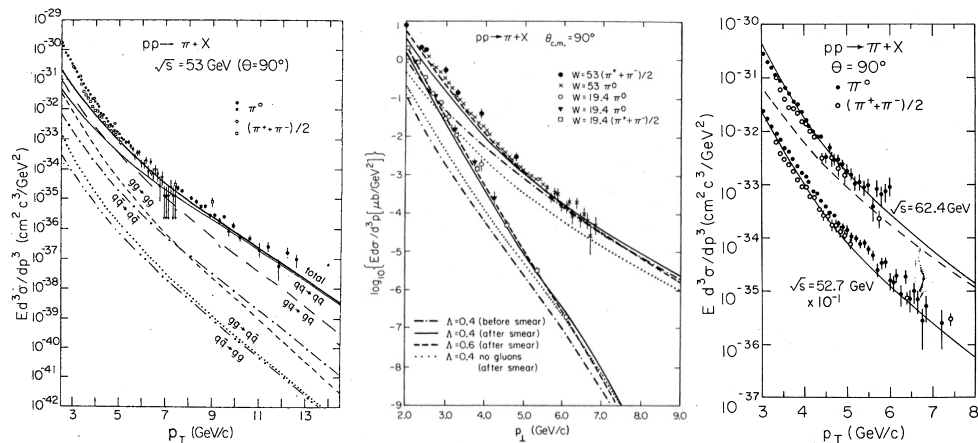


Fig. 14. a) (left) QCD calculation [Owens 1978a], with subprocess contributions shown, compared to preliminary CCOR π^0 measurements [Pope 1978]. QCD calculations including the k_T effect: (b) (center) Feynman Field and Fox [Feynman 1978] and (c) (right) Owens and Kimel [Owens 1978b] compared to CERN-ISR and Fermilab pion measurements indicated.

that go into the calculation; but the total, which fits the data well for $p_T > 5$ GeV/c, falls below the data for $p_T < 5$ GeV/c. Note that the data are preliminary results of CCOR [Pope 1978] which agree with the final publication [Angelis 1978] shown in Fig. 12. The FFF calculations in Fig. 14b follow the BS [Alper 1975b] $(\pi^+ + \pi^-)/2$ and CCRS π^0 [Büsser 1976a] measurements at $\sqrt{s} = 53$ GeV/c, as well as $\sqrt{s} = 19.4$ GeV/c measurements from Fermilab, from $p_T \approx 7$ GeV/c down to $p_T \approx 2$ GeV/c

because the effect of k_T smearing was included. k_T , the transverse momentum of a parton in a nucleon, had been introduced by FFF the previous year [Feynman 1977] to explain ISR measurements of two-particle correlations which will be discussed in detail in a later section. A second calculation by Owens [Owens 1978b] which included the k_T effect also fit the CCRS [Büsser 1976a] data down to $p_T = 3$ GeV/c.

These calculations all assume that high p_T particles are produced from states with two roughly back-to-back jets which are the result of scattering of a parton from each nucleon. The calculations require the purely theoretical elementary QCD subprocesses plus other quantities which must come from measurements. It is also important to understand the kinematics of parton-parton scattering and the definition of the various kinematic quantities. These are given in the Appendix (section 14).

6 Elements of QCD for Experimentalists

QCD calculations at the parton level are relatively straightforward. For example consider the scattering:

$$a + b \rightarrow c + d$$

where a and b are incident partons with c.m. energy $\sqrt{\hat{s}}$ that scatter elastically through angle θ^* , with 4-momentum-transfer-square:

$$Q^2 = -\hat{t} = \hat{s} \frac{(1 - \cos \theta^*)}{2} \quad . \quad (15)$$

The QCD cross section for this subprocess is simply:

$$\left. \frac{d\sigma}{d\hat{t}} \right|_{\hat{s}} = \frac{\pi \alpha_s^2(Q^2)}{\hat{s}^2} \Sigma^{ab}(\cos \theta^*) \quad ; \quad (16)$$

where the elementary QCD subprocesses involving quarks (q) and gluons (g) in hadron-hadron collisions and their characteristic angular distributions [Combridge 1977] [Cutler 1978] $\Sigma^{ab}(\cos \theta^*)$ are enumerated in Fig. 15a-h.

6.1 The Elementary QCD Subprocesses

At the elementary level, the lowest order QCD Born diagrams, shown in Fig. 15-(right), are analogous to the QED processes of Møller, Bhabha and Compton scattering indicated; and tests of their validity would be quite analogous to the studies of the validity of Quantum Electrodynamics (QED) which occupied the 1950's and 1960's [Brodsky 1970]. The \hat{t} and \hat{u} channels and \hat{s} and \hat{t} channels are indicated for the qq and $\bar{q}q$ diagrams respectively. It is important to note that the diagrams in the dashed box are unique to QCD since the gluons carry color charge and interact with each other while the photons in QED do not carry electric charge and so do not self-interact.

Although the different combinations of \hat{s} , \hat{t} and \hat{u} for the cross sections in Fig. 15a-h may at first seem to be formidable, it can be seen by substituting $\hat{t} = -\hat{s}(1 - \cos \theta^*)/2$, $\hat{u} = -\hat{s}(1 + \cos \theta^*)/2$, that indeed the $\Sigma^{ab}(\cos \theta^*)$ are nothing other than angular distributions. For example, for $qq' \rightarrow qq'$ Fig. 15a:

$$\Sigma^{qq'}(\cos \theta^*) = \frac{4}{9} \frac{\hat{s}^2 + \hat{u}^2}{\hat{t}^2} = \frac{4}{9} \left[\left(\frac{2}{1 - \cos \theta^*} \right)^2 + \left(\frac{1 - \cos \theta^*}{1 + \cos \theta^*} \right)^2 \right] \quad (17)$$

However, bringing Eqs. 16 and 17 to the p+p collision level leads to complications.

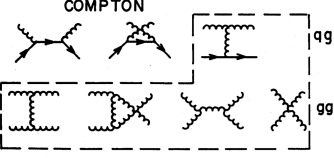
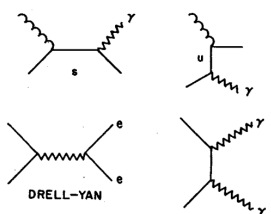
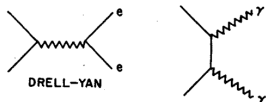
a)	$qq' \rightarrow qq'$ $\bar{q}q' \rightarrow \bar{q}q'$	$\frac{4}{9} \frac{\hat{s}^2 + \hat{u}^2}{\hat{t}^2}$		qq MOLLER
b)	$qq \rightarrow qq$	$\frac{4}{9} \left(\frac{\hat{s}^2 + \hat{u}^2}{\hat{t}^2} + \frac{\hat{s}^2 + \hat{t}^2}{\hat{u}^2} \right) - \frac{8}{27} \frac{\hat{s}^2}{\hat{u}\hat{t}}$		$\bar{q}q$ BHABHA
c)	$\bar{q}q \rightarrow \bar{q}'q'$	$\frac{4}{9} \frac{\hat{t}^2 + \hat{u}^2}{\hat{s}^2}$		
d)	$\bar{q}q \rightarrow \bar{q}q$	$\frac{4}{9} \left(\frac{\hat{s}^2 + \hat{u}^2}{\hat{t}^2} + \frac{\hat{t}^2 + \hat{u}^2}{\hat{s}^2} \right) - \frac{8}{27} \frac{\hat{u}^2}{\hat{s}\hat{t}}$		
e)	$\bar{q}q \rightarrow gg$	$\frac{32}{27} \frac{\hat{u}^2 + \hat{t}^2}{\hat{u}\hat{t}} - \frac{8}{3} \frac{\hat{u}^2 + \hat{t}^2}{\hat{s}^2}$		
f)	$gg \rightarrow \bar{q}q$	$\frac{1}{6} \frac{\hat{u}^2 + \hat{t}^2}{\hat{u}\hat{t}} - \frac{3}{8} \frac{\hat{u}^2 + \hat{t}^2}{\hat{s}^2}$		
g)	$qq \rightarrow qq$	$-\frac{4}{9} \frac{\hat{u}^2 + \hat{s}^2}{\hat{u}\hat{s}} + \frac{\hat{u}^2 + \hat{s}^2}{\hat{t}^2}$		
h)	$gg \rightarrow gg$	$\frac{9}{2} \left(3 - \frac{\hat{u}\hat{t}}{\hat{s}^2} - \frac{\hat{u}\hat{s}}{\hat{t}^2} - \frac{\hat{s}\hat{t}}{\hat{u}^2} \right)$		

Fig. 15. a)-h) (left) Hard scattering subprocesses in QCD [Combridge 1977] [Cutler 1978] for quarks q and gluons g where the q' indicates a different flavor quark from q , with their lowest order cross section angular distribution $\Sigma^{ab}(\cos\theta^*)$ as defined in Eq. 16. (right) Lowest order diagrams involving initial state q and g scattering.

6.2 p+p hard-scattering in QCD

The overall hard-scattering cross section $A + B \rightarrow C + X$ (Fig. 16) in “leading

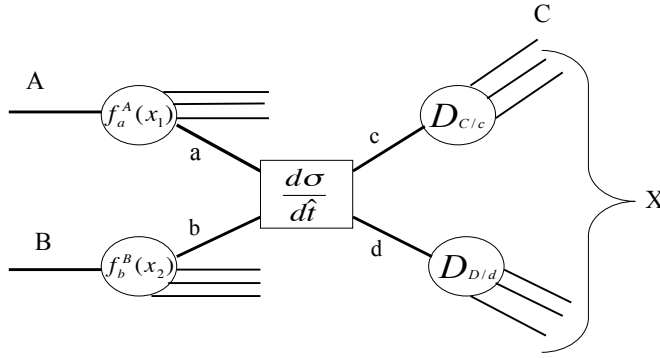


Fig. 16. Sketch (inspired by Fig. 3 of [Feynman 1978]) of the reaction of initial colliding particles $A+B$ producing a particle C in the final state where X represents all other particles.

logarithm” pQCD is the sum over parton reactions $a + b \rightarrow c + d$ (e.g. $g + q \rightarrow g + q$) at parton-parton center-of-mass (c.m.) energy $\sqrt{\hat{s}}$ as given in Eq. 18 [Owens 1987]

$$\frac{d^3\sigma}{dx_1 dx_2 d\cos\theta^*} = \frac{sd^3\sigma}{d\hat{s}d\hat{y}d\cos\theta^*} = \frac{1}{s} \sum_{ab} f_a^A(x_1) f_b^B(x_2) \frac{\pi\alpha_s^2(Q^2)}{2x_1 x_2} \Sigma^{ab}(\cos\theta^*) \quad (18)$$

where $f_a^A(x_1)$, $f_b^B(x_2)$, are parton distribution functions (PDF), the differential probabilities for partons a and b to carry momentum fractions x_1 and x_2 of their respective protons (e.g. $u(x_2)$), and where θ^* is the scattering angle in the parton-parton c.m. system. The parton-parton c.m. energy squared is $\hat{s} = x_1 x_2 s$, where \sqrt{s} is the c.m. energy of the p+p collision. The parton-parton c.m. system moves with rapidity $\hat{y} = (1/2) \ln(x_1/x_2)$ in the p+p c.m. system. The quantities $f_a(x_1)$ and $f_b(x_2)$, the “number” distributions of the constituents, are related (for the electrically charged quarks) to the structure functions measured in $e + A$ lepton-hadron Deeply Inelastic Scattering (DIS), where A is p or n, e.g.

$$F_1^A(x, Q^2) = \frac{1}{2} \sum_a e_a^2 f_a^A(x, Q^2) \quad \text{and} \quad F_2^A(x, Q^2) = x \sum_a e_a^2 f_a^A(x, Q^2) \quad (19)$$

where e_a is the electric charge of the quark a .

The transverse momentum of a scattered constituent is:

$$p_T = p_T^* = \frac{\sqrt{\hat{s}}}{2} \sin \theta^*, \quad (20)$$

and the scattered constituents c and d in the outgoing parton-pair have equal and opposite momenta in the parton-parton (constituent) c.m. system. A naive experimentalist would think of $Q^2 = -\hat{t}$ for a scattering subprocess and $Q^2 = \hat{s}$ for a Compton or annihilation subprocess.

Equation 18 gives the p_T spectrum of outgoing parton c , which then fragments into a jet of hadrons, including e.g. π^0 . To go to the particle level the fragmentation function $D_c^{\pi^0}(z)$ which is the probability for a π^0 to carry a fraction $z = p^{\pi^0}/p^c$ of the momentum of outgoing parton c must be multiplied in along with its differential dz . Equation 18 must be summed over all subprocesses leading to a π^0 in the final state weighted by their respective fragmentation functions. In this formulation, $f_a^A(x_1)$, $f_b^B(x_2)$ and $D_c^{\pi^0}(z)$ represent the “long-distance phenomena” to be determined by experiment; while the characteristic subprocess angular distributions, $\Sigma^{ab}(\cos \theta^*)$ (Fig. 15) and the coupling constant, $\alpha_s(Q^2) = \frac{12\pi}{25 \ln(Q^2/\Lambda^2)}$, are fundamental predictions of QCD [Cambridge 1977] [Cutler 1978] for the short-distance, large- Q^2 , phenomena. When higher order effects are taken into account, it is necessary to specify factorization scales μ for the distribution and fragmentation functions in addition to renormalization scale Λ which governs the running of $\alpha_s(Q^2)$. As noted above, the momentum scale $Q^2 \approx p_T^2$ for the scattering subprocess, while $Q^2 \approx \hat{s}$ for a Compton or annihilation subprocess, but the exact meanings of Q^2 and μ^2 tend to be treated as parameters rather than as dynamical quantities.

7 Direct single photon production, the most elegant QCD reaction

Direct single photon (γ) production with a ratio $\gamma/\pi^0 \sim 10 - 20\%$ [Farrar 1976] was one of the first proposed explanations of the direct single e^\pm discovery at the ISR but was excluded with 95% confidence level to $\gamma/\pi^0 < 5\%$ for $p_T > 1.3$ GeV/c [Büsser 1976a]¹.

7.1 Direct- γ QCD elementary subprocesses: 1977

The first QCD calculation of direct- γ production, “the inverse QCD Compton Effect”, via the constituent reaction $g + q \rightarrow \gamma + q$ was presented by Fritzsche and Minkowski in 1977 [Fritzsche 1977]. This reaction has many beautiful aspects as a hadronic probe.

1. The γ -ray participates directly in the hard-scattering and then emerges freely and unbiased from the reaction, isolated, with no accompanying particles.
2. The energy of this outgoing parton (the γ -ray) can be measured precisely.
3. No fragmentation function is required for Eq. 18.
4. Since there are many fewer \bar{q} in a nucleon than quarks or gluons, the $g+q$ reaction dominates so that the parton opposite the γ -ray is most likely a quark.
5. The scattered quark has equal and opposite transverse momentum to the direct- γ , so the transverse momentum of the jet from the outgoing quark is also precisely known (modulo k_T).

The cross-section for the elementary QCD subprocess, $g+q \rightarrow \gamma+q$ is simply:

$$\left. \frac{d\sigma}{d\hat{t}} \right|_{\hat{s}} = \frac{\pi\alpha_s \alpha e_q^2}{3\hat{s}^2} \left(\frac{\hat{s} + \hat{t}}{\hat{s}} + \frac{\hat{s}}{\hat{s} + \hat{t}} \right) \quad , \quad (21)$$

Using the same argument as item 4 above, the QCD cross-section for the reaction $A+B \rightarrow \gamma+q$ with the direct- γ produced at rapidity y_c with p_T , and the quark-jet at y_d with p_T is analytical:

$$\begin{aligned} \frac{d^3\sigma}{dp_T^2 dy_c dy_d} &= x_1 G_A(x_1) F_{2B}(x_2) \frac{\pi\alpha\alpha_s(Q^2)}{3\hat{s}^2} \left(\frac{1 + \cos\theta^*}{2} + \frac{2}{1 + \cos\theta^*} \right) \\ &+ F_{2A}(x_1) x_2 G_B(x_2) \frac{\pi\alpha\alpha_s(Q^2)}{3\hat{s}^2} \left(\frac{1 - \cos\theta^*}{2} + \frac{2}{1 - \cos\theta^*} \right) \end{aligned} \quad (22)$$

where

$$\cos\theta^* = \tanh \frac{(y_c - y_d)}{2} \quad x_{1,2} = x_T \frac{e^{\pm y_c} + e^{\pm y_d}}{2} \quad \sqrt{\hat{s}} = 2p_T \cosh \frac{(y_c - y_d)}{2}. \quad (23)$$

Here $F_2(x, Q^2)$ is the sum of the PDF's over all the quarks and anti-quarks (predominantly u and d) in the nucleons or nuclei A and B and $G(x, Q^2)$ is the gluon PDF which is the principal theoretical problem in the calculation since it is the least well known. However, the main difficulty with the measurement of direct photon production is experimental: a huge background from the decays $\pi^0 \rightarrow \gamma + \gamma$ and $\eta \rightarrow \gamma + \gamma$.

7.1.1 R_γ , 'the double ratio' for signal/background

For measurements at mid-rapidity, the π^0 cross section is typically a power law with $d\sigma/p_T dp_T \propto p_T^{-n}$. In this case the p_T spectrum of the background γ rays from $\pi^0 \rightarrow \gamma + \gamma$ relative to the π^0 spectrum is given by the simple expression [Ferbel 1984]¹:

$$\left. \frac{\gamma}{\pi^0} \right|_{\pi^0} = \frac{2}{n-1} \implies \left. \frac{\gamma}{\pi^0} \right|_{\text{bkg}} \approx 1.19 \times \frac{2}{n-1} \quad (24)$$

where $(\gamma/\pi^0)_{\text{bkg}}$ includes the $\eta \rightarrow \gamma + \gamma$ background ($\eta/\pi^0 \approx 0.5$ for $p_T > 3$ GeV/c with $\eta \rightarrow \gamma + \gamma$ branching ratio 0.38 [Büsser 1975c]).

Generally, the background is calculated using Monte Carlo calculations including efficiency, acceptance, etc. However the signal/background ratio is best presented by the double ratio:

$$R_\gamma = \frac{(\gamma/\pi^0)_{\text{Measured}}}{(\gamma/\pi^0)_{\text{Background}}} \approx \frac{\gamma_{\text{Measured}}}{\gamma_{\text{Background}}} \quad (25)$$

because the calculated background in the form $(\gamma/\pi^0)_{\text{Background}}$ can be checked by comparison to Eq. 24. $R_\gamma > 1.0$ indicates a direct- γ signal.

7.2 Experimental results

As in many reactions studied for the first time, the experimental results at the ISR, where direct- γ were eventually discovered, started with an incorrect measurement [Darriulat 1976a] while other early experiments set limits using low mass e^+e^- pairs¹. The first correct results from an experiment specifically designed to detect real single photons at the ISR [Amaldi 1979] set a 95% confidence upper limit of $\gamma/\pi^0 < 4\%$ for $2.3 \leq p_T \leq 3.4$ GeV/c.

The first experiment to actually correctly claim the observation of a signal for direct- $\gamma/\pi^0 \approx 0.2$ for $p_T \geq 4.5$ GeV/c and generally given credit for the discovery of direct- γ production was the measurement by the AABC experiment [Diakonou 1979] a modification of the ABCS experiment using the high resolution calorimeters which could resolve the two γ 's from π^0 decay. The first measurement of the direct- γ cross section was by CCOR [Angelis 1980a] who could not resolve the two γ s in a cluster but instead measured the fraction of clusters of a given p_T that would pass through the 1.0 radiation length thin-wall of the superconducting solenoid without making a conversion (47% for a single γ and $\approx 20-24\%$ for 2 or more γ rays in the cluster). This led to a large systematic uncertainty which was not too bad for $9 \leq p_T \leq 13$ GeV/c (Fig 17a). The cross-sections in this region were in surprisingly good agreement with the final AABC (R806) results (Fig 17b) [Anassontzis 1982] as discussed in detail by [Ferber 1984]. The final ISR direct- γ measurement [Angelis 1989] also includes a summary of the previous measurements, which are all in impressive agreement over the range $4 \leq p_T \leq 13$ GeV/c as shown in Fig 17c.

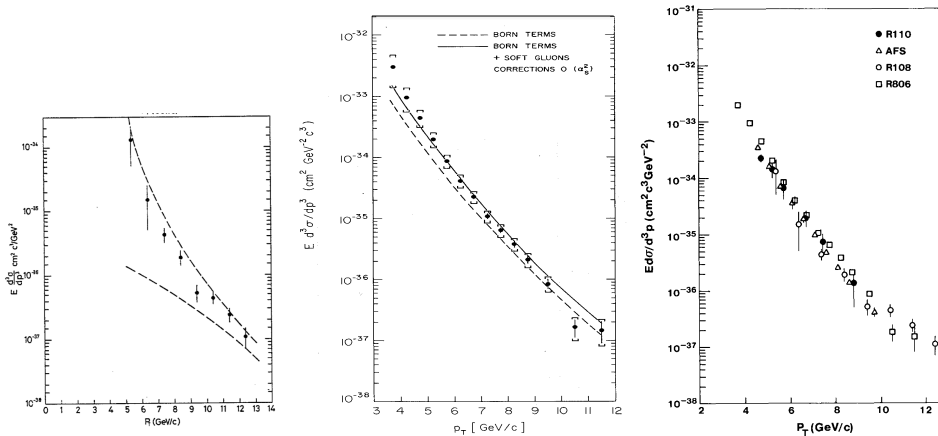


Fig. 17. Inclusive direct- γ cross sections at $\sqrt{s} = 63$ GeV: a)(left) CCOR [Angelis 1980a] (dashed lines are systematic uncertainty), b)(center) R806 [Anassontzis 1982] (lines are QCD calculations [Contogouris 1981]), c) (right) CMOR [Angelis 1989].

7.2.1 Theoretical predictions of direct- γ data show that QCD really works.

The theoretical predictions of direct- γ cross-sections lagged behind the experimental measurements because the gluon structure functions (PDF), $G(x, Q^2)$, in deeply inelastic e+p or neutrino scattering are not measured directly as are the quark PDF's, $F_2(x, Q^2)$, but are measured via the scaling violations, the Q^2 evolution of $F_2(x, Q^2)$ [Abramowicz 1982]. In fact, the first attempted direct measurement of $G(x, Q^2)$ was made at the ISR by the AFS experiment [Akeson 1987] with measurements of direct- γ +jet, both at mid-rapidity, solving Eq. 22 for $xG(x)$ (Fig. 18a).

It is interesting and informative to skip ahead to the present, where next-to-leading-order QCD calculations using the latest PDF's as well as "joint resummation of both threshold and recoil effects due to soft multigluon emission" are in excellent agreement with all existing direct- γ measurements at the time of publication [Aurenche 2006] (Fig. 18b.)

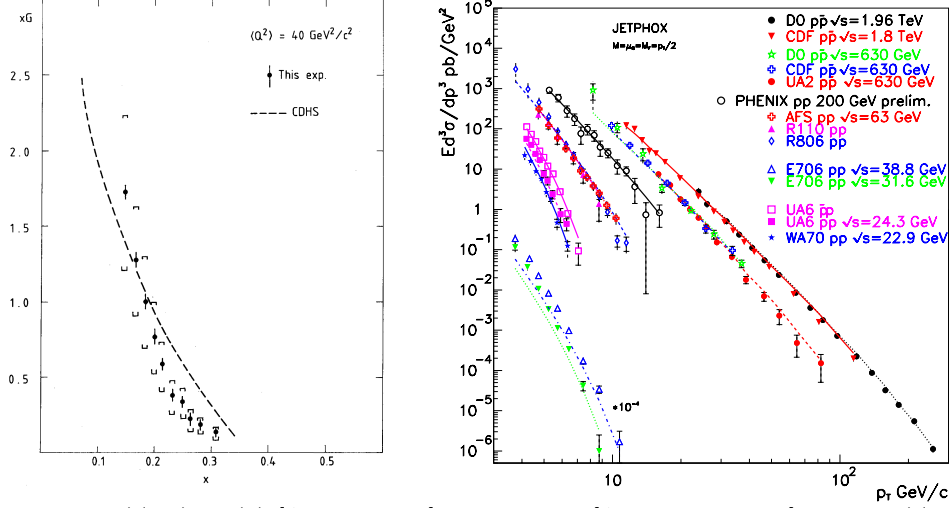


Fig. 18. a)(left) $xG(x)$ [Akesson 1987] compared to [Abramowicz 1982] dashes. b)(right) Plot of all direct- γ $Ed^3\sigma/dp^3$ measurements in p+p and \bar{p} +p collisions circa 2006 compared to "JETPHOX" NLO QCD predictions [Aurenche 2006].

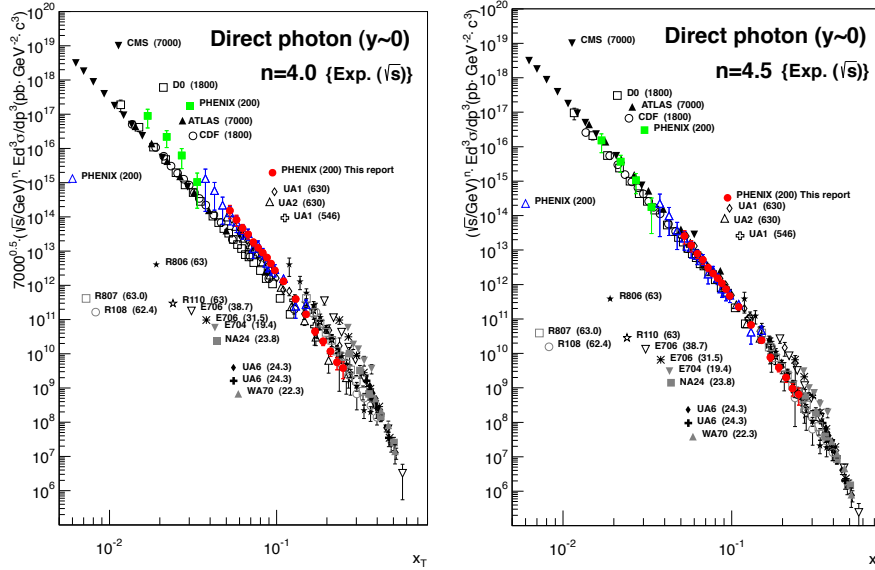


Fig. 19. a)(left) $\sqrt{s}^{n_{\text{eff}}} \times Ed^3\sigma/dp^3$, as a function of $x_T = 2p_T/\sqrt{s}$, with $n_{\text{eff}} = 4.0$, for direct- γ measurements in p+p and \bar{p} -p experiments at the $(\sqrt{s}$ GeV) indicated. [Adare 2012]. b)(right) same as (a) with $n_{\text{eff}} = 4.5$

From the experimental point of view, a better illustration of QCD in action is given by the x_T scaling of all the existing direct- γ measurements (Fig. 19). For x_T scaling with $n_{\text{eff}}=4.0$ (the parton model) QCD non-scaling is visible; but x_T scaling with $n_{\text{eff}}=4.5$ accounts for the non-scaling evolution which is a key element of QCD .

8 Two-particle correlations.

It was natural for the experiments that had searched for single leptons and lepton-pairs at mid-rapidity but were overwhelmed by pions at large p_T to look for what was balancing the p_T of the pions: an outgoing parton with opposite p_T , as described by Bjorken [Bjorken 1971] [Bjorken 1973], that fragmented into a collimated group of particles, “a jet” with a configuration like ordinary particle production e.g. $e^{-6p'_T}$ where p'_T is perpendicular to the outgoing parton. In this case, the jets should be coplanar with the beam direction and balance transverse momenta. Viewed down the beam axis, in azimuthal projection (Fig. 20), the events should show strong azimuthal correlation. Another possibility was balance as required by kinematics [Di Lella 1974].

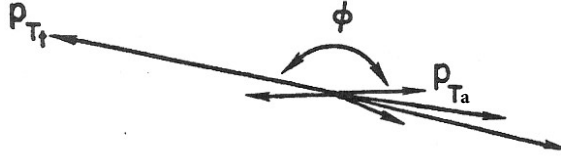


Fig. 20. Sketch of view down the beam axis of dijet event triggered by particle with p_{T_t} (circa 1973)

In Fig. 20 the different distribution of fragments in the jet \hat{p}_{T_t} , triggered by a particle with p_{T_t} , and the away jet is no accident. Bjorken made a very important point in his parton scattering prediction, that the single high p_T particle used as a trigger to search for the opposite jet, would carry “a major fraction (60-80%) of the total trigger parton (or jet) momentum. This is known as “trigger bias” [Jacob 1976] and is related to the Bjorken parent-child relation [Jacob 1978].

The cross-section for a pion with p_{T_t} which is a fragment with momentum fraction $z = p_{T_t}/\hat{p}_T$ in a jet from a parton q with \hat{p}_T where $D_\pi^q(z)$ is the fragmentation function (e.g. $\sim e^{-bz}$) is:

$$\frac{d^2\sigma_\pi(\hat{p}_T, z)}{\hat{p}_T d\hat{p}_T dz} = \frac{d\sigma_q}{\hat{p}_T d\hat{p}_T} \times D_\pi^q(z) = \frac{A}{\hat{p}_T^n} \times D_\pi^q(z) \quad . \quad (26)$$

The change of variables, $\hat{p}_T = p_{T_t}/z$, $d\hat{p}_T/dp_{T_t}|_z = 1/z$, then gives the joint probability of the pion with transverse momentum p_{T_t} and fragmentation fraction z :

$$\frac{d^2\sigma_\pi(p_{T_t}, z)}{p_{T_t} dp_{T_t} dz} = \frac{A}{p_{T_t}^n} \times z^{n-2} D_\pi^q(z) \quad . \quad (27)$$

Thus, the effective fragmentation function, for a trigger particle with p_{T_t} is weighted upward in z by a factor z^{n-2} , where n is the simple power fall-off of the jet invariant cross section (Eq. 26). This is the ‘trigger bias’ [Jacob 1976].

The pion p_{T_t} distribution is the integral of Eq. 27 over all values of the parton \hat{p}_T from $\hat{p}_T = p_{T_t}$, $z = 1$, to $\hat{p}_T = \sqrt{s}/2$, $z = x_{T_t}$, which has the same power n as the parton \hat{p}_T distribution:

$$\frac{d\sigma_\pi(p_{T_t})}{p_{T_t} dp_{T_t}} = \frac{1}{p_{T_t}^n} \int_{x_{T_t}}^1 A z^{n-2} D_\pi^q(z) dz \approx \frac{\text{constant}}{p_{T_t}^n}, \quad (28)$$

since typically $x_{T_t} \ll 1$, so the integral depends only weakly on p_{T_t} . Thus the invariant p_{T_t} spectrum of the π^0 fragment is a power law with the same power n as the original parton \hat{p}_T spectrum, for $p_{T_t} \ll \sqrt{s}/2$. This is the Bjorken parent-child relation.

8.1 Two particle correlation measurements 1975-1977.

Historically, at the ISR [Darmiulat 1976b, Della Negra 1977], since the trigger bias implied that the p_{Tt} of the trigger particle was a reasonable approximation to the \hat{p}_T of the triggered jet, and the away jet would be approximately equal and opposite to the trigger jet, the transverse momentum of the away particle p_{Ta} was decomposed into components (Fig. 21) of which two are commonly used: one perpendicular to the trigger plane $p_{out} = p_{Ta} \sin \Delta\phi$, and one in the trigger plane:

$$x_E = \frac{-p_x}{p_{Tt}} = \frac{-p_{Ta} \cos(\Delta\phi)}{p_{Tt}} \simeq \frac{p_{Ta}/\hat{p}_{Ta}}{p_{Tt}/\hat{p}_{Tt}} \approx \frac{z}{z_{\text{trig}}} \quad (29)$$

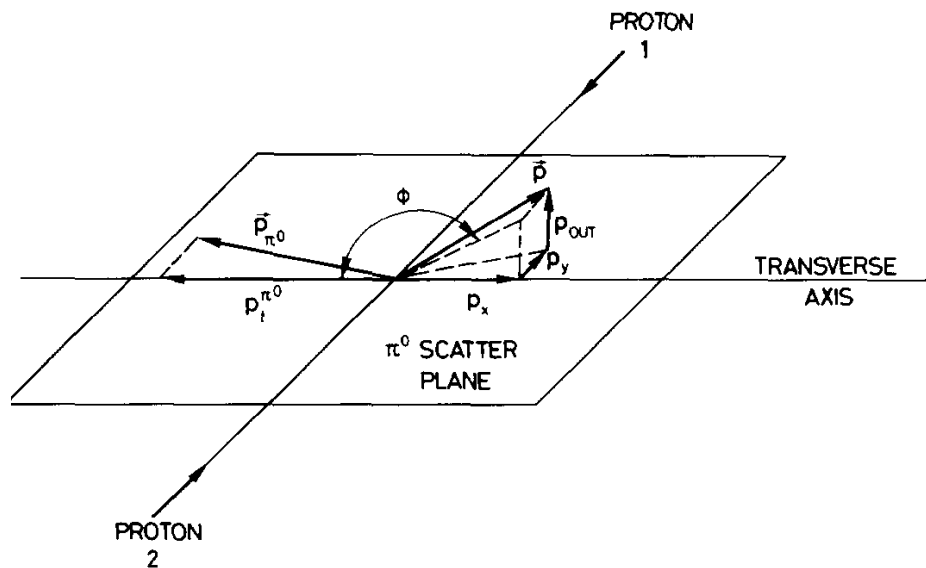


Fig. 21. Diagram [Darmiulat 1976b] of kinematical quantities for π^0 -hadron correlations. The trigger π^0 has momentum \mathbf{p}_{π^0} and transverse momentum $p_{Tt}^{\pi^0}$. The away hadron momentum \mathbf{p} is broken into four components: i) p_{out} , perpendicular to the scattering plane formed by the colliding protons and \mathbf{p}_{π^0} ; ii) p_y parallel to the p+p collision axis in the scattering plane; iii) p_T , not labelled, the component of \mathbf{p} transverse to the p+p collision axis; and iv) $p_x = p_T \cos \phi$, opposite to the direction of $p_{Tt}^{\pi^0}$ in the scattering plane, where ϕ (often called $\Delta\phi$) is the azimuthal angle between $p_{Tt}^{\pi^0}$ and p_T .

With the assumption that the trigger and away jets balance transverse momenta, $\hat{p}_{Ta} = -\hat{p}_{Tt}$, as assumed in the last step of Eq. 29, the variable x_E was thought to measure the fragmentation fraction z of the away jet from the highly biased trigger jet with $z_{\text{trig}} \rightarrow 1$. It was generally assumed that the p_{Ta} distribution of away side hadron fragments from an away-side parton opposite a single particle trigger with p_{Tt} , would be the same as that from a jet-trigger and follow the same fragmentation function of partons as observed in e^+e^- or DIS [Darmiulat 1976b] (Fig. 22). Because of the relatively large trigger bias at ISR energies and small range of $\langle z_{\text{trig}} \rangle$, $0.8 \lesssim \langle z_{\text{trig}} \rangle \lesssim 0.9$, it was also assumed that x_E scaling [Jacob 1976] would hold, i.e. all x_E distributions measured at different p_{Tt} would be the same.

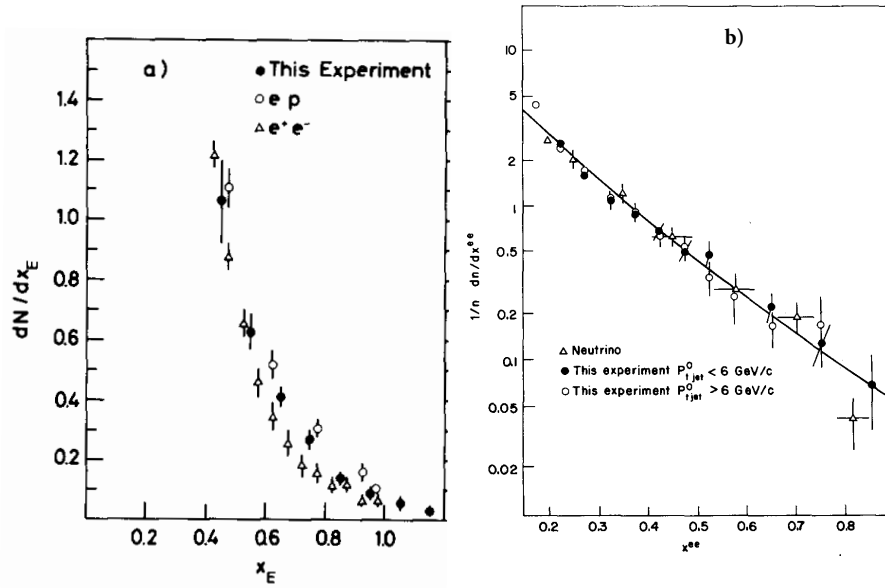


Fig. 22. a) x_E distribution for π^0 -h correlations with $2.0 < p_{T_t} < 4.1 \text{ GeV}/c$ and $1.2 < p_x < 3.2 \text{ GeV}/c$ together with e+p DIS and e^+e^- measurements [Darriulat 1976b]. b) jet fragmentation functions from ν +p (triangles), e^+e^- (full line) compared to measured p+p x_E distributions [Clark 1979].

These ideas were further clarified by Feynman, Field and Fox [Feynman 1977], who showed that the away side correlations for a single-particle trigger with p_{T_t} would be roughly the same as the away-side correlations for a jet trigger with $\hat{p}_{T_t} = p_{T_t}/\langle z_{\text{trig}} \rangle$ due to the fact that “the ‘quark’ from which the single hadron trigger came had a higher \hat{p}_{T_t} than did the quark producing the jet trigger (by a factor of $1/\langle z_{\text{trig}} \rangle$)”. (Fig 23). The ideas of x_E scaling according to a fragmentation function were supported by later ISR measurements but first a contemporary experiment (CCHK) [Della Negra 1977] did not find x_E scaling for values of $p_{T_t} < 4 \text{ GeV}/c$ which led to an important discovery.

8.1.1 k_T , the transverse momentum of a parton in a proton

The CCHK experiment at the CERN-ISR [Della Negra 1977] observed that x_E scaling [Jacob 1976] didn't work in the range $2.0 \leq p_{T_t} \leq 3.2 \text{ GeV}/c$; i.e. different values of trigger p_{T_t} did not produce a universal x_E distribution (Fig. 24a). CCHK also looked at the p_{out} variable and plotted $\langle p_{\text{out}} \rangle$ versus x_E for triggers in the range $2.0 \leq p_{T_t} \leq 3.2 \text{ GeV}/c$. They found that the $\langle p_{\text{out}} \rangle$ increased with increasing x_E up to a maximum value of $\langle p_{\text{out}} \rangle \sim 0.65 \text{ GeV}/c$ (Fig. 24b). The original parton model did not assign transverse motion to quarks in the proton, only longitudinal x , but it had been proposed by Levin and Ryskin [Levin 1975] that quarks in the proton also carry transverse momentum. This idea, coupled with the lack of x_E scaling for $p_{T_t} < 3 \text{ GeV}/c$, was taken by CCHK [Della Negra 1977] as evidence for the transverse momentum of quarks inside the proton. Calculations from their parton scattering model with $k_T = 0$ and $\langle k_T \rangle = 610 \text{ MeV}/c$ are shown in Fig. 24b. This result led Feynman, Field and Fox (FFF) [Feynman 1977] to formally introduce \vec{k}_T , the transverse momentum of a parton in a nucleon into their model of parton-parton scattering.

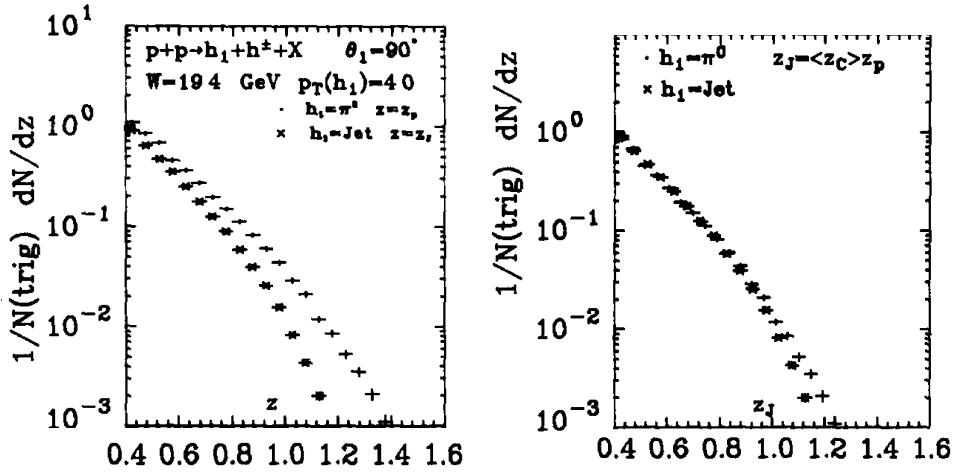


Fig. 23. [Feynman 1977]: a)(left) $dn/dz|_{trig}$ plotted vs. $z = x_E$ for a single particle trigger with p_{Tt} (dots) and $z = z_J = p_x/p_{Tjet}$ for a trigger by the jet (crosses); b)(right) same plot except now $z_J = \langle z_{trig} \rangle x_E$ is plotted for the single particle trigger instead of $z = x_E$.

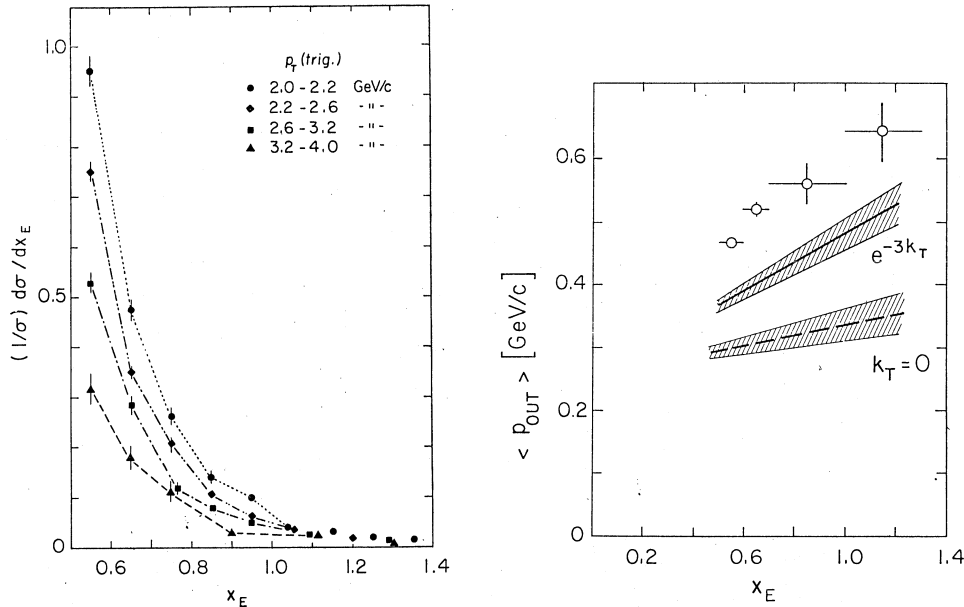


Fig. 24. a)(left) CCHK [Della Negra 1977] measurement of x_E distributions, $dn/dx_E|_{p_{Tt}}$, for intervals of p_{Tt} in the range 2.0–4.0 GeV/c. b) (right) CCHK [Della Negra 1977] measurement of $\langle p_{out} \rangle$ versus x_E for triggers in the range $2.0 \leq p_{Tt} \leq 3.2$ GeV/c. Also shown are the predictions of their parton scattering Monte Carlo model with $k_T = 0$ and $dN/k_T dk_T \propto e^{-3k_T}$ (with the restriction $k_T < 5/3$ GeV/c).

8.2 The second round of two-particle correlation measurements 1978-1979

The two experiments on two particle correlations at the CERN-ISR discussed above both used the Split Field Magnet Facility (SFM) [Bilan 1972] which could measure the momenta of charged particles in nearly the full polar angular range but was optimized for measurements at forward and backward angles. One experiment [Darriulat 1976b]

moved their small E.M. calorimeter to mid-rapidity of the SFM transverse to the beam axis while the CCHK measurement [Della Negra 1977] used only the SFM in a self-triggering mode at polar angles of 20° and 45° .

The second round of two particle correlations with improved detectors started to present data in 1978. The BFS collaboration [Albrow 1978] had moved the British Scandinavian wide angle spectrometer to the SFM at an angle of 90° at mid rapidity. They could trigger on identified charged particles with detection of the associated charged particles in the Split Field Magnet. The acceptance for associated charged particles, which was the same as CCHK, covered a rapidity range $-4 \leq y \leq +4$, with an azimuthal aperture of $\pm 40^\circ$ on the trigger side and $\pm 25^\circ$ on the away side. This experiment presented one of the most interesting results, a dramatic map of the two particle correlation function over nearly the full region in rapidity. Figure 25 shows the ratio of the density of tracks with $p_T > 0.5$ GeV/c, as a function of rapidity y and azimuthal angle ϕ , from a high p_{T_t} trigger with $3 < p_{T_t} < 4$, GeV/c located at $y = 0$ $\phi = 180^\circ$, relative to minimum bias events ($p_{T_t} \geq 0.5$ GeV/c with elastic scattering events removed). They called this ratio, which cancels the effects of acceptance variation, $R + 1$. The main features of Fig. 25 are an increase in the value

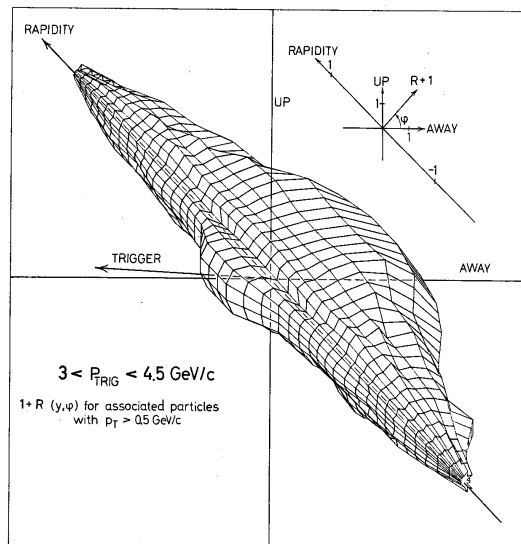


Fig. 25. BFS [Albrow 1978] measurement of $R+1$, ratio of charged particle track distribution from a high p_T trigger to that from minimum bias events

of the correlation function in a small region in y and ϕ near the trigger particle and a much larger increase on the away side, mainly within $|\phi| < 45^\circ$ (the limit of their acceptance), but extending in rapidity to $|y| \simeq 3$. This illustrates the di-jet coplanar structure of high p_{T_t} triggered events. One can also see a smaller same side correlation extending out to $|y| \simeq 2$.

The CCOR experiment, which was proposed in May 1973 [CCOR 1973] and approved in March 1974, was installed in the ISR as R108 (8th experiment at Intersection 1) at the end of 1976 along with a low β insertion for higher luminosity. It was debugged, tuned-up and started taking data in July 1977. This experiment [Angelis 1979a] with its thin-coil superconducting solenoid and cylindrical drift chambers was the first at the CERN-ISR to provide charged particle measurement with full and uniform acceptance over the entire azimuth, with pseudorapidity cov-

erage $-0.7 \leq \eta \leq 0.7$, so that the jet structure of high p_T scattering could be easily seen and measured. However, from August to October the liquid He refrigerator was broken, so the solenoid was turned off and only π^0 measurements in the EMcalorimeter could continue [Angelis 1978] (Section 5). The measurements of charged-particles associated to a π^0 trigger came a few months later (Fig. 26) [Angelis 1979a].

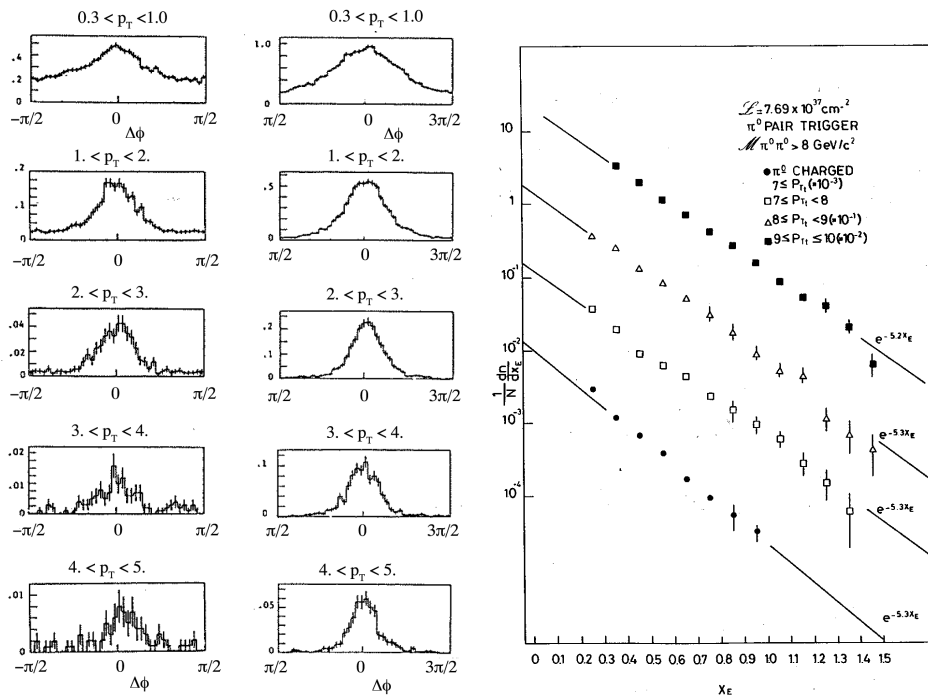


Fig. 26. a,b) Azimuthal distributions of charged particles of transverse momentum p_T , with respect to a trigger π^0 with $p_{Tt} \geq 7$ GeV/c, for 5 intervals of p_T [Angelis 1979a]: a) (left-most panel) for $\Delta\phi = \pm\pi/2$ rad about the trigger particle, and b) (middle panel) for $\Delta\phi = \pm\pi/2$ about π radians (i.e. directly opposite in azimuth) to the trigger. The trigger particle is restricted to $|\eta| < 0.4$, while the associated charged particles are in the range $|\eta| \leq 0.7$. c) (right panel) x_E distributions corresponding to the data of the center panel.

In Fig. 26a,b, the azimuthal distributions of associated charged particles relative to a π^0 trigger with transverse momentum $p_{Tt} > 7$ GeV/c are shown for five intervals of associated particle transverse momentum p_T . In all cases, strong correlation peaks on flat backgrounds are clearly visible, indicating the di-jet structure which is contained in an interval $\Delta\phi = \pm 60^\circ$ about a direction towards and opposite the to trigger for all values of associated p_T (> 0.3 GeV/c) shown. The width of the peaks about the trigger direction (Fig. 26a), or opposite to the trigger (Fig. 26b) indicates out-of-plane activity from the individual fragments of jets. If the width of the away distributions (Fig. 26b) corresponding to the out of plane activity were due entirely to jet fragmentation, then $\langle |\sin(\Delta\phi)| \rangle = \langle |j_{T\phi}|/p_T \rangle$ would decrease in direct proportion to $1/p_T$, since $j_{T\phi}$, the component of the jet fragmentation transverse momentum, \vec{j}_T , in the azimuthal plane, should be independent of p_T . These data were also further analyzed to measure \vec{j}_T as well as \vec{k}_T , the transverse momentum of a parton in a nucleon, as originally shown by the CCHK collaboration [Della Negra 1977], and elaborated by Feynman, Field and Fox (FFF) [Feynman 1977].

The x_E distributions [Angelis 1979a], [Jacob 1979] from the data of Fig. 26b are shown in Fig. 26c. The x_E scaling is evident for all values of p_{T_t} , with the expected fragmentation behavior, $e^{-6z} \sim e^{-6x_E(z_{\text{trig}})}$. This figure also showed that there were no di-jets, each of a single particle, as claimed by another ISR experiment of that period [Kourkouvelis 1979b], and by Jacob and Landshoff [Jacob 1976], since there is no peak at $x_E = 1$. There is a small anecdote concerning this measurement and Maurice Jacob's talk at the EPS1979 HEP Conference [Jacob 1979]. Maurice was originally only going to show a plot from the ABCS experiment [Kourkouvelis 1979b] which appeared to show "a systematic wiggle departure from an exponential...The wiggle could bear witness to a specific process where the two jets would each only consist of one high $p_T \pi^0$ " as he had predicted [Jacob 1976]. I insisted that Maurice also show Fig. 26c, a plot that I had made with three higher p_T points than the CCOR plot in Ref. [Angelis 1979a], "which challenged the one high $p_T \pi^0$ only jet idea" after I nearly broke the telephone in the ISR counting room when I heard that Maurice was only going to show the plot with the "wiggle" [Kourkouvelis 1979b].

Even though this period ended with the strong belief [Darriulat 1980] that jet fragmentation functions from $\nu+p$ and e^+e^- reactions are the same as $p+p$ x_E distributions, with the same dependence of the exponential slope b on p_{T_t} or $\sqrt{s}/2$ for e^+e^- (Fig. 22b), it turned out that nature had the last laugh. This belief was one of the very few results from the "high p_T discovery period" that did not stand the test of time. It was discovered at RHIC [Adler 2006], a quarter of a century later, that the shape of the x_E distribution triggered by the fragment of a jet, such as a π^0 had nothing to do with fragmentation functions but instead measured the ratio of the away jet to the trigger jet ($\hat{x}_h \equiv \hat{p}_{T_a}/\hat{p}_{T_t}$) and depended only on the power n of the invariant single particle high p_T cross section:

$$\left. \frac{d\mathcal{P}}{dx_E} \right|_{p_{T_t}} = N(n-1) \frac{1}{\hat{x}_h} \frac{1}{(1 + \frac{x_E}{\hat{x}_h})^n} \quad (30)$$

8.3 Measurement of the jet fragmentation transverse momentum, j_T , and k_T , the transverse momentum of a parton in a nucleon

Following the idea of Levin and Ryskin [Levin 1975] and CCHK [Della Negra 1977], Feynman, Field and Fox [Feynman 1977] established the formalism for \vec{k}_T , the transverse momentum of a parton in a nucleon. In this formulation (Fig. 27), the net

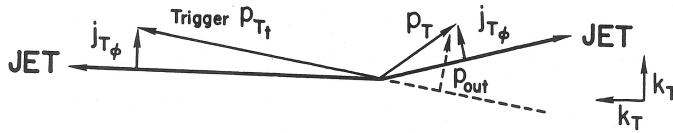


Fig. 27. Azimuthal projection of di-jet with trigger particle p_{T_t} and associated away-side particle p_{T_a} , and the azimuthal components $j_{T\phi}$ of the fragmentation transverse momentum. The initial state \vec{k}_T of a parton in each nucleon is shown schematically: one vertical which gives an azimuthal decorrelation of the jets and one horizontal which changes the transverse momentum of the trigger jet.

transverse momentum of an outgoing parton pair, where the two \vec{k}_T add randomly, is $\sqrt{2}k_T$, which is composed of two orthogonal components, $\sqrt{2}k_{T_\phi} = k_T$, out of the scattering plane, which makes the jets acoplanar, i.e. not back-to-back in azimuth, and $\sqrt{2}k_{T_x} = k_T$, along the axis of the trigger jet, which makes the jets unequal in energy.

FFF [Feynman 1977] gave the approximate formula to derive k_T from the measurement of p_{out} as a function of x_E :

$$\langle |p_{\text{out}}| \rangle^2 = x_E^2 [2\langle |k_{T_\phi}| \rangle^2 + \langle |j_{T_\phi}| \rangle^2] + \langle |j_{T_\phi}| \rangle^2 \quad (31)$$

This formula assumed that $\langle z_{\text{trig}} \rangle = 1$ and that the jet energies are equal.

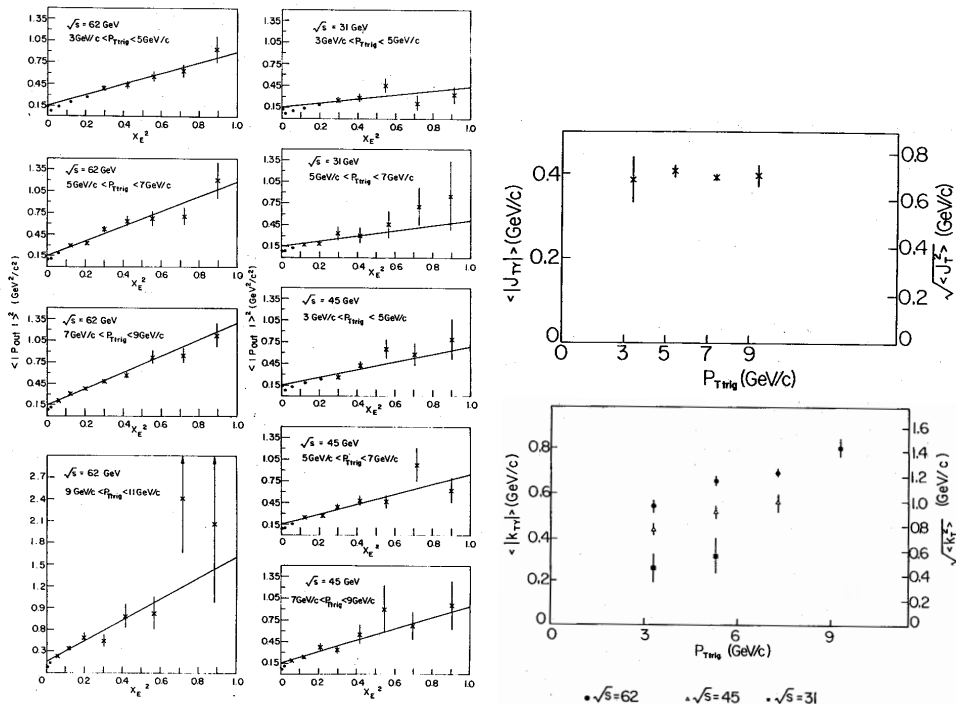


Fig. 28. [Angelis 1980b] a)(left) CCOR $\langle |p_{\text{out}}| \rangle^2$ versus x_E^2 for nine different data samples. The crosses are those points used in the fit to Eq. 31. The straight lines shown are obtained keeping the intercept the same for all nine data samples. b)(right): (top) Fitted values of $\langle |j_{T_\phi}| \rangle$ and $\sqrt{\langle j_T^2 \rangle}$ as a function of p_{T_t} . These values were all equal as a function of \sqrt{s} and constrained to be equal in the fit shown; (bottom) $\langle |k_{T_\phi}| \rangle$ and $\sqrt{\langle k_T^2 \rangle}$ as a function of p_{T_t} for the 3 values of \sqrt{s} indicated.

CCOR [Angelis 1980b] used a fit to this formula (Fig. 28a) to derive $\langle |k_{T_\phi}| \rangle$ and $\langle |j_{T_\phi}| \rangle$ as a function of p_{T_t} and \sqrt{s} (Fig. 28b) from the data of Fig. 26b. This important result showed that $\langle |j_{T_\phi}| \rangle$ is constant, independent of p_{T_t} and \sqrt{s} , as expected for fragmentation, but that $\langle |k_{T_\phi}| \rangle$ varies with both p_{T_t} and \sqrt{s} , suggestive of a radiative, rather than an intrinsic origin for k_T . Large values of $\sqrt{\langle k_T^2 \rangle} \approx 1$ GeV/c were also reported in other CERN-ISR measurements [Clark 1979], [Kourkoumelis 1979c] but it took the e^+e^- people several more years to get j_T correct [Althoff 1984] because they hadn't understood the "seagull effect" [Satz 1976]: with increased momentum of fragments in a jet, their momentum transverse to the jet axis also increases until it reaches its true j_T .

9 Multiparticle correlations—the search for jets 1977–1980

The jet searches like many other new measurements, but perhaps the worst in this regard, started off with a major incorrect claim of the observation of the jets of hard

scattering at Fermilab. Several fixed target experiments searched for jets using the energy detected in calorimeters with limited aperture ($\Delta\phi = \pm 45^\circ$, $\Delta y \approx \pm 0.35$ to 0.55) at mid-rapidity in the p+p c.m. system. The first claim for discovering the jets from the “quark-quark scattering model” was by Fermilab E260 [Bromberg 1978] who found that for $\sqrt{s} = 19.4$ GeV the cross section for the jet, which was defined by summing all the energy in their calorimeter, was “similar in shape to the single particle cross section but two orders of magnitude larger.”

As calorimeters in experiments got larger, the “jet” to single particle ratio kept getting larger until the jet fiasco ended dramatically when the NA5 fixed target experiment at CERN, with a hadron calorimeter which covered the full azimuth with a c.m. polar angular interval $54^\circ < \theta^* < 135^\circ$ ($\Delta y \approx \pm 0.9$) in the p+p c.m. system at $\sqrt{s} = 23.8$ GeV, presented their results [Pretzl 1980]. The coup de grace was their conclusion: “The events selected by the full calorimeter trigger show no dominant jet structure. They appear to originate from processes other than two constituent scattering.” The actual publication of the NA5 result [De Marzo 1982] was perhaps even clearer: “The large transverse energy observed in the calorimeter is the result of a large number of particles with a rather small transverse momentum”.

The problem with the mistaken claim of ‘jets’ was that the difference between single particle and multiparticle measurements was not understood. The principal multiparticle variables are the charge multiplicity distribution $dN_{ch}/d\eta$ and the transverse energy (E_T) distribution [Landshoff and Polkinghorne 1978] :

$$E_T \equiv \sum_i E_i \sin \theta_i \quad , \quad (32)$$

where the sum is over all particles emitted on an event into a fixed but large solid angle. The NA5 result [De Marzo 1982] was the first E_T measurement in the form that is still in use at present [Tannenbaum 1989][Adler 2014].

The difference between single and multi-particle distributions is shown in Fig. 29. Single particle p_T distributions (left) follow the e^{-6p_T} [Cocconi 1961] soft physics particle spectrum until $p_T \approx 1 - 2$ GeV/c where the hard-scattering power law begins to dominate, roughly 2–3 orders of magnitude down in cross section. On the other

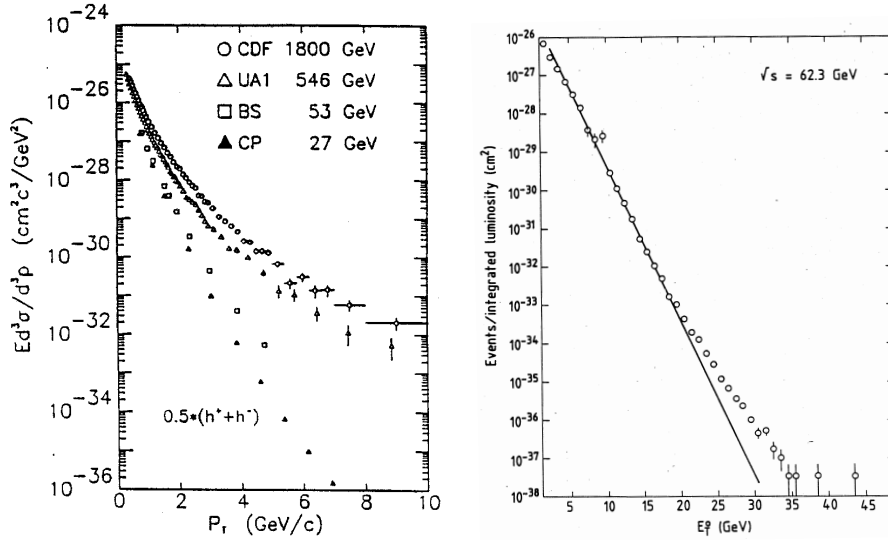


Fig. 29. a) (left) $E d^3\sigma/d^3p$ for single hadrons at mid-rapidity as a function of \sqrt{s} in p+p and $\bar{p}+p$ collisions [Abe 1988]. b) (right) E_T^0 spectrum at $\sqrt{s} = 62$ GeV [Angelis 1983].

hand, the spectrum of the neutral transverse energy E_T^0 at $\sqrt{s} = 62.4$ GeV (right) falls exponentially for ≥ 6 orders of magnitude until the hard scattering component of the E_T^0 distribution becomes evident by the break from the exponential spectrum. In the exponential region there was a uniform azimuthal distribution of E_T^0 , with a dominant 2 jet structure for $E_T^0 > 24$ GeV [Angelis 1983].

A much clearer separation between “soft” and “hard” physics in such spectra was determined at the ISR by the AFS collaboration [Akesson 1983] with a full azimuth EM and hadron calorimeter covering the rapidity range $|y| < 0.9$. A study of the event shape as a function of E_T , was performed using a principal axis analysis. A quantity, “circularity”, was defined which would be 1 for a totally uniform azimuthal distribution of the components of E_T and zero if all the E_T were in two narrow jets back to back in azimuth. The distributions (Fig.30) show no evidence of jets for $E_T < 25$ GeV at any c.m. energy. However for $E_T > 25$ GeV, there is an increase in low circularity events, leading up to a dominance of low-circularity events from a two-jet structure for $E_T \geq 31$ GeV at $\sqrt{s} = 63$ GeV.

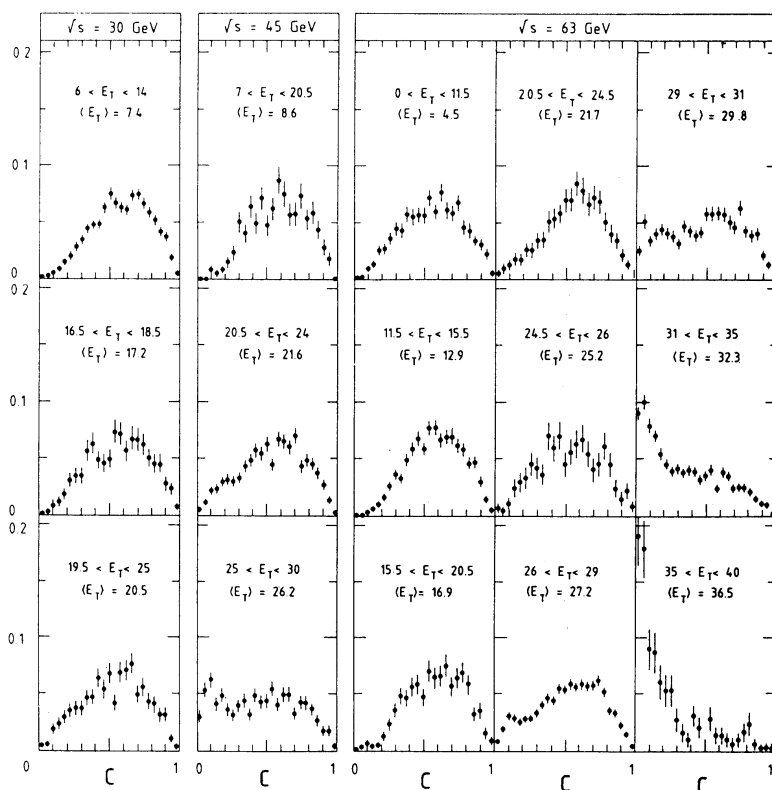


Fig. 30. Circularity distributions for bins in E_T and \sqrt{s} . The error bars are statistical only [Akesson 1983].

These beautiful measurements from the year 1983 made it clear that the jets of hard scattering could indeed be observed using E_T distributions; but that hard scattering effects have negligible influence on the shape of E_T spectra in proton-(anti)proton collisions for the first 4, or even 6, orders of magnitude of cross section, depending on the c.m. energy. However the first convincing evidence of jets and the validity of QCD as the mechanism for hard-scattering came at the ICHEP1982 conference in Paris.

10 The final proof of jets and QCD by measurements 1980–1982

The rejection of the Fermilab E260 [Bromberg 1978] jet claim by the observation of no jets in a better measurement at CERN [Pretzl 1980], presented at the ICHEP1980, led to confusion in the High Energy Physics community in the U. S. during the period from the ICHEP1980 to the ICHEP1982. There was no clear understanding of why the jets of QCD were not observed in the full azimuth calorimeter which led to doubts by many of the utility and validity of QCD tests in hadron-hadron collisions. To get an idea of the thinking during this period, I had to give a seminar at my laboratory, BNL, in March 1982 with the title: “Why I believe in jets in spite of calorimeter experiments. For QCD tests try to minimize the effect of jets.”

In March 1980, I had moved from the Rockefeller University to BNL to help save ISABELLE, the $\sqrt{s} = 800$ GeV superconducting p+p collider under construction. My assignment was to help sort out the problems they were having with the superconducting magnets that quenched at a much lower magnetic field than expected. I described my work in this period in a previous EPJH article [Tannenbaum 2016], so I’ll skip to March 1982 when I transferred to the BNL Physics Department and resumed work on the CCOR experiment. One of the problems with the CCOR full azimuth superconducting solenoid detector was that it did not have any specific electron identification device like the Cherenkov counters in CCRS, so that in trying to measure e^+e^- pairs we had to trigger on clusters with energy > 2.5 GeV in each arm of our EMcalorimeters (as described in Section 4.3.1). This left us with $\approx 750,000$ π^0 pairs which we decided to analyze in the same way we would analyze e^+e^- pairs in the detector, namely the invariant mass $M_{\pi\pi}$ of the pair, its net P_t and rapidity Y and $\cos\theta^*$ in the c.m. system of the pair.

There were enough events so that we could select π^0 pairs with net $P_t < 1$ GeV/c (or $P_t < 2$ GeV/c for $M_{\pi\pi} > 11$ GeV/c²) and $|Y| < 0.35$. Then we moved to the c.m. system of the pair, in which the two π^0 are back to back at an angle $\cos\theta^*$, by the simple rapidity shift $y^* = y - Y$ (Sec. 14.1) for each π^0 . We knew from FFF [Feynman 1977] that the trigger π^0 had almost the same p_{Tt} as the parton \hat{p}_{Tt} ($\langle z_{\text{trig}} \rangle \approx 1.0$). Thanks to the full azimuth charged particle tracking we were able to measure $\langle z_{\text{trig}} \rangle$ from our own data by summing over all charged particles within an azimuthal angle $\pm 60^\circ$ of the trigger in the rapidity range $|y| < 0.7$, multiplying by 1.5 to account for the missing neutrals [Angelis 1982a]. We noted that the large measured values of $\langle z_{\text{trig}} \rangle > 0.9$ for $M_{\pi\pi} > 8$ GeV/c² and measured value of $\langle |j_{Ty}| \rangle = 0.44$ GeV/c justify the assumption that the axis of the di-pion system in the pair c.m. system follows closely that of the original parton-parton scattering with $\sqrt{\hat{s}} \approx M_{\pi\pi}$. These measured $\cos\theta^*$ distributions are shown in Fig. 31 and should be able to be compared directly to the $\cos\theta^*$ distributions of the elementary QCD subprocesses in terms of $d\sigma/d\cos\theta^*$ at fixed \hat{s} , Eq. 33, easily derived from Eq. 16:

$$\left. \frac{d\sigma}{d\cos\theta^*} \right|_{\hat{s}} = \frac{\pi\alpha_s^2(Q^2)}{2\hat{s}} \Sigma^{ab}(\cos\theta^*) \quad . \quad (33)$$

The effect of $\langle |j_{Ty}| \rangle$ is negligible, well within the bins in $\cos\theta^*$.

In fact the measured distributions for the various $M_{\pi\pi} \approx \hat{s}$ all have the same shape which we compared directly to the QCD angular distributions from Eq. 33 for the subprocesses, gg , qg , qq' and qq elastic scattering [Tannenbaum 1982] also shown in Fig. 31. The measured distributions are steeper than all the QCD constituent scattering subprocess distributions with constant $\alpha_s(Q^2)$. However once the increase of the QCD coupling constant $\alpha_s(Q^2)$, with decreasing $Q^2 = -\hat{t}$ as $\cos\theta^*$ increases, is taken into account as shown as the dashed curve for qq with $\alpha_s(Q^2)$, the measurement and QCD predictions agree very well. We had this data for two years until Dave Levinthal and Steve Pordes realized that we had to include the QCD $\alpha_s(Q^2)$ evolution.

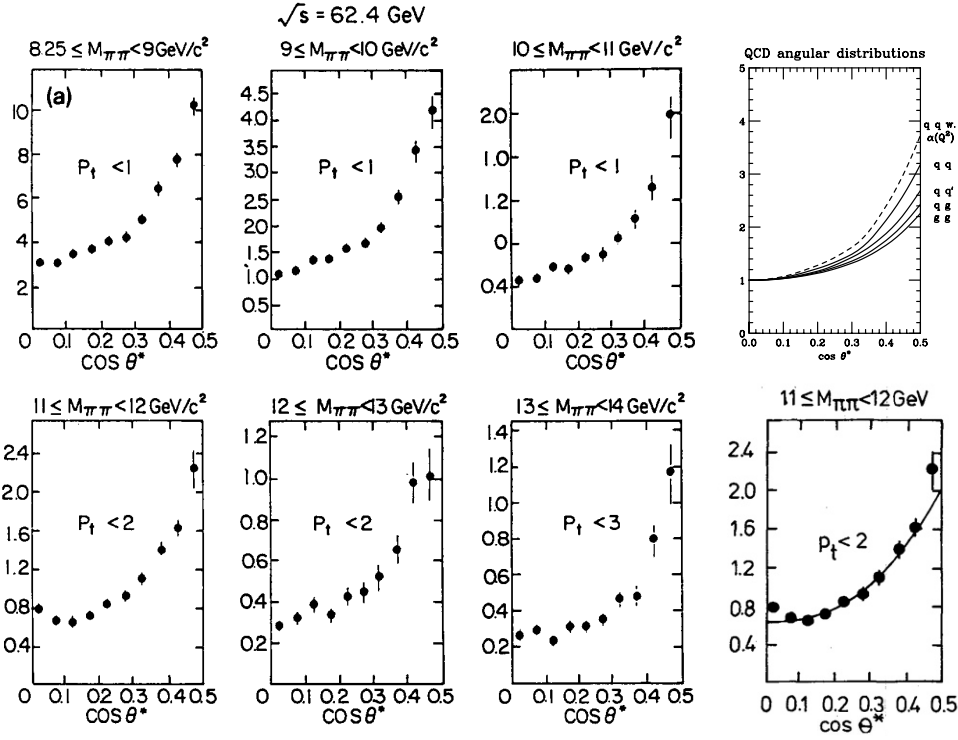


Fig. 31. a) (left 6 panels) CCOR measurement [Angelis 1982a] of polar angular distributions of π^0 pairs, with $M_{\pi\pi}$ and net P_t indicated, in p+p collisions at $\sqrt{s} = 62.4$ GeV. b) (right 2 panels) (top) QCD elementary subprocess angular distributions at fixed \hat{s} , normalized at 90° , $\cos\theta^* = 0$, which I showed as an overlay on the $9 \leq M_{\pi\pi} \leq 10 \text{ GeV}/c^2$ plot [Tannenbaum 1982]. (bottom) Günter Wolf's calculation of $\Sigma^{ab}(\cos\theta^*)$ for qq overlaid on the CCOR $11 \leq M_{\pi\pi} \leq 10 \text{ GeV}/c^2$ measurement [Wolf 1982].

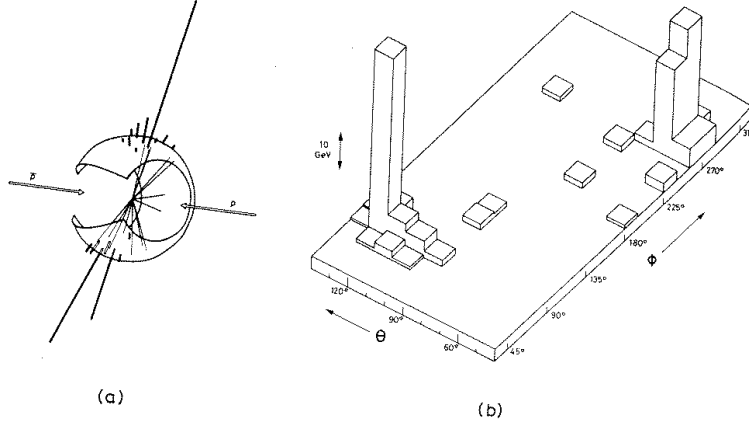


Fig. 32. Configuration of the UA2 event [Repellin 1982] with the largest value of ΣE_T , 127 GeV ($M = 140$ GeV): (a) charged tracks pointing to the inner face of the central calorimeter are shown together with cell energies (indicated by heavy lines with lengths proportional to cell energies). (b) the cell energy distribution as a function of polar angle θ and azimuth ϕ .

I was lucky enough to present this result [Tannenbaum 1982] at the ICHEP82 meeting in Paris after the session where UA2 [Repellin 1982] revealed their di-jet LEGO plot measured in a highly segmented total absorption calorimeter covering the azimuthal range $\Delta\phi = 300^\circ$ with $|y| < 1.0$. This now famous plot (Fig. 32) clearly indicated di-jets in collisions at $\sqrt{s} = 540$ GeV, one of the first results at the CERN $S\bar{p}pS$ $\bar{p}+p$ collider, which immediately convinced everybody that jets existed.

These two measurements and Günter Wolf's outstanding rapporteur talk, in which he also verified the $\cos\theta^*$ calculation with his own overlay plot (lowest right plot in Fig. 31), convinced all observers, and as the news spread, everybody else, that QCD and jets were the cornerstone of the Standard Model. Quotes from Günter's proceedings [Wolf 1982] are worth repeating: "Amongst the most exciting results are the direct measurement of the parton-parton scattering angular distribution and the observation of very energetic jets at the SPS collider." "QCD provides a consistent description for the underlying constituent scattering processes." Since that time QCD and jets have become the standard tools of high energy particle physics.

10.1 A few more recent collider results on QCD and jets

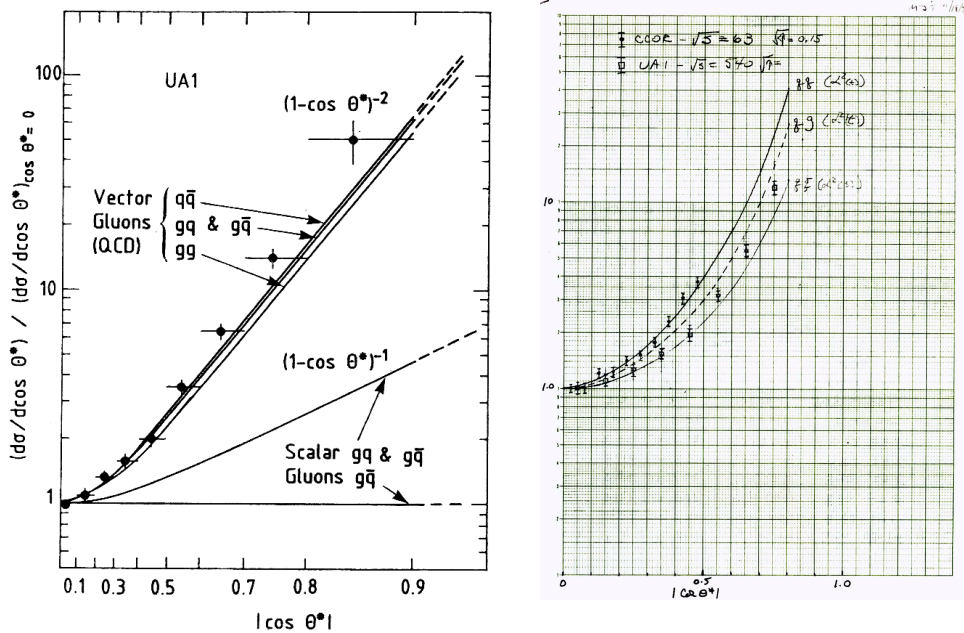


Fig. 33. a) (left) UA1 $\cos\theta^*$ distribution for dijets in $\bar{p}+p$ collisions at $\sqrt{s} = 540$ GeV with QCD $\Sigma^{ab}(\cos\theta^*)$ calculations [Arnison 1984]. b) (right) My comparison of UA1 $\bar{p}+p$ and CCOR $p+p$ $\cos\theta^*$ distributions and QCD subprocesses, November 1983.

When the CERN $\bar{p}+p$ collider experiments started to publish di-jet angular distribution measurements compared to QCD constituent scattering subprocess distributions, e.g. UA1 [Arnison 1984] (Fig. 33a), I made a plot (Fig. 33b) of their data for $\sqrt{s} = 540$ GeV and the CCOR measurement at $\sqrt{s} = 62.4$ GeV with my calculations of the QCD qq , gq and $\bar{q}q$ subprocess angular distributions. The $p+p$ data aligned best with the gq calculation while the $\bar{p}+p$ data aligned beautifully with the $\bar{q}q$ calculation for $|\cos\theta^*| \leq 0.5$ which I thought was pretty neat in 1983 but I never published it.

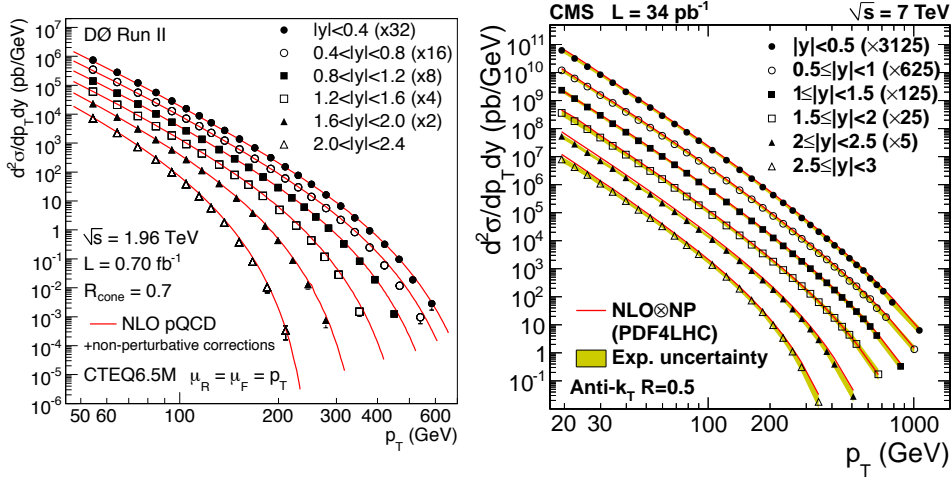


Fig. 34. a) (left) D0 [Abazov 2008] inclusive jet cross sections at $\sqrt{s} = 1.96$ TeV as a function of jet p_T in bins of jet rapidity y with NLO pQCD predictions. b) CMS [Chatrchyan 2011a] measurements at $\sqrt{s} = 7$ TeV (data points) with NLO theoretical predictions.

The relatively recent jet cross section measurements (Fig. 34) as a function of p_T and rapidity at the Fermilab Tevatron in $\bar{p} + p$ collisions at $\sqrt{s} = 1.96$ TeV and the CERN LHC $p + p$ collider at $\sqrt{s} = 7$ TeV agree incredibly well with Next to Leading Order (NLO) QCD. Note that at mid-rapidity the D0 data follow the typical hard-scattering power law but drop sharply at large p_T and y , due to conservation of energy. The drop is much weaker at large p_T and y for the CMS data because of the 3.5 times larger c.m. energy.

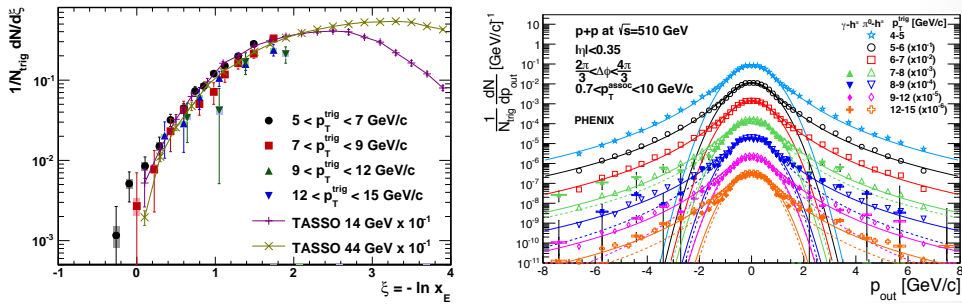


Fig. 35. a) (left) Direct- γ - h correlations in $\sqrt{s} = 200$ GeV $p+p$ collisions as a function of $\xi = -\ln x_E$ [Adare 2010] b) (right) p_{out} distributions of charged hadrons in $\pi^0 + h$ and $\gamma + h$ correlations with $0.7 < p_{T_a} < 10$ GeV/c for 7 values of p_{T_t} in $\sqrt{s} = 510$ GeV $p+p$ collisions [Adare 2017].

Recent two-particle correlation measurements at RHIC (Fig. 35) nicely show that the x_E distribution of direct- γ - h correlations plotted as a function of $\xi = -\ln x_E$ really does measure the fragmentation function as measured in e^+e^- collisions at $\sqrt{s} = 14$ and 44 GeV [Braunschweig 1990] and that the p_{out} distribution has two components, a Gaussian likely to be from the intrinsic k_T of partons in the nucleon, and a power-law tail from NLO QCD gluon emission as suggested in [Adare 2017].

11 Hadron Collider discoveries, not exactly QCD 1983–2012

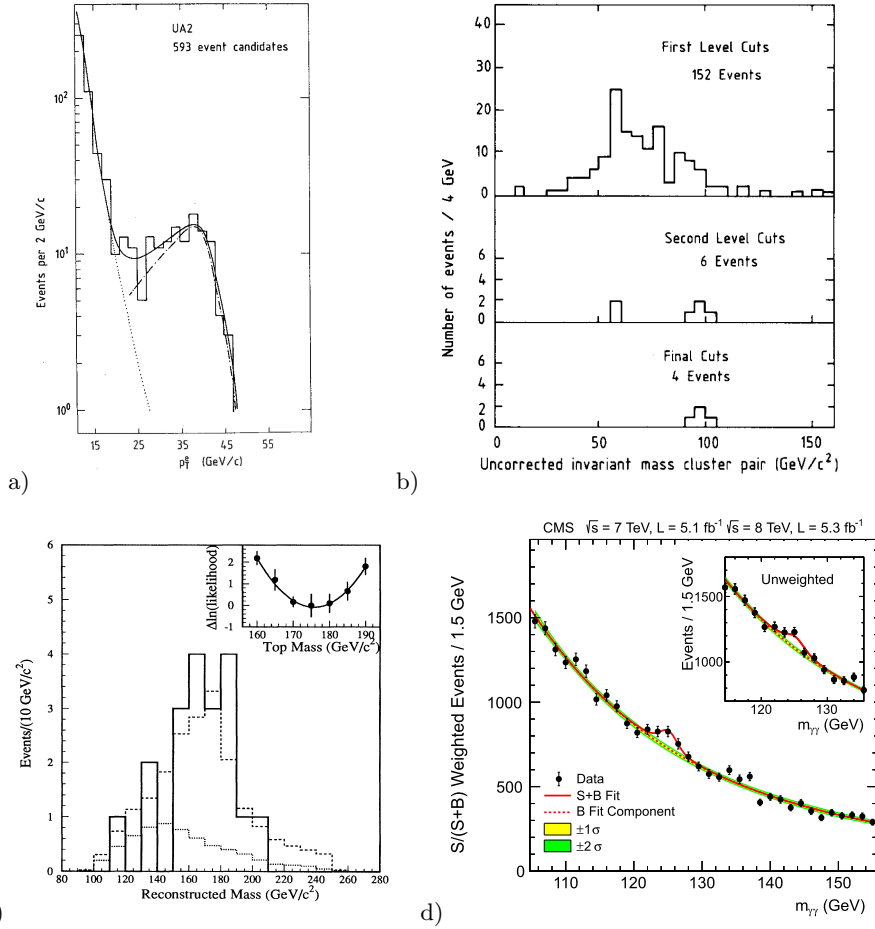


Fig. 36. a) UA2 p_T^e spectrum [Appel 1986]. b) UA1 $Z^0 \rightarrow e^+e^-$ discovery [Arnison 1983b]. c) CDF b -tagged $W + \geq 4$ jet top quark mass plot [Abe 1995]. d) CMS $m_{\gamma\gamma}$ plot with 125 GeV Higgs $\rightarrow \gamma\gamma$ [Chatrchyan 2012].

To keep the record straight, I think that it is important to note several major discoveries at hadron colliders that are not exactly QCD but nevertheless are key elements of the Standard Model. The W and Z bosons of the Weak interactions were discovered at the CERN $\bar{p}+p$ collider in 1983 by experiments UA1 (W) [Arnison 1983a], (Z) [Arnison 1983b]; and UA2 (W) [Banner 1983] (Z) [Bagnaia 1983]. Figure 36a shows a UA2 measurement of $W^\pm \rightarrow e^\pm + X$ with a nice Zichichi signature and Fig. 36b the actual UA1 discovery plot of the $Z^0 \rightarrow e^+ + e^-$.⁵ The top quark was discovered at the Fermilab Tevatron $\bar{p}p$ collider by D0 [Abachi 1995] and CDF [Abe 1995] (Fig. 36c) and the Higgs Boson was discovered at the CERN-LHC by ATLAS [Aad 2012] and CMS [Chatrchyan 2012] (Fig. 36d).

⁵ The Z^0 plot reminds me of Fig. 6b; but for Fig. 36b it was Carlo Rubbia who had the last laugh, a well deserved Nobel Prize.

12 QCD at Relativistic Heavy Ion Colliders 2000–2017

12.1 From Bjorken Scaling to QCD to the QGP

Bjorken scaling not only led to the parton model and QCD as we have already discussed, but also led to the conclusion [Collins and Perry 1975] that “superdense matter (found in neutron-star cores, exploding black holes, and the early big-bang universe) consists of quarks rather than of hadrons”, because the hadrons overlap and their individuality is confused. This is different from earlier models which take hadrons as the basic entities [Hagedorn 1994]. Collins and Perry [Collins and Perry 1975] called this state “quark soup” but used the equation of state of a gas of free massless quarks from which the interacting gluons acquire an effective mass which provides long-range screening. They also pointed out that for the theory of strong interactions (QCD), “high density matter is the second situation where one expects to be able to make reliable calculations—the first is Bjorken scaling”. In the Bjorken scaling region, the theory is asymptotically free at large momentum transfers while in high-density nuclear matter long range interactions are screened by many-body effects, so they can be ignored and short distance behavior can be calculated with the asymptotically-free QCD and relativistic many-body theory. Shuryak [Shuryak 1980] codified and elaborated on these ideas and provided the name “QCD (or quark-gluon) plasma” QGP for “this phase of matter”, a plasma being an ionized gas.

It didn’t take long for others to realize that relativistic heavy ion (RHI) collisions could provide the means of obtaining superdense nuclear matter in the laboratory [Lederman and Weneser 1975] [Bjorken 1983]. The kinetic energy of the incident projectiles would be dissipated in the large volume of nuclear matter involved in the reaction. The system is expected to come to equilibrium, thus heating and compressing the nuclear matter so that it undergoes a phase transition from a state of nucleons containing bound quarks and gluons to a state of deconfined quarks and gluons, the Quark Gluon Plasma (QGP), in chemical and thermal equilibrium, covering the entire volume of the colliding nuclei or a volume that corresponds to many units of the characteristic length scale.

In the terminology of high energy physics, this is called a “soft” (low Q^2) process, related to the QCD confinement scale

$$\Lambda_{\text{QCD}}^{-1} \simeq (0.2 \text{ GeV})^{-1} \simeq 1 \text{ fm} \quad . \quad (34)$$

With increasing temperature, T , in analogy to increasing Q^2 , the strong coupling constant $\alpha_s(T)$ becomes smaller, reducing the binding energy, and the string tension, $\sigma(T)$, becomes smaller, increasing the confining radius, effectively screening the potential[Satz 2000]:

$$V(r) = -\frac{4}{3} \frac{\alpha_s}{r} + \sigma r \rightarrow -\frac{4}{3} \frac{\alpha_s}{r} e^{-\mu_D r} + \sigma \frac{(1 - e^{-\mu_D r})}{\mu_D} \quad (35)$$

where $\mu_D = \mu_D(T) = 1/r_D$ is the Debye screening mass [Satz 2000]. For $r < 1/\mu_D$ a quark feels the full color charge, but for $r > 1/\mu_D$, the quark is free of the potential and the string tension, effectively deconfined. The properties of the QGP can not be calculated in QCD perturbation theory but only in Lattice QCD Calculations [Soltz 2015].

12.2 From ISABELLE to CBA to RHIC 1983

Following the discovery of the W and Z bosons at CERN, the $\sqrt{s} = 800 \text{ GeV}$ p+p collider at BNL, ISABELLE, which had been renamed Colliding Beam Accelerator

(CBA), was cancelled by HEPAP (the U.S. High Energy Physics Advisory Panel) on July 11, 1983, but was miraculously immediately resuscitated by NSAC (the U.S. Nuclear Science Advisory Committee) to eventually become the $\sqrt{s_{NN}} = 200$ GeV A+A Relativistic Heavy Ion Collider (RHIC) [Crease 2008] whose purpose was to discover the properties of nuclear matter under extreme conditions with possible discovery of new states of matter, e.g. the QGP. In Ref. [Tannenbaum 2016], I discussed several lucky breaks that I had in being able to attend the ICHEP82 and then to present the lecture with the results shown in Fig. 31. Well, it turned out that I had another important lucky break in August 1983 just after RHIC became a gleam in the eye of NSAC. The chair of the BNL physics department, Arthur Schwartzschild, a Nuclear Physicist, offered me five BNL Nuclear Physicists to participate in the set-up and data taking of an $\alpha + \alpha$ run which had been scheduled for 16–30 August 1983 at the CERN ISR, as well as to help analyze the data. The purpose was to get collider experience for the RHIC proposal and to help understand an “exciting result” from the previous $\alpha + \alpha$ run at the ISR.

12.2.1 “Exciting result”? How I became a nuclear physicist!

It started in 1979, when Martin Faessler [Faessler 1979] and collaborators proposed to measure $p + \alpha$ and $\alpha + \alpha$ collisions in the CERN-ISR using the SFM. The proposal was approved which led to runs with $\alpha + \alpha$ at $\sqrt{s_{NN}} = 31$ GeV and $p + \alpha$ at $\sqrt{s_{NN}} = 44$ GeV in 1980, with a subsequent run in 1983 with $\alpha + \alpha$, $p + \alpha$, $d + d$ and p+p interactions all at the same $\sqrt{s_{NN}} = 31$ GeV. The high energy physicists at the ISR had the option of turning off their detectors and resting for a few weeks or continuing to operate their detectors for the nuclear collisions, with the possibility of exciting new physics results. They all opted to continue. Exactly same option and, predictably, exactly the same outcome occurred at the LHC 30 years later.

Once again, the publications from measurements in a new field started out with an incorrect result from the 1980 run, this time where I was a co-author [Angelis 1982b]. Incredibly, it eventually turned out that this result was helpful. The 1980 $\alpha + \alpha$ run was at the full ISR energy, $\sqrt{s} = 62.4$ GeV for p+p collisions which was only $\sqrt{s_{NN}} = 31.2$ GeV for $\alpha + \alpha$ where $Z/A=1/2$. There was no comparison p+p data at $\sqrt{s} = 31.2$ GeV in the 1980 run, only $\sqrt{s} = 62.4$ GeV data. However, there was comparison p+p data at $\sqrt{s} = 31.2$ GeV from the 1979 run which was not used because of uncertainty of a change in the absolute p_T scale for the EM calorimeter by $\approx 5\%$, a huge effect when trying to measure a cross section that drops like $1/p_T^n$ with $n \approx 10$. The $\sqrt{s} = 62.4$ GeV p+p data were used for comparison, but extrapolated to $\sqrt{s} = 31.2$ GeV by a method that I kept saying was wrong whenever I was able to communicate with my collaborators adequately (no internet!!!) because I was still making magnets at BNL ≈ 6000 km away. I told them to use x_T scaling but they ignored my advice.

For high p_T hard-scattering, which is the result of scattering of pointlike partons, the ratio of the cross sections in p+A or B+A collisions to the p+p cross section should be simply equal to the product of the number of nucleons in the projectile and target, a factor A times larger for p+A and $B \times A$ for B+A collisions. However an ‘anomalous nuclear enhancement’ was found in p+A collisions by Jim Cronin and collaborators at Fermilab [Antreasyan, Cronin 1979]. The pion cross section ratio increased as $A^{\alpha(p_T)}$ where $\alpha(p_T)$ peaked at ~ 1.15 for $p_T = 4-5$ GeV/c for $19.4 \leq \sqrt{s_{NN}} \leq 27.4$ GeV. By contrast, the COR measurement in $\alpha + \alpha$ collisions [Angelis 1982b] for $p_T \geq 5$ GeV/c was equivalent to $\alpha(p_T) = 1.3$ a factor of ~ 1.6 larger for the $\alpha\alpha/pp$ cross section ratio than the extrapolation of Cronin’s measurement. To quote a review by [Faessler 1984] of the results from the 1980 $\alpha + \alpha$ run: “If this trend is confirmed, it could eventually signify that something very interesting is going on in nucleus nucleus collisions.”

The interesting results from the $\alpha + \alpha$ collisions spread to the CERN management and through the nuclear physics grapevine to the chairman of the BNL physics department, Arthur Schwartzschild, who offered me the five BNL Nuclear Physicists. My CERN collaborators were happy about this because they also wanted Nuclear Physicists to help them understand the “exciting result”.

Well, of course, we found out that the “exciting result” was wrong because our new result from the 1983 $\alpha + \alpha$ and p+p runs at $\sqrt{s_{NN}} = 31$ GeV [Angelis 1987] was $\alpha(p_T) = 1.14 \pm 0.01$ which now agreed with Cronin’s result. We also had a preliminary result which Sanki Tanaka [Angelis, Tanaka 1984] was able to complete in time to present at the Quark Matter 1983 conference, the last week in September 1983, which had been moved from Helsinki to BNL. This result showed that the ratio of the cross sections for $\alpha\alpha/pp$ as a function of E_T varied by 2 to 6 orders of magnitude, so that the $A^{\alpha(p_T)}$ Cronin formalism was completely inadequate. We soon understood that this was because E_T was a multiparticle distribution [Tannenbaum 1985] which turned out to be very useful in Relativistic Heavy Ion collisions. Based on these ISR $\alpha + \alpha$ results, I joined with Chellis Chasman, Ole Hansen, Andy Sunyar of BNL, Lee Grodzins of MIT ⁶, Shoji Nagamiya of Columbia and others in an experiment (E802) to explore all aspects of relativistic heavy ion collisions at the new heavy ion beam at the BNL-AGS built to prepare for RHIC.

12.3 RHIC and its Experiments: Design and Construction-1991–2000

The initial proposal by BNL to the U.S. Department of Energy to build RHIC was in 1984; the first funds for construction of RHIC were in the U.S. budget for Fiscal Year 1991; construction was completed and the first Au+Au collisions at $\sqrt{s_{NN}} = 130$ GeV were in 2000 and with the standard c.m. energy $\sqrt{s_{NN}} = 200$ GeV in 2001 [Harrison 2003]. The first call for Letters of Intent for experiments was in April 1990 which were evaluated in November 1990 with updated LOI submitted in July 1991. The first Program Advisory Committee (PAC) to evaluate these updated LOI’s approved the STAR proposal to join with a BNL TPC proposal to build a large Time Projection Chamber (TPC) concentrating on hadrons. Three other proposals: di-muon, OASIS and TALES/SPARHC were rejected but told by the Associate Lab Director Mel Schwartz to merge into an experiment (most like TALES/SPARHC, my affiliation) to study electrons and photons emerging from the QGP, which became the PHENIX experiment. Two smaller experiments were also approved [Harrison 2003].

The STAR experiment is similar to a conventional solenoid collider detector of the late 1980’s except that its solenoid with 2.6m radius and magnetic field $B=0.5$ T is not superconducting. The TPC covers the full azimuth at mid-rapidity, $|\eta| \leq 1.0$. Particle identification is done with dE/dx in the TPC and Time of Flight counters. An EMcalorimeter outside the solenoid has segmentation $\Delta\eta \times \Delta\phi = 0.05 \times 0.05$ with a shower-maximum pre-converter/detector $5 X_o$ deep for improved γ/π^0 separation.

The PHENIX experiment is a two-arm spectrometer with a fine grain EMcalorimeter $\Delta\eta \times \Delta\phi \approx 0.01 \times 0.01$ to separate single- γ and resolve $\pi^0 \rightarrow \gamma + \gamma$ with p_T up to ≈ 20 GeV/c. Each arm has a Ring Imaging Cerenkov counter, time-of-flight (TOF) and drift-chamber tracking for e^\pm , γ and identified hadron measurements at mid-rapidity; with full azimuth muon spectrometers at forward and backward rapidity $1.1 < |y| < 2.2 - 2.4$. Full azimuth Beam Beam Counters at $3.0 \leq |\eta| \leq 3.9$ and Zero Degree hadron Calorimeters that measure forward going neutrons within a 2 mrad ($|\eta| > 6$) cone are used for triggering and luminosity measurement.

⁶ Sunyar and Grodzins along with Maurice Goldhaber had made the famous measurement of the helicity of the neutrino at BNL [Goldhaber 1958].

It was no accident that PHENIX had all the features of CCRS (Section:4.1) plus precision TOF for particle identification: I was one of the principal proponents of TALES/SPARHC. This gave PHENIX the possibility of measuring single e^\pm for $p_T > 0.3$ GeV/c which was crucial for J/Ψ and charm measurements. Measurements of identified hadrons (including charm), although not part of Mel Schwartz's directive, were obviously necessary for understanding the background from their decay. Also, it was always my intention to use single e^\pm to measure charm [Tannenbaum 1996], because there is no combinatoric background. This is a serious problem in A+A collisions where charged multiplicities rise to $\approx A$ times that in p+p for the most central collisions where the two nuclei fully overlap [Adler 2005] (Fig. 37).

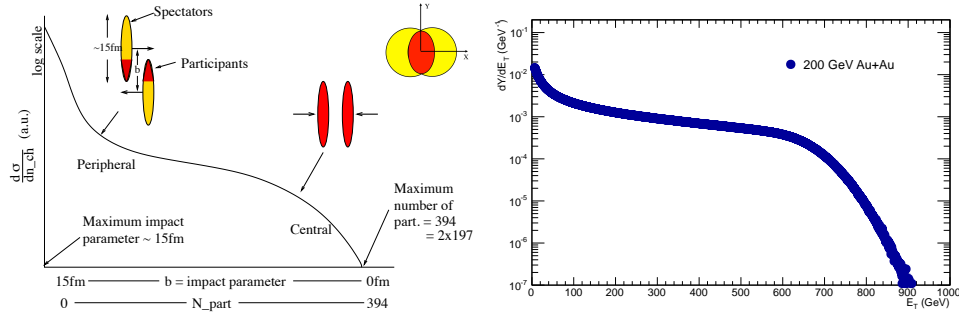


Fig. 37. a) (left) [Tannenbaum 2008] Schematic of collision in the c.m. system of two Lorentz contracted Au+Au nuclei with radius R and impact parameter b . N_{part} is the number of nucleons struck in the collision. The curve with the ordinate labeled $d\sigma/dn_{\text{ch}}$ represents the relative probability of charged particle multiplicity n_{ch} . The upper right corner shows the almond shape overlap of the nuclei in peripheral collisions. It should be rotated so that the X axis is perpendicular to the page. More particles will be emitted along the X axis than the Y axis because of the stronger pressure gradient. This is called elliptical flow. b)(right) E_T distribution in Au+Au at $\sqrt{s_{NN}} = 200$ GeV from PHENIX [Adler 2014]. The E_T is corrected to the region $\Delta\eta = 1.0$, $\Delta\phi = 2\pi$. The charged multiplicity, $dN_{\text{ch}}/d\eta \approx 1.14 \times E_T$.

12.4 How to find the QGP 1986–2000

At the time of the proposals for experiments at RHIC (also for the LHC [Aamodt 2008]) in 1990-91, there were two proposed signatures of the QGP: strangeness enhancement [Koch, Müller and Rafelski 1986] and the “gold-plated” signature for deconfinement in the QGP, J/Ψ suppression [Matsui and Satz 1986]. Matsui and Satz predicted that J/Ψ production in A+A collisions will be suppressed by Debye screening of the quark color charge in the QGP. The J/Ψ is produced when two gluons interact to produce a $c\bar{c}$ pair which then resonates to form the J/Ψ . In the QGP, the $c\bar{c}$ interaction is screened so that the $c\bar{c}$ go their separate ways and eventually pick up other quarks at the periphery to become *open charm*. However, as pointed out a year later [Matsui 1987], enhanced production of c and \bar{c} quarks in A+A collisions, so that many of the “other quarks” picked up are c or \bar{c} , could lead to recombination of $c\bar{c}$ into J/Ψ which might “hinder” J/Ψ suppression as evidence for the QGP. Another problem was that the J/Ψ is suppressed in p+A collisions [Prino 2001]. These issues were worked out in further detail by analysis of J/Ψ measurements at the CERN fixed-target heavy ion program [Braun-Munzinger and Stachel 2000] with the prediction of enhancement of J/Ψ at LHC energies.

12.4.1 A hard-scattering QGP signature based on QCD 1997–1998

A new tool for probing the color response function of the QGP with a firm basis in QCD was developed shortly before RHIC turned on. I found out about this in 1998 at the QCD workshop in Paris [Baier also Tannenbaum 1998], when Rolf Baier asked me whether jets could be measured in Au+Au collisions because he had made studies in pQCD [Baier 1997] of the energy loss, by ‘coherent’ (LPM) gluon bremsstrahlung, of hard-scattered partons “with their color charge fully exposed” traversing a medium, “with a large density of similarly exposed color charges”. This leads to a reduction of the p_T of both the outgoing partons and their fragments, hence a reduction in the number of partons or fragments at a given p_T , which is called jet quenching. The effect is absent in p+A or d+A collisions because no medium is produced (Fig. 38a)

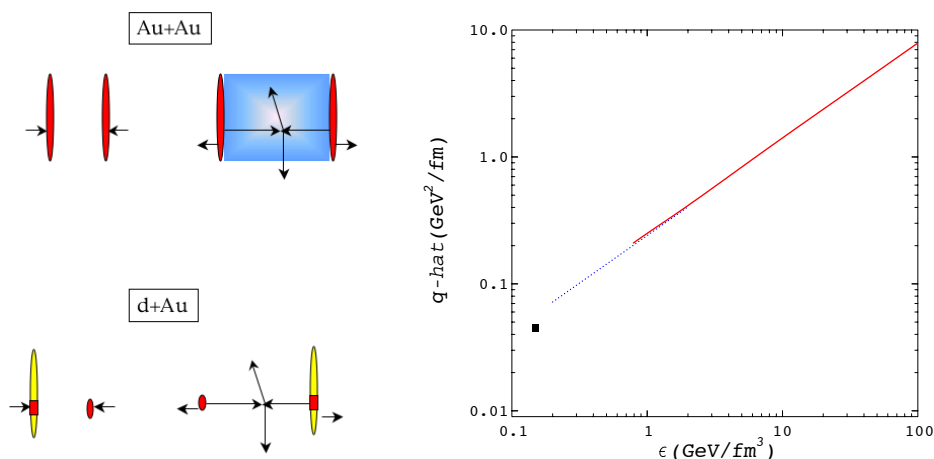


Fig. 38. a) (left) [Tannenbaum 2006] Schematic diagram of hard scattering in Au+Au and d(p)+Au collisions. Parton scattering occurs when the nuclei overlap, and for Au+Au the scattered high p_T partons emerge sideways through the medium formed. For d+Au no medium is formed and the outgoing partons travel in vacuum until they fragment. b) (right) Transport coefficient \hat{q} as a function of energy density ϵ for different media [Baier 2003]: cold nuclear matter (filled square), massless hot pion gas (dotted) and ‘ideal’ QGP (solid curve).

The energy loss of an outgoing parton, $-dE/dx$, per unit length (x) of a medium with total length L due to coherent gluon bremsstrahlung is proportional to the 4-momentum-square, $q^2(L)$, transferred to the medium and takes the form:

$$\frac{-dE}{dx} \simeq \alpha_s \langle q^2(L) \rangle = \alpha_s \hat{q} L \quad . \quad (36)$$

\hat{q} , the transport coefficient of a gluon in the medium, is defined as the mean 4-momentum transfer-square, q^2 , to the medium by a radiated gluon, *per gluon mean free path*, which can be calculated with QCD [Baier 2000]. Figure 38b shows an early calculation of \hat{q} [Baier 2003].

I told Rolf (and put in the proceedings) that because the expected energy in a typical jet cone $R = \sqrt{(\Delta\eta)^2 + (\Delta\phi)^2}$ in central Au+Au collisions at $\sqrt{s_{NN}} = 200$ GeV would be $\pi R^2 \times 1/2\pi \times dE_T/d\eta = R^2/2 \times dE_T/d\eta \sim 300$ GeV for $R = 1$, where the kinematic limit is 100 GeV, jets can not be reconstructed in Au+Au central

collisions at RHIC. This is still correct at present (19 years later) where the solution is to make smaller jet cones, which may (or may not) be a problem.

I also told Rolf the good news that the jet suppression could be measured by single particle inclusive and two-particle correlations at RHIC as we had done at the CERN-ISR and that the PHENIX detector had actually been designed to make such measurements.

12.5 Measurements relevant to QCD in A+A collisions at RHIC and LHC

Measuring and understanding the properties of nuclear matter under extreme conditions and possibly the QGP requires knowledge of Statistical Physics, Thermo- and Hydro- dynamics without much QCD input. However, there were several important discoveries and measurements which did involve QCD.

12.5.1 Baryon chemical potential measured without particle identification

In an equilibrated thermal medium, particles should follow a Boltzmann distribution in the local rest frame [Cooper and Frye 1974]

$$\frac{d^2\sigma}{dp_L p_T dp_T} = \frac{d^2\sigma}{dp_L m_T dm_T} \propto \frac{1}{e^{(E-\mu)/T} \pm 1} \sim e^{-(E-\mu)/T}, \quad (37)$$

where $m_T = \sqrt{p_T^2 + m^2}$ and μ is a chemical potential. In fact, the ratios of particle abundances (which are dominated by low p_T particles) for central Au+Au collisions at RHIC, even for strange and multi-strange particles, are well described [Adams 2005] by fits to a thermal distribution,

$$\frac{d^2\sigma}{dp_L p_T dp_T} \sim e^{-(E-\mu)/T} \rightarrow \frac{\bar{p}}{p} = \frac{e^{-(E+\mu_B)/T}}{e^{-(E-\mu_B)/T}} = e^{-(2\mu_B)/T}, \quad (38)$$

with similar expressions for strange particles. μ_B (and μ_S) are chemical potentials associated with each conserved quantity: baryon number, μ_B , (and strangeness, μ_S).

However for this problem there is also Lattice QCD thermodynamics which can calculate μ_B from the net electric charge distributions of non-identified charged particles ($n^+ - n^-$) [Bazavov 2012]. The theoretical analyses are made by a Taylor expansion of the free energy $F = -T \ln Z$ around the freezeout temperature T_f where Z is the partition function, or sum over states, which is of the form

$$Z \propto e^{-(E - \sum_i \mu_i Q_i)/kT} \quad (39)$$

and μ_i are chemical potentials associated with conserved charges Q_i . The terms of the Taylor expansion, which are obtained by differentiation, are called susceptibilities, denoted χ .

The only connection of this method to mathematical statistics is that the Cumulant generating function in mathematical statistics for a random variable x is also a Taylor expansion of the ln of an exponential:

$$g_x(t) = \ln \langle e^{tx} \rangle = \sum_{n=1}^{\infty} \kappa_n \frac{t^n}{n!} \quad \kappa_m = \left. \frac{d^m g_x(t)}{dt^m} \right|_{t=0}. \quad (40)$$

Thus, the susceptibilities are Cumulants in mathematical statistics terms. The first four Cumulants are $\kappa_1 = \mu \equiv \langle x \rangle$, $\kappa_2 = \langle (x - \mu)^2 \rangle \equiv \sigma^2$, $\kappa_3 = \langle (x - \mu)^3 \rangle$,

$\kappa_4 = \langle (x - \mu)^4 \rangle - 3\kappa_2^2$. Two so-called normalized or standardized Cumulants are common in this field, the skewness, $S \equiv \kappa_3/\sigma^3$ and the kurtosis, $\kappa \equiv \kappa_4/\sigma^4$. The theoretical results are presented as ratios of Cumulants so that the volume dependences of μ , σ , S , κ cancel.

The measured values of the temperature T_f and μ_B are obtained [Adare 2016] by comparing the measured values of κ_1/κ_2 and κ_3/κ_1 to the Lattice QCD calculations [Bazavov 2012], which are given as functions of T_f and μ_B . Figure 39 shows that the PHENIX + Lattice results for μ_B from net-charge fluctuations, *with no particle identification*, are in excellent agreement with the best accepted analysis of μ_B from baryon/anti-baryon ratios [Cleymans 2006]. Both the μ_B and T_f (not shown) results [Adare 2016] also agree with the more conventional best accepted values, which I believe was a first for measurements plus Lattice QCD calculations in A+A collisions!

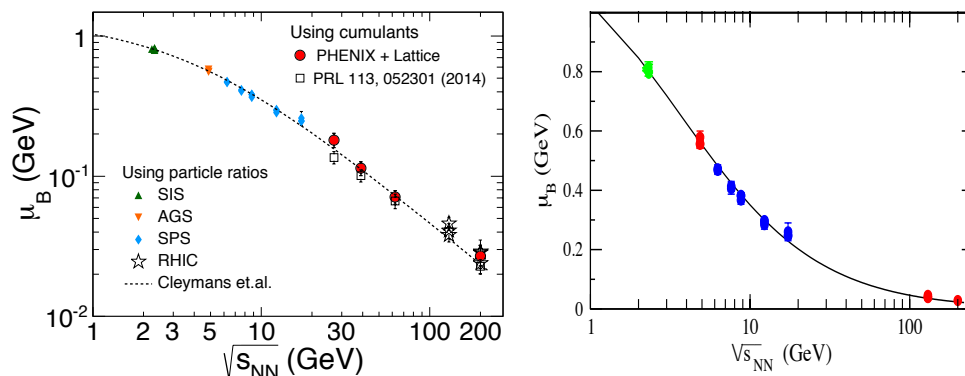


Fig. 39. a)(left) $\sqrt{s_{NN}}$ dependence of μ_B from PHENIX+Lattice [Adare 2016] net-charge results. Open squares are from STAR net-charge [Adamczyk 2014] together with net-protons [Borsanyi 2014]. Dashed line and other data points are from b)(right), the best accepted analysis of μ_B vs $\sqrt{s_{NN}}$ from baryon/anti-baryon ratios [Cleymans 2006].

12.5.2 Discovery of the QGP at RHIC by suppression of high p_T particles—2002

The discovery at RHIC [Adcox 2002b] that high p_T π^0 produced by hard parton-parton scattering in the colliding Au+Au nuclei are suppressed in central Au+Au collisions by a factor of ~ 5 compared to pointlike scaling from $p+p$ collisions is arguably *the* major discovery in Relativistic Heavy Ion Physics.

In Fig. 40, the suppression of the many identified particles measured by PHENIX at RHIC is presented as the Nuclear Modification Factor, $R_{AA}(p_T)$, the ratio of the yield of e.g. π per central Au+Au collision (upper 10%-ile of observed multiplicity) to the pointlike-scaled $p+p$ cross section at the same p_T , where $\langle T_{AA} \rangle$ is the average overlap integral of the nuclear thickness functions:

$$R_{AA}(p_T) = \frac{(1/N_{AA}) d^2 N_{AA}^\pi / dp_T dy}{\langle T_{AA} \rangle d^2 \sigma_{pp}^\pi / dp_T dy} . \quad (41)$$

The striking differences of $R_{AA}(p_T)$ in central Au+Au collisions for the many particles measured by PHENIX (Fig. 40) illustrates the importance of particle identification for understanding the physics of the medium produced at RHIC. The most notable observations are:

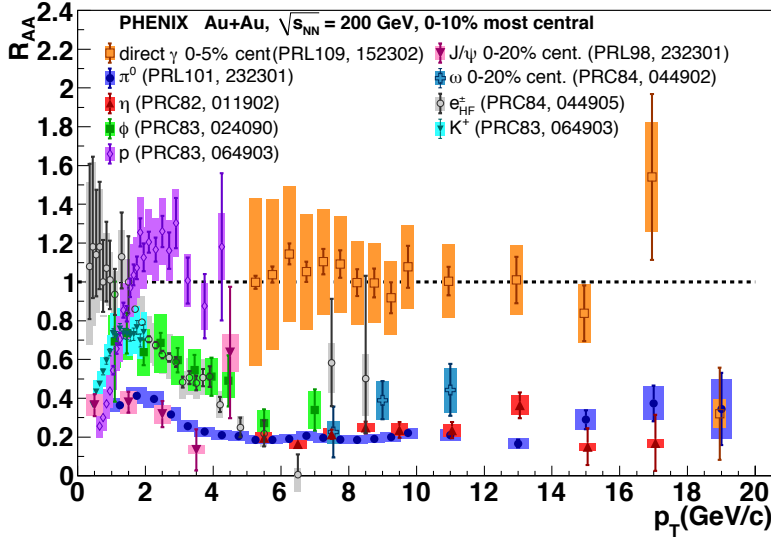


Fig. 40. [Tannenbaum 2014] PHENIX measurements of the suppression R_{AA} of identified particles with references to publication as a function of transverse momentum p_T .

1. the equal suppression of π^0 and η mesons by a constant factor of 5 ($R_{AA} = 0.2$) for $4 \leq p_T \leq 15$ GeV/c, with suggestion of an increase in R_{AA} for $p_T > 15$ GeV/c;
2. the equality of suppression of direct-single e_{HF}^{\pm} from heavy flavor (c , b quark) decay, and π^0 at $p_T \gtrsim 5$ GeV/c;
3. the non-suppression of direct- γ for $p_T \geq 4$ GeV/c.

For $p_T \gtrsim 4$ GeV/c, the hard-scattering region, the fact that all hadrons are suppressed, but direct- γ are not suppressed, indicates that suppression is a medium effect on outgoing color-charged partons, likely due to energy loss by coherent Landau-Pomeranchuk-Migdal radiation of gluons, predicted in pQCD [Baier 2000].

12.5.3 QGP, the perfect liquid, from charm suppression and flow–2007

The measurement of direct single e^{\pm} (also called heavy flavor e^{\pm} at RHIC) at mid-rapidity by PHENIX [Adare 2006] in p+p collisions at $\sqrt{s} = 200$ GeV is shown in Fig. 41a,b. The background from internal and external γ conversions was determined by the converter method as in section 4.2.1. The data are compared to a fixed-order-plus-next-to-leading-log (FONLL) pQCD calculation [Vogt, Cacciari and Nason 2006] which is in excellent agreement with the measurement and gives the relative contributions of c and b quark decay.

Figure 41c shows the R_{AA} of direct single heavy flavor e^{\pm} and π^0 in $\sqrt{s_{NN}} = 200$ GeV Au+Au collisions [Adare 2007a] which become equal in the range $4 \leq p_T \leq 7$ GeV/c. Initially this result was a surprise because heavy flavor quarks were predicted to lose less energy than light quarks due to the “dead cone effect” which happens in QED bremsstrahlung [Dokshitzer and Kharzeev 2001]. Figure 41d shows the anisotropic elliptical flow measurement v_2^{HF} for the heavy flavor quarks and for π^0 [Adare 2007a]. The heavy quarks at $p_T \approx 2$ GeV/c are actually barely relativistic, because $\gamma\beta = p_T/m = 2.0/1.3 \approx 1.5$, but have a significant v_2^{HF} .

The v_2^{HF} in this region suggested [Moore and Teaney 2005] that the charm quarks thermalize in the medium which responds as a thermalized fluid with a small trans-

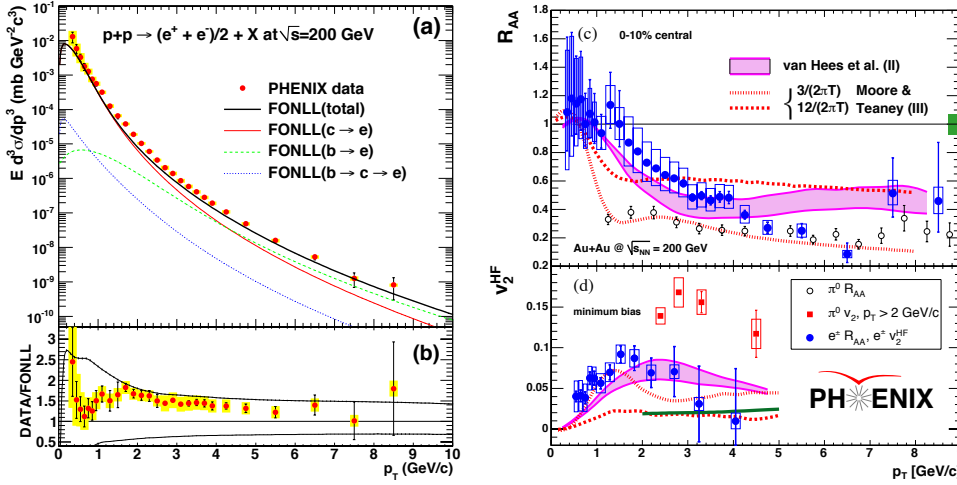


Fig. 41. (left) a) [Adare 2006] Invariant differential cross sections of electrons from heavy flavor quark decays. The curves are FONLL calculations [Vogt, Cacciari and Nason 2006] b) The ratio of the measurement to the FONLL calculation. c) [Adare 2007a] R_{AA} from direct-single e^\pm and π^0 , d) elliptical flow v_2 for Heavy Flavor quarks and π^0 . Dashed and filled lines are theoretical predictions of the diffusion coefficient D .

port mean free path. Thus they treat the heavy quark in the medium as a thermal diffusion problem with diffusion coefficient $D = 6\eta/(\epsilon + p)$ where η is the shear viscosity, ϵ is the energy density, and p the pressure. The enthalpy $(\epsilon + p) = Ts$ for zero baryon chemical potential, μ_B (a reasonable assumption at $\sqrt{s_{NN}} = 200$ GeV, Fig. 39), where T is the temperature and s is the entropy density. Obviously this is a thermodynamic/hydrodynamic problem with some QCD in the Monte Carlo to get R_{AA} but the results, shown as the dashes for two different values of $D = 3/(2\pi T)$ and $D = 12/(2\pi T)$ on Fig. 41c,d, lead to a spectacular conclusion. Taking $D = 6\eta/Ts \approx (6 \text{ to } 4)/(2\pi T)$ as the most reasonable range that fits both R_{AA} and v_2^{HF} in Fig. 41c,d [van Hees, Greco and Rapp 2006], gives the result:

$$\eta/s = (2 \text{ to } 4/3)/4\pi \quad (42)$$

which is intriguingly close to the conjectured [Kovtun, Son and Starinets 2005] quantum lower bound, $\eta/s = 1/4\pi$.

This is why we claimed the discovery of the QGP, the perfect liquid, at RHIC [Lee 2005], [Arsene 2005], [Back 2005],[Adams 2005], [Adcox 2005].

12.5.4 J/Ψ enhancement not suppression proves the existence of the QGP at the LHC

PHENIX measurements of J/Ψ suppression (R_{AA}) in Au+Au collisions at $\sqrt{s_{NN}} = 200$ GeV relative to point-like scaling of p+p collisions at mid-rapidity [Adare 2007b] Fig. 42a turned out to be nearly identical to the NA50 fixed-target measurements in $\sqrt{s_{NN}} = 17.2$ Pb+Pb collisions at CERN [Alessandro 2005]. The equality of J/Ψ suppression at $\sqrt{s_{NN}} = 17.2$ and 200 GeV was elegantly explained as recombination or coalescence of c and \bar{c} quarks in the QGP to regenerate J/Ψ [Zhao and Rapp 2008].

Miraculously this made the observed R_{AA} equal at SpS and RHIC c.m. energies. I called this my “Nightmare Scenario” because I thought that nobody would believe it. The good news was that such models are testable because they predicted the reduction of J/Ψ suppression or even an enhancement ($R_{AA} > 1$) at LHC energies [Braun-Munzinger and Stachel 2000], [Thews, Schroedter and Rafelski 2001],

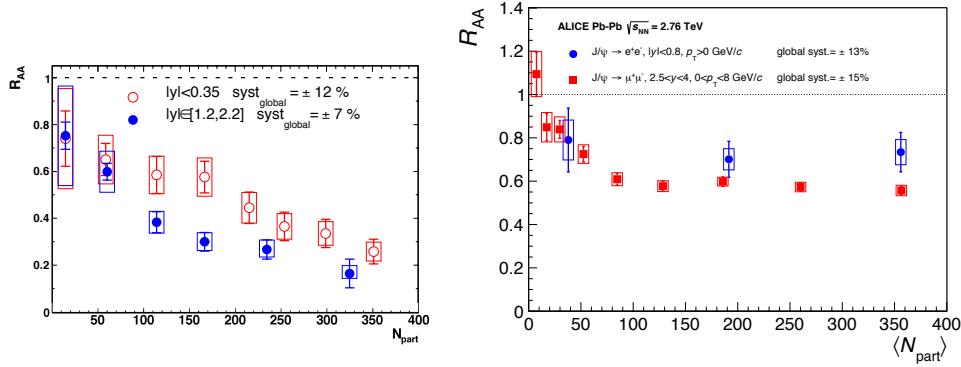


Fig. 42. a) (left) PHENIX [Adare 2007b] R_{AA} of J/Ψ in Au+Au at $\sqrt{s_{NN}} = 200$ GeV for e^+e^- ($|y| < 0.8$), and $\mu^+\mu^-$ ($1.2 \leq y \leq 2.2$) decay. b)(right) ALICE [Abelev 2014] R_{AA} of J/Ψ in Au+Au at $\sqrt{s_{NN}} = 2.76$ TeV for e^+e^- ($|y| < 0.35$), and $\mu^+\mu^-$ ($2.5 \leq y \leq 4.0$) decay.

[Andronic, Braun-Munzinger, Redlich and Stachel 2007], which would be spectacular, if observed.

As shown in Fig. 42b, the most recent ALICE [Abelev 2014] measurement of R_{AA} for J/ψ at $\sqrt{s_{NN}} = 2.76$ TeV exhibits considerably less suppression for both $J/\psi \rightarrow e^+e^-$ at mid rapidity and $J/\psi \rightarrow \mu^+\mu^-$ at forward rapidity than the PHENIX measurements at $\sqrt{s_{NN}} = 200$ GeV in Fig. 42a. The reduction of J/Ψ suppression at the LHC compared to RHIC is a clear observation of regeneration at LHC which directly proves the existence of the QGP, since it is evidence that the large number of c and \bar{c} quarks produced (with their color charge hidden by Debye screening) freely traversed the medium (with a large density of similarly screened color charges) until they met another quark close enough within the screening radii to form J/Ψ 's.

However [Satz 2013], these beautiful results do not prove that J/Ψ are deconfined in the QGP. According to Satz, the crucial issue is whether the medium modifies the fraction of produced $c\bar{c}$ pairs which form J/Ψ . Dissociation of J/Ψ in the medium would reduce the observed $J/\Psi/c\bar{c}$ ratio in A+A compared to p+p collisions, i.e. $R_{AA}^{J/\Psi}/R_{AA}^{c\bar{c}} \ll 1$. Personally, I think that Debye screening which is the basis of suppression of J/Ψ in the QGP is proved by Fig. 42 but Satz's requirement may be important to find how low in $\sqrt{s_{NN}}$ the QGP is formed.

12.5.5 jet quenching at the LHC

Although nobody at RHIC had claimed to measure the quenching of fully reconstructed jets in $\sqrt{s_{NN}} = 200$ GeV Au+Au collisions, because the multiparticle background is too large, as soon as the LHC started its 2760 GeV run, unbalanced jets were visible on the event displays for both ATLAS [Aad 2010] and CMS (Fig. 43) [Chatrchyan 2011b]

13 Summary and Conclusions

In the years 1972-1982 experiments at Hadron Colliders made major contributions to the theory of QCD which was developed in this same period. More recently, Heavy Ion Colliders have opened up a new field of the study of superdense nuclear matter

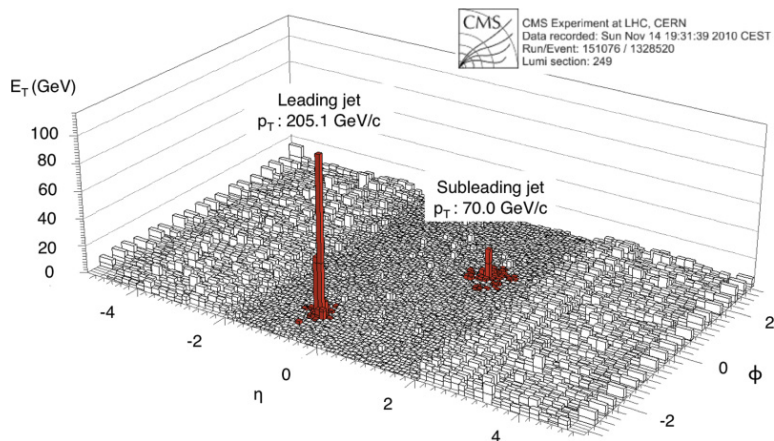


Fig. 43. Example [Chatrchyan 2011b] of an unbalanced dijet in a PbPb collision event at $\sqrt{s_{NN}} = 2.76$ TeV. The summed transverse energy in the electromagnetic and hadron calorimeters is plotted vs. η and ϕ , with the identified jets highlighted, and labeled with the corrected jet transverse momentum.

in the laboratory, leading to the discovery of the Quark Gluon Plasma which can be analyzed with lattice QCD. Highlights of these achievements can be summarized as follows.

13.1 Hadron Colliders and QCD

The CERN Intersecting Storage Rings (ISR), Geneva, SZ, 1971–1983.

This was the first hadron collider, with p+p collisions at c.m. energy $\sqrt{s} = 23.5 - 62.4$ GeV. Also d+d $\alpha + \alpha$ p+ α and p+p experiments were performed. The largest contributions for the development of QCD were from the ISR.

1. Discovery of particle production at high $p_T \geq 3$ GeV/c, 1972.
2. Discovery of charm particles by direct single e^\pm production in 1974, but not understood until 1976.
3. First application of QCD theory to ISR π^\pm and π^0 spectra with $3 \leq p_T \leq 14$ GeV/c, 1978.
4. Discovery of direct- γ production 1979-1980 as predicted by QCD in 1977.
5. Observation of the di-jet structure of hard-scattering via two-particle correlations including discovery and measurements of k_T , the transverse momentum of a parton in a nucleon, and measurement of $\langle j_T \rangle$ the average momentum of jet fragments transverse to the jet axis, 1977-1979.
6. First measurement of the $\cos\theta^*$ distribution of elementary QCD subprocesses including the increase of the QCD coupling constant $\alpha_s(Q^2)$ with decreasing Q^2 at more forward angles, 1982.
7. First direct measurement of the gluon structure function $G(x, Q^2)$, 1987.

The CERN S $\bar{p}p$ S Collider 1981–1991. Nobel Prize winning hadron collider with $\bar{p}+p$ collisions at $\sqrt{s} = 546 - 630$ GeV.

1. First definitive observation of jets in hadron collisions, 1982.
2. Discovery of the W^\pm ‘intermediate boson’ of weak interactions, 1983.
3. Discovery of the Z^0 boson of weak interactions, 1983.

ISABELLE at BNL, Upton, NY, USA, 1978–1983 (cancelled)

ISABELLE was designed as p+p collider with $\sqrt{s} = 800$ GeV. This was the first collider with superconducting magnets, which led to problems during construction. Eventually greatly improved superconducting accelerator magnets were developed and tested, known as the Palmer Magnet [Palmer 1985]. This design has been used by all following colliders except for the Fermilab Tevatron Collider.

Tevatron Collider at Fermilab, Batavia, Illinois, USA, 1986–2011

This was a $\sqrt{s} = 1.8$ TeV $\bar{p}+p$ collider with a different superconducting magnet design than ISABELLE. However, the Palmer Magnet developed at ISABELLE was based on the superconducting cable developed for the Tevatron.

1. Discovery of the top quark, 1995
2. Measurement of jet cross sections over a wide range of p_T and rapidity in agreement with QCD.

Superconducting Super Collider (SSC), Waxahachie, Texas, USA, 1990–1993 (cancelled)

The SSC was designed as a $\sqrt{s} = 40$ TeV p+p collider. Its demise hurt High Energy Physics in the U.S.A; but on the positive side, in 1994, the U.S. High Energy Physics Advisory Panel recommended that the U.S. significantly participate in the CERN Large Hadron Collider to help maintain U.S. involvement in High Energy Physics. In 1997 the DOE recommended spending a total of more than \$531 million for U.S. contributions to both the accelerator and the experiments, the first agreement between CERN and the U.S. government. This allowed CERN to build the LHC in a single stage of $\sqrt{s} = 14$ GeV rather than the originally approved two stage construction with missing magnets [Evans and Bryant 2008].

The CERN Large Hadron Collider, LHC, 2008–present.

The largest and highest energy p+p collider with $\sqrt{s} = 7 - 13$ TeV. Also Pb+Pb and p+Pb collisions.

1. Measurement of jet cross sections over a wide range of p_T and rapidity in agreement with QCD.
2. Discovery of the Higgs Boson, 2012.
3. Discovery of suppression of jets in Pb+Pb collisions, 2010.
4. Discovery of J/Ψ enhancement compared to measurements at RHIC, evidence for the Quark Gluon Plasma, 2014.

RHIC, the Relativistic Heavy Ion Collider at BNL, 2000–present.

RHIC is a Heavy Ion Collider with c.m. energy per nucleon pair, $\sqrt{s_{NN}} = 19.6 - 200$ GeV, and the first polarized p+p collider with $\sqrt{s} = 500$ GeV. RHIC has provided collisions of p+p, p+Au, p+Al, d+Au, $^3\text{He}+\text{Au}$, Cu+Cu, Cu+Au, Au+Au and U+U.

1. Discovery of jet quenching predicted for the QGP, 2002.
2. Discovery of the QGP as a perfect liquid with shear viscosity/entropy density near the quantum limit, 2005–2007.

13.2 Future Possibilities for QCD

A remaining problem with QCD is the need to utilize structure and fragmentation functions, which come from experimental measurements, in the calculations. An excellent possibility for the future is to be able to also calculate the structure and fragmentation functions in QCD.⁷

⁷ Thanks to Norman Christ for this suggestion.

14 Appendix

14.1 The relativistic longitudinal variable, y , rapidity

Any particle with momentum P and energy E can be represented by its longitudinal momentum P_L , which is subject to a Lorentz transformation, and its transverse momentum P_T which is not affected, so $E^2 = p^2 + m^2 = p_T^2 + p_L^2 + m^2$ in the nomenclature where the speed of light $c \equiv 1$. The ‘transverse mass’, $m_T \equiv \sqrt{p_T^2 + m^2} = \sqrt{E^2 - P_L^2}$, is invariant under a Lorentz transformation. The definition of the rapidity of this particle is:

$$\cosh y = E/m_T \quad \sinh y = p_L/m_T \quad dy = dp_L/E \quad (43)$$

$$y = \frac{1}{2} \ln \left(\frac{E + P_L}{E - P_L} \right) = \ln \left(\frac{E + P_L}{m_T} \right) \quad . \quad (44)$$

The advantage of rapidity is that if the rapidity of a particle is y^* in a frame moving with velocity $\beta = v/c$ with respect to our system, then the rapidity y of the particle in our system is related to y^* by simple addition, $y = Y + y^*$, where Y is the rapidity of the moving frame

$$Y = \frac{1}{2} \ln \left(\frac{1 + \beta}{1 - \beta} \right) \quad .$$

Using the rapidity variable, the invariant differential single particle inclusive cross section for a scattered particle with longitudinal momentum p_L along the collision axis, and transverse momentum p_T at azimuthal angle ϕ in cylindrical coordinates, can be written in the Lorentz invariant form:

$$\frac{E d^3 \sigma}{dp^3} = \frac{E d^3 \sigma}{p_T dp_T dp_L d\phi} = \frac{d^3 \sigma}{p_T dp_T dy d\phi} \quad . \quad (45)$$

14.1.1 Pseudorapidity, η

In the limit when ($P \gg m$) for a particle, $E \rightarrow P$, $m_T \rightarrow p_T \rightarrow E \sin \theta$, $p_L \rightarrow E \cos \theta$, where θ is the polar angle, the rapidity y (Eq. 43) reduces to the pseudorapidity, η :

$$\cosh \eta = \csc \theta \quad \sinh \eta = \cot \theta \quad \tanh \eta = \cos \theta \quad (46)$$

$$\eta = -\ln \tan \theta/2 \quad . \quad (47)$$

14.2 Parton-parton scattering

In hadron colliders, collisions usually take place with protons of equal and opposite vector momenta \mathbf{P} and $-\mathbf{P}$ so that the p+p center of mass (c.m.) system is at rest in the laboratory. However, the partons in each proton have fractional momenta x_1 and x_2 which are not generally equal so that the parton-parton c.m. system moves longitudinally in the p+p c.m. system (Fig. 44). For kinematic calculations, the gluon and quark partons are massless; and for simplicity the proton mass M can be ignored because $P \gg M$ for the colliders discussed, so that $E^2 = P^2 + M^2 \rightarrow P^2$ and the particles all have relativistic velocities so that Lorentz Transformations are required.

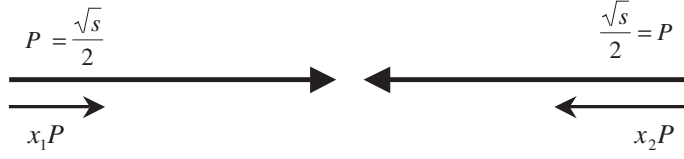


Fig. 44. Proton-proton collision with colliding parton momenta illustrated

The c.m. energy of the p+p collision is given by the Lorentz invariant Mandelstam variable $\sqrt{s} = 2P$, where

$$s = -(p_1 + p_2)^2 = -[(0, 0, P, iP) + (0, 0, -P, iP)]^2 = 4P^2 \quad . \quad (48)$$

The partons (with notation $\hat{}$) are assumed to travel along the longitudinal directions of their protons so that the c.m. energy of the parton-parton collision $\sqrt{\hat{s}}$ is given by:

$$\begin{aligned} \hat{s} &= -(\hat{p}_1 + \hat{p}_2)^2 = -[(0, 0, x_1 P, ix_1 P) + (0, 0, -x_2 P, ix_2 P)]^2 = 4P^2 x_1 x_2 \\ &= s x_1 x_2 \quad . \end{aligned} \quad (49)$$

The parton-parton c.m. system has longitudinal momentum $P_L = (x_1 - x_2)P$ and total energy $E = (x_1 + x_2)P$ in the p+p c.m. system, transverse mass $m_T = \sqrt{E^2 - P_L^2} = \sqrt{\hat{s}}$ and thus has rapidity (Eq. 44) \hat{y} :

$$\hat{y} = \ln \left(\frac{E + P_L}{\sqrt{\hat{s}}} \right) = \ln \sqrt{\frac{x_1}{x_2}} \quad . \quad (50)$$

Also, Eqs. 50, 49 can be solved for x_1 and x_2 :

$$x_1 = \sqrt{\frac{\hat{s}}{s}} e^{\hat{y}} \quad x_2 = \sqrt{\frac{\hat{s}}{s}} e^{-\hat{y}} \quad . \quad (51)$$

14.2.1 Kinematics of parton-parton scattering

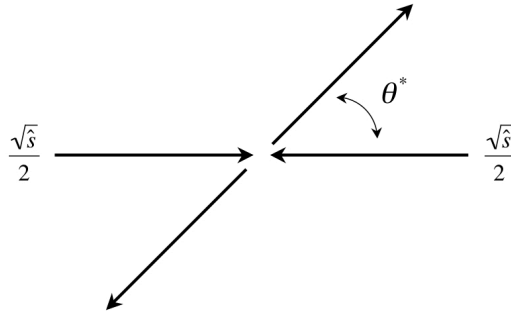


Fig. 45. Elastic scattering in parton-parton c.m. system

Figure 45 shows the elastic scattering of the two initial partons through angle θ^* in the parton-parton c.m. system, where the two colliding partons have equal and opposite momenta, $\sqrt{\hat{s}}/2$. The scattered parton 3-momenta are equal and opposite,

$\mathbf{P}_3^* = -\mathbf{P}_4^*$, and their energies are equal, and equal to the magnitude of their 3-momenta, $E_3^* = E_4^* = P_3^* = P_4^* = \sqrt{\hat{s}}/2$, because both outgoing partons are assumed to be massless. For the z axis along the direction of the initial partons and the y axis perpendicular to the z axis in the scattering plane, the parton 4-momenta in the parton-parton c.m. system can be written as:

$$p_1^* = \frac{\sqrt{\hat{s}}}{2}(0, 0, 1, i) \quad p_2^* = \frac{\sqrt{\hat{s}}}{2}(0, 0, -1, i) \quad (52)$$

$$p_3^* = \frac{\sqrt{\hat{s}}}{2}(0, \sin \theta^*, \cos \theta^*, i) \quad p_4^* = \frac{\sqrt{\hat{s}}}{2}(0, -\sin \theta^*, -\cos \theta^*, i) \quad , \quad (53)$$

so that

$$P_{L_3}^* = -P_{L_4}^* = \frac{\sqrt{\hat{s}}}{2} \cos \theta^* \quad P_{T_3}^* = -P_{T_4}^* \equiv p_T = m_T = \frac{\sqrt{\hat{s}}}{2} \sin \theta^* \quad . \quad (54)$$

For the outgoing partons, the rapidities are equal and opposite in the parton-parton c.m. system:

$$y_3^* = \sinh^{-1} P_{L_3}^*/m_T = -y_4^* \quad (55)$$

The other two Mandelstam invariants of the parton-parton scattering, \hat{t} , the 4-momentum-transfer-squared, and \hat{u} can be easily computed from Eqs. 52 and 53. The invariants are related by the c.m. scattering angle:

$$\hat{Q}^2 = -\hat{t} = (p_1^* - p_3^*)^2 = \hat{s} \frac{(1 - \cos \theta^*)}{2} \quad ; \quad (56)$$

and likewise

$$-\hat{u} = (p_1^* - p_4^*)^2 = \hat{s} \frac{(1 + \cos \theta^*)}{2} \quad . \quad (57)$$

Acknowledgements

Research supported by U.S. Department of Energy, Contract No. de-sc0012704.

References

- 't Hooft, G., 1999. *Nucl. Phys. B(Proc. Suppl.)* **74**: 413–425.
Aad, G. et al. (ATLAS) 2010. *Phys. Rev. Lett.* **105**: 252303.
Aad, G. et al. (ATLAS) 2012. *Phys. Lett. B* **716**: 1–29.
Aamodt, K. et al. (ALICE) 2008. *JINST* **3**: S08002.
Abachi, S. et al. (D0) 1995. *Phys. Rev. Lett.* **74**: 2632–2637.
Abazov, V. M. et al. (D0) 2008. *Phys. Rev. Lett.* **101**: 062001.
Abe, F. et al. (CDF) 1988. *Phys. Rev. Lett.* **61**: 1819–1822.
Abe, F. et al. (CDF) 1995. *Phys. Rev. Lett.* **74**: 2626–2631.
Abelev, B. et al. (ALICE) 2014. *Phys. Lett. B* **734**: 314–327.
Abramov, V. V. et al. 1976. *Phys. Lett. B* **64**: 365–368.
Abramowicz, H. et al. (CDHS) 1982. *Z. Phys. C* **12**: 289–295.
Abrams, G.-S. et al. 1974. *Phys. Rev. Lett.* **33**: 1453–1455.
Acosta, D. et al. (CDF). 2005. *Phys. Rev. D* **71**: 032001.
Adamczyk, L. et al. (STAR) 2014. *Phys. Rev. Lett.* **113**: 092301.
Adams, J. et al. 2005. *NPA* **757**: 102–183.
Adare, A. et al. (PHENIX) 2006. *Phys. Rev. Lett.* **97**: 252002.

- Adare, A. et al. (PHENIX) 2007a. *Phys. Rev. Lett.* **98**: 172301.
- Adare, A. et al. (PHENIX) 2007b. *Phys. Rev. Lett.* **98**: 232301.
- Adare, A. et al. (PHENIX) 2010. *Phys. Rev. D* **82**: 072001.
- Adare, A. et al. (PHENIX) 2012. *Phys. Rev. D* **86**: 072008.
- Adare, A. et al. (PHENIX) 2016. *Phys. Rev. C* **93**: 011910(R).
- Adare, A. et al. (PHENIX) 2017. *Phys. Rev. D* **95**: 072002.
- Adcox, K. et al. (PHENIX). 2002a. *Phys. Rev. Lett.* **88**: 192303.
- Adcox, K. et al. (PHENIX) 2002b. *Phys. Rev. Lett.* **88**: 022301.
- Adcox, K. et al. (PHENIX) 2005. *Nucl. Phys. A* **757**: 184–283.
- Adler, S. S. et al. (PHENIX) 2005. *Phys. Rev. C* **71**: 034908.
- Adler, S. S. et al. (PHENIX) 2006. *Phys. Rev. D* **74**: 072002.
- Adler, S. S. et al. (PHENIX) 2014. *Phys. Rev. C* **89**: 044905.
- Akesson, T. et al. (AFS) 1983. *Phys. Lett. B* **128**: 354–360.
- Akesson, T. et al. (AFS) 1987. *Z. Phys. C* **34**: 293–302.
- Albrow, M. G. et al. (BFS) 1978. *Nucl. Phys. B* **145**: 305–348.
- Alessandro, B. et al. (NA50) 2005. *Eur. Phys. J. C* **39**: 335–345.
- Alper, B. et al. (British-Scandinavian ISR Collaboration). 1973. *Phys. Lett. B* **44**: 521–526.
- Alper, B. et al. p. V-9, Fig. 1 in Ref. [Segler 1974].
- Alper, B. et al. (British-Scandinavian) 1975a. *Nucl. Phys. B* **87**: 19–40.
- Alper, B. et al. (BS) 1975b. *Nucl. Phys. B* **100**: 237–290.
- Altarelli, G., R. A. Brandt and G. Preparata. 1971. *Phys. Rev. Lett.* **26**: 42–46.
- Altarelli, G. and G. Parisi. 1977. *Nucl. Phys. B* **126**: 298–318.
- Althoff, M. et al. (TASSO) 1984. *Z. Phys. C* **22**: 307–340.
- Amaldi, E. et al. 1979. *Nucl. Phys. B* **150**: 326–344.
- Anassontzis, E. et al. (R806) 1982. *Z. Phys. C* **13**: 277–289.
- Andronic, A., p. Braun-Munzinger, K. Redlich and J. Stachel. 2007. *Nucl. Phys. A* **789**: 334–356.
- Angelis, A. L. S. et al. (CCOR) 1978. *Phys. Lett. B* **79**: 505–510.
- Angelis, A. L. S. et al. (CCOR) 1979a. *Physica Scripta* **19**: 116–123.
- Angelis, A. L. S. et al. (CCOR). 1979b. *Phys. Lett. B* **87**: 398–402.
- Angelis, A. L. S. et al. (CCOR). 1980a. *Phys. Lett. B* **94**: 106–112.
- Angelis, A. L. S. et al. (CCOR) 1980b. *Phys. Lett. B* **97**: 163–168.
- Angelis, A. L. S. et al. (CCOR) 1982a. *Nucl. Phys. B* **209**: 284–300.
- Angelis, A. L. S. et al. (COR) 1982b. *Phys. Lett. B* **116**: 379–382.
- Angelis, A. L. S. et al. (COR) 1983. *Phys. Lett. B* **126**: 132–136.
- Angelis, A. L. S. et al. (BCMOR) 1987. *Phys. Lett. B* **185**: 213–217.
- Angelis, A. L. S. et al. (CMOR). 1989. *Nucl. Phys. B* **327**: 541–568.
- Angelis, A. L. S., Tanaka, M. et al. (BCMOR) 1984. *Nucl. Phys. A* **418**: 321c–326c.
- Antreasyan, D., J. W. Cronin et al. 1979. *Phys. Rev. D* **19**: 764–778.
- Appel, J. A. et al. 1974. *Phys. Rev. Lett.* **33**: 722–725.
- Appel, J. A. et al. (UA2) 1986. *Z. Phys. C* **30**: 1–22.
- Appelquist, T. and H. D. Politzer. 1975. *Phys. Rev. Lett.* **34**: 43–45.
- Arnison, G. et al. (UA1) 1983a. *Phys. Lett. B* **122**: 103–116.
- Arnison, G. et al. (UA1) 1983b. *Phys. Lett. B* **126**: 398–410.
- Arnison, G. et al. (UA1) 1984. *Phys. Lett. B* **136**: 294–300.
- Arsene, I. et al. (BRAHMS) 2005. *Nucl. Phys. A* **757**: 1–27.
- Aubert, J. J. et al. 1974. *Phys. Rev. Lett.* **33**: 1404–1406.
- Augustin, J.-E. et al. 1974. *Phys. Rev. Lett.* **33**: 1406–1408.
- Aurenche, P., J. Ph. Guillet, E. Pilon, M. Werlen and M. Fontannaz. 2006. *Phys. Rev. D* **73**: 094007.
- Büsser, F. W. et al. (CCR). 1973. *Phys. Lett. B* **46**: 471–476.
- Büsser, F. W. et al. (CCRS). 1974. *Phys. Lett. B* **53**: 212–216.
- Büsser, F. W. et al. (CCRS). 1975a. *Phys. Lett. B* **56**: 482–486.
- Büsser, F. W. et al. (CCRS). 1975b. Fig. 12a, p. 281 in Ref [Lederman 1975].
- Büsser, F. W. et al. (CCRS). 1975c. *Phys. Lett. B* **55**: 232–2236.
- Büsser, F. W. et al. (CCRS). 1976a. *Nucl. Phys. B* **106**: 1–30.

- Büsser, F. W. et al. (CCRS). 1976b. *Nucl. Phys. B* **113**: 189–245.
- Back, B. B. et al. (PHOBOS). 2005. *Nucl. Phys. A* **757**: 28–101.
- Bagnaia, P. et al. (UA2) 1983. *Phys. Lett. B* **129**: 130–140.
- Baier, R., Yu. L. Dokshitzer, A. H. Mueller, S. Peigné and D. Schiff, 1997. *Nucl. Phys. B* **483**: 291–320.
- Baier, R., D. Schiff and B. G. Zakharov. 2000. *Ann. Rev. Nucl. Part. Sci.* **50**: 37–69.
- Baier, R. 2003. *Proceedings of the 16th International Conference on Ultra-Relativistic Nucleus-Nucleus Collisions*, Nantes, France, July 18–24, 2002, H. Gutbrod, J. Aichelin and K. Werner (eds.) 2003. *Nucl. Phys. A* **715**: 209c–218c.
- Baier, R. also M. J. Tannenbaum. *Proc. IV Workshop on Quantum Chromodynamics*, Paris, France, June 1–6, 1998, H. M. Fried and B. Müller (eds.) (World Scientific, Singapore, 1999) pp. 272–285.
- Banner, M. et al. (Saclay-Strasbourg Collaboration). 1973. *Phys. Lett. B* **44**: 537–540.
- Banner, M. et al. (UA2). 1983. *Phys. Lett. B* **122**: 476–485.
- Basile, M. et al. 1981. *Nuovo Cimento* **A65**: 421–456.
- Baum, L. et al. (CHORMN) 1976. *Phys. Lett. B* **60**: 485–490.
- Bazavov, A. et al. 2012. *Phys. Rev. Lett.* **109**: 192302.
- Berman, S. M., J. D. Bjorken and J. B. Kogut. 1971. *Phys. Rev. D* **4**: 3388–3418.
- Bernardini, G., J. K. Bienlein, G. Von Dardel, H. Faissner, F. Ferrerero, J. M. Gaillard, H. J. Gerber, B. Hahn, V. Kaftanov, F. Krienen, C. Manfredotti, M. Reinharz and R. A. Salmeron, 1964. *Phys. Lett.* **13**: 86–91.
- Bernstein, J. 1963. *Phys. Rev.* **129**: 2323–2325.
- Billan, J., R. Perin and V. Sergo, 1972. *Proc. 4th International Conference on Magnet Technology*, (Upton, NY, 19–22 September, 1972) Y. Winterbottom (editor) (Brookhaven National Laboratory, Upton, NY, 1972) pp. 433–443. <http://inspirehep.net/record/80276/files/C720919-p433.PDF>
- Bjorken, B. J. and S. L. Glashow 1964. *Phys. Lett.* **11**: 255–257.
- Bjorken, J. D, 1971. *Proc. 1971 International Symposium on Electron and Photon Interactions at High Energies*, (Cornell University, 23–27 August, 1971) N. B. Mistry (editor) (Cornell, Ithaca, NY, 1971) pp. 282–297.
- Bjorken, J. D. 1973. *Phys. Rev. D* **8**: 4098–4106.
- Bjorken, J. D. 1969. *Phys. Rev.* **179**: 1547–1553.
- Bjorken, J. D. 1983. *Phys. Rev. D* **27**: 140–151.
- Bjorken, J. D. and E. A. Paschos. 1969. *Phys. Rev.* **185**: 1975–1982.
- Blankenbecler, R., S. J. Brodsky and J. F. Gunion, 1972. *Phys. Lett. B* **42**: 461–465.
- Borsanyi, S. et al. 2014. *Phys. Rev. Lett.* **113**: 052301.
- Bourquin, M. and J.-M. Gaillard, 1976. *Nucl. Phys. B* **114**: 334–364.
- Boyerski, A. M. et al. 1975. *Phys. Rev. Lett.* **35**: 196–199.
- Boymond, J. P. et al. 1974. *Phys. Rev. Lett.* **33**: 112–115.
- Braun-Munzinger, P. and J. Stachel. 2000. *Phys. Lett. B* **490**: 196–202.
- Braunschweig, W. et al. (TASSO) 1990. *Z. Phys. C* **47**: 187–198.
- Breidenbach, M., J. I. Friedman, H. W. Kendall, E. D. Bloom, D. H. Coward, H. DeStabler, J. Drees, L. W. Mo and R. E. Taylor. 1969. *Phys. Rev. Lett.* **23**: 935–939.
- Brodsky, S. J. and S. D. Drell. 1970. *Ann. Rev. Nucl. Part. Sci.* **20**: 147–194.
- Bromberg, C., G. C. Fox et al. (E260) 1978. *Nucl. Phys. B* **134**: 189–241.
- Burns, R., K. Goulios, E. Hyman, L. Lederman, W. Lee, N. Mistry, J. Rettberg, M. Schwartz, J. Sunderland and G. Danby. 1965a. *Phys. Rev. Lett.* **15**: 42–45.
- Burns, R., K. Goulios, E. Hyman, L. Lederman, W. Lee, N. Mistry, J. Rettberg, M. Schwartz, and J. Sunderland, 1965b. *Phys. Rev. Lett.* **15**: 830–834.
- Cahalan, R. F., K. A. Geer, J. Kogut and L. Susskind. 1975. *Phys. Rev. D* **11**: 1199–1212.
- CCR Collaboration. 1973. *Proposal for a continuation with Increased Sensitivity of the Search for e^\pm , e^+e^- pairs, High p_T π^\pm and multiple pion correlations in collisions with high p_T* , CERN/ISRC/73-13, 14 May 1973. <http://cds.cern.ch/record/732024/files/cm-p00048643.pdf>
- CCOR Collaboration. 1974. *Proposal for a High Sensitivity Search at the ISR For High Mass States Decaying Into Two Electrons*, CERN/ISRC/74-56, 25 November 1974. <http://cds.cern.ch/record/1004373/files/CM-P00063282.pdf>

- CCRS Collaboration. 1973. *Addendum 2 to Proposal: Measurement of High Transverse Momentum Charged Particles*, CERN/ISRC/72-13/Add. 2, April 1973. <http://cds.cern.ch/record/835104/files/CM-P00053349.pdf>
- CERN-Saclay Collaboration. 1974. *Proposal to Search for Charmed Particles and e^+e^- Pairs at the ISR*, CERN/ISRC/74-55, 25 November 1974. <http://cds.cern.ch/record/738399/files/cm-p00047665.pdf>
- Chatrchyan, S. et al. (CMS) 2011a. *Phys. Rev. Lett.* **107**: 132001.
- Chatrchyan, S. et al. (CMS) 2011b. *Phys. Rev. C* **84**: 024906.
- Chatrchyan, S. et al. (CMS) 2012. *Phys. Lett. B* **716**: 30–61.
- Chilton, F., A. M. Saperstein and E. Shrauner. 1966. *Phys. Rev.* **148**: 1380–1384.
- Christenson, J. H., G. S. Hicks, L. M. Lederman, P. J. Limon, B. G. Pope and E. Zavattini. 1970. *Phys. Rev. Lett.* **25**: 1523–1526.
- Clark, A. G. et al. (CSZ). 1978. *Nucl. Phys. B* **142**: 29–52.
- Clark, A. G. et al. (CS) 1979. *Nucl. Phys. B* **160**: 397–425.
- Cleymans, J., H. Oeschler, K. Redlich and S. Wheaton. 2006. *Phys. Rev. C* **73**: 034905.
- Cobb, J. H. et al. (BCSY). 1977. *Phys. Lett. B* **72**: 273–277.
- Cocconi, G., L. J. Koester, and D. H. Perkins, Technical Report No. UCRL- 10022 (1961), Lawrence Radiation Laboratory (unpublished), p. 167, <https://www.osti.gov/scitech/biblio/4695660/> as cited by [Orear 1964].
- Collins, J. C. and M. J. Perry. 1975. *Phys. Rev. Lett.* **34**: 1353–1356.
- Combridge, B. L., J. Kripfganz and J. Ranft. 1977. *Phys. Lett. B* **70**: 234–238.
- Contogouris, A. P., S. Papadopoulos and J. Ralston. 1981. *Phys. Lett. B* **104**: 70–74.
- Cool, R., L. DiLella, L. Lederman and E. Zavattini. 1969. *Intersecting Storage Ring Study Of Dileptons*, CERN/ISRC/69-43, 20 June 1969. <http://cds.cern.ch/record/1005387/files/CM-P00062888.pdf>
- Cool, R. L. et al. 1973. (CCR) *Proc. XVI International Conference on High Energy Physics* (Chicago-Batavia,1972). J. D. Jackson and A. Roberts (eds.) (NAL, Batavia, IL,1973) Vol. 3 p. 317.
- Cooper, F. and G. Frye. 2010. *Phys. Rev. D* **10**: 186–189.
- Crease, R. P. 2008. *Hist. Stud. Nat. Sci.* **38**: 535–568.
- Cronin, J. W. 1977. *Proc. 1977 Int. Symposium on Lepton and Photon Interactions at High Energies*, (Hamburg, Germany 25-31 August, 1977), F. Gutbrod (editor) (DESY, Hamburg, 1977) pp. 579–598.
- Cutler, R. and D. Sivers. 1978. *Phys. Rev. D* **17**: 196–211.
- Danby, G., J.-M. Gaillard, K. Goulianos, L. M. Lederman, N. Mistry, M. Schwartz, and J. Steinberger, 1962. *Phys. Rev. Lett.* **9**: 36–44.
- Darriulat, P. et al. 1976a. *Nucl. Phys. B* **110**: 365–379.
- Darriulat, P. et al. 1976b. *Nucl. Phys. B* **107**: 429–456.
- Darriulat, P. 1980. *Large Transverse Momentum Hadronic Processes*, CERN-EP/80-16 <http://cds.cern.ch/record/133947/files/198004343.pdf>
- Darriulat, P. 2012. *40th Anniversary of the First Proton-Proton Collisions in the CERN Intersecting Storage Rings (ISR)*, CERN-2012-004, 2012. pp 63–73. <http://cds.cern.ch/record/1456765>
- De Marzo, C. et al. (NA5) 1982. *Phys. Lett. B* **112**: 173–177.
- De Rujula, A. and S. L. Glashow. 1975. *Phys. Rev. Lett.* **34**: 46–49.
- Della Negra, M. et al. (CCHK) 1977. *Nucl. Phys. B* **127**: 1–42.
- Di Lella, L. pp. V-13–V20 in Ref. [Segler 1974].
- Diakonou, M. et al. (AABC). 1979. *Phys. Lett. B* **87**: 292–296.
- Djhelyadin, R. I. et al. 1980. *Phys. Lett. B* **94**: 548–550.
- Dokshitzer, Yu. L. and D. E. Kharzeev. 2001. *Phys. Lett. B* **519**: 199–206.
- Drell, S. D. and J. D. Walecka, 1964. *Ann. Phys. (NY)* **28**: 18–33.
- Drell, S. D. and T.-M. Yan 1970. *Phys. Rev. Lett.* **25**: 316–320.
- Drijard, D. et al. (CCHK) 1979. *Phys. Lett. B* **81**: 250–254.
- Eichten, E. et al. 1975. *Phys. Rev. Lett.* **34**: 369–372.
- Eichten, E. and K. Gottfried. 1977. *Phys. Lett. B* **66**: 286–290.

- Evans, L. and P. Bryant (editors). 2008. *JINST* **3**: S08001 <http://dx.doi.org/10.1088/1748-0221/3/08/S08001>.
- Fabjan, C. W. and N. McCubbin. 2004. *Phys. Repts.* **403–404**: 165–175.
- Faessler, M. A. et al. (CHL) $p-\alpha$ and $\alpha-\alpha$ Collisions in the ISR, Proposal to CERN-ISRC, CERN/ISRC/79-10; ISRC/P101, April 10, 1979. <http://cds.cern.ch/record/719842/files/cm-p00048087.pdf>
- Faessler, M. A. 1984. *Phys. Repts.* **115**: 1–91.
- Farrar, G. R. and S. C. Frautschi. 1976. *Phys. Rev. Lett.* **36**: 1017–1020.
- Ferbel, T. and W. R. Molzon. 1984. *Rev. Mod. Phys.* **56**: 181–221.
- Feynman, R. P., R. D. Field and G. C. Fox. 1977. *Nucl. Phys. B* **128**: 1–65.
- Feynman, R. P., R. D. Field and G. C. Fox. 1978. *Phys. Rev. D* **18**: 3320–3343.
- Friedman, J. I. 1991. *Rev. Mod. Phys.* **63**: 615–627.
- Fritzsche, H. and P. Minkowski. 1977. *Phys. Lett. B* **69**: 316–320.
- Fritzsche, H. and M. Gell-Mann *Proc. XVI International Conference on High Energy Physics* (Chicago-Batavia, 1972). J. D. Jackson and A. Roberts (eds.) (NAL, Batavia, IL, 1973) Vol. 2 pp. 135–165.
- Fritzsche, H., M. Gell-Mann and H. Leutwyler, 1973. *Phys. Lett. B* **47**: 365–368.
- Gell-Mann, M. 1964. *Phys. Lett.* **8**: 214–215.
- Gell-Mann, M. 2013. *Int. J. Mod. Phys. A* **28**: 1330016.
- Glashow, S. L., J. Iliopoulos and L. Maiani. 1970. *Phys. Rev. D* **2**: 1285–1292.
- Goldhaber, M., L. Grodzins and A. W. Sunyar. 1958. *Phys. Rev.* **109**: 1015–1017.
- Goldhaber, G. et al. 1976. *Phys. Rev. Lett.* **37**: 255–259.
- Greenberg, O. W. 1964. *Phys. Rev. Lett.* **13**: 598–602.
- Gross, D. J. and F. Wilczek, 1973. *Phys. Rev. Lett.* **30**: 1343–1346.
- Hagedorn, R. 1995. *NATO Sci. Ser.* **B346**: 13–46. https://link.springer.com/chapter/10.1007%2F978-3-319-17545-4_17
- Harrison, M., T. Ludlam and S. Ozaki (eds.). 2003. “The Relativistic Heavy Ion Collider Project: RHIC and its Detectors”, 2003. *Nucl. Instrum. Methods A* **499**: 235–880.
- Herb, S. W. et al. (CFS). 1977. *Phys. Rev. Lett.* **39**: 252–255.
- Hinchliffe, I. and C. H. Llewellyn Smith. 1976a. *Phys. Lett. B* **61**: 472–476.
- Hinchliffe, I. and C. H. Llewellyn Smith. 1976b. *Nucl. Phys. B* **114**: 45–60.
- Hom, D. C. et al. (CFS). 1976a. *Phys. Rev. Lett.* **36**: 1236–1239.
- Hom, D. C. et al. (CFS). 1976b. *Phys. Rev. Lett.* **37**: 1374–1377.
- Jacob, M. and P. V. Landshoff. 1976. *Nucl. Phys. B* **113**: 395–412.
- Jacob, M. and P. V. Landshoff. 1978. *Phys. Repts.* **48**: 285–350.
- Jacob, M. *Proc. EPS International Conference on High Energy Physics*, (Geneva, 27 June–4 July 1979) (CERN, Geneva, SZ, 1980) pp. 473–522. http://inspirehep.net/record/141851/files/19399_473-522.pdf
- Jacob, M. 1984. *HISTORY OF ISR PHYSICS*, Ref.TH.3807-CERN <http://cds.cern.ch/record/150654/files/CM-P00062099.pdf>
- Jane, M. R. et al. 1975. *Phys. Lett. B* **59**: 103–105. Erratum 1978. *Phys. Lett. B* **73**: 503.
- Jarlskog, C. and H. Pilkuhn. 1967. *Nucl. Phys. B* **1**: 264–268.
- Koch, P., B. Müller and J. Rafelski. 1986. *Phys. Repts.* **142**: 167–262.
- Kourkouvelis, C. et al. (ABCS) 1979a. *Phys. Lett. B* **84**: 271–276.
- Kourkouvelis, C. et al. (ABCS) 1979b. *Phys. Lett. B* **86**: 391–394.
- Kourkouvelis, C. et al. (ABCS) 1979c. *Nucl. Phys. B* **158**: 39–56.
- Kourkouvelis, C. et al. (ABCSY). 1980a. *Phys. Lett. B* **91**: 481–486.
- Kourkouvelis, C. et al. (ABCSY) 1980b. *Phys. Lett. B* **91**: 475–480.
- Kovtun, P. K., D. T. Son and A. O. Starinets. 2005. *Phys. Rev. Lett.* **94**: 111601.
- Kroll, N. M. and W. Wada. 1955. *Phys. Rev.* **98**: 1355–1359.
- Lamb, R. C., R. A. Lundy, T. B. Novey, D. D. Yovanovitch, M. L. Good, R. Hartung, M. W. Peters and A. Subramanian. 1965. *Phys. Rev. Lett.* **15**: 800–802.
- Landsberg, L. G. 1985. *Phys. Repts.* **128**: 301–376.
- Landshoff, P. V. and J. C. Polkinghorne 1978. *Phys. Rev. D* **18**: 3344–3352.
- Lebedev, V. et al. pp. 328–335 in Ref. [Cool 1973].

- Lederman, L. M., W. Lee, J. Appel, M. Tannenbaum, L. Read, J. Sculli, T. White and T. Yamanouchi, *Study of Lepton Pairs From Proton-Nuclear Interactions; Search For Intermediate Bosons and Lee-Wick Structure*, June 17, 1970, NAL PROPOSAL No. 70 <http://lss.fnal.gov/archive/test-proposal/0000/fermilab-proposal-0070.pdf>.
- Lederman, L. M. p. V-55 in Ref. [Segler 1974].
- Lederman, L. M. 1975. *Proc. 1975 International Symposium on Lepton and Photon Interactions at High Energies*, (Stanford University, 21-27 August, 1975) W. T. Kirk (editor) (SLAC, Stanford CA, 1975) pp. 265–316.
- Lederman, L. M. 1976. *Phys. Repts.* **26**: 149–181.
- Lederman, L. and J. Weneser (eds.) *Report of the Workshop on BeV/Nucleon Collisions of Heavy Ions—How and Why* (Bear Mountain, NY, 29 November–1 December, 1974) (BNL 50445, Upton, NY, 1975).
- Lee, T. D. *CERN SEMINARS 1961*, CERN 61-30, 1961, pp. 65–72. <http://cds.cern.ch/record/285663/files/CERN-61-30.pdf>
- Lee, T. D. et al. 2005. *Nucl. Phys. A* **750**: 1–171.
- Lee, T. D. and C. N. Yang. 1960. *Phys. Rev.* **119**: 1410–1419.
- Levin, E. M. and M. G. Ryskin 1975. *Sov. Phys.-JETP* **42**: 783–789. http://www.jetp.ac.ru/cgi-bin/dn/e_042_05_0783.pdf
- Matsui, T. 1987. "On the Charm Production in Ultra-relativistic Heavy Ion Collisions", *Proc. 2nd Workshop on Experiments and detectors for RHIC*, Berkeley, CA, May 1987, eds. H. G. Ritter, A. Shor, LBL-24604. <http://www.osti.gov/scitech/biblio/5302565>
- Matsui, T. and H. Satz 1986. *Phys. Lett. B* **17**: 416–422.
- Moore, G. D. and D. Teaney. 2005. *Phys. Rev. C* **71**: 064904.
- Nearing, J. 1963. *Phys. Rev.* **132**: 2323-2324.
- Nearing, J. 1964. *Phys. Rev.* **135**: AB2.
- Orear, J. 1964. *Phys. Rev. Lett.* **12**: 112–113.
- Owens, J. F., E. Reya and M. Glück. 1978a. *Phys. Rev. D* **18**: 1501–1514
- Owens, J. F. and J. D. Kimel. 1978b. *Phys. Rev. D* **18**: 3313–3319.
- Owens, J. F. 1987. *Rev. Mod. Phys.* **59**: 465–503.
- Palmer, R. B., E. J. Bleser et al. 1985. *Nucl. Instrum. Methods A* **235**: 435–463.
- Panofsky, W. K. H. 1968. *Proc. 14th International Conference on High Energy Physics, Vienna, Austria, 28 Aug.–5 Sept, 1968*. J. Prentki and J. Steinberger (eds.) (CERN, Geneva, 1968) pp. 23–39.
- Perkins, D. H. *Proc. XVI International Conference on High Energy Physics, Chicago-Batavia, 1972*. J. D. Jackson and A. Roberts (eds.) (NAL, Batavia, IL, 1973) Vol. 4 pp. 189–247.
- Piccioni, O., R. Good, W. Melhop and R. Swanson. 1966. *Proc. XII International Conference on High Energy Physics*, (Dubna, 1964). Ya. A. Smorodinskii (editor-in-chief) (Atomizdat, Moscow, 1966), Vol. 2, p. 32–36. <http://inspirehep.net/record/1376999/files/C64-08-05-p032.pdf>
- Politzer, H. D., 1973. *Phys. Rev. Lett.* **30**: 1346–1349.
- Pontecorvo, B. 1959. *JETP* **37**: 1751–1757.
- Pope, B. G. et al. (CCOR) 1978. *AIP Conf. Proc.* **43**: 239–242.
- Pretzl, K., C. Favuzzi et al. (NA5) *Proc. XX International Conference on High Energy Physics* (Madison, WI 1980). L. Durand and L. G. Pondrom (editors) (AIP, New York, 1980), pp. 435–468. <http://aip.scitation.org/doi/pdf/10.1063/1.32442>
- Prino, F. et al. (NA50) *Proc. XXX International Symposium on Multiparticle Dynamics (ISMD2000)*, Tihany, Hungary, October 9–15, 2000, T. Csorgo, S. Hegy and W. Kittel (eds.) (World Scientific, New Jersey, 2001). <https://arxiv.org/pdf/hep-ex/0101052.pdf>.
- Rak, J. and M. J. Tannenbaum. 2013. *High p_T Physics in the Heavy Ion Era*, (Cambridge University Press, 2013).
- Repellin, J.-P. 1982 (UA2) *Proc. 21st International Conference on High Energy Physics (ICHEP)*, Paris, France, July 26–31, 1982 P. Petiau and M. Porneuf (eds.) *J. Phys. Colloques.* **43**: C3-571–C3-578. <https://doi.org/10.1051/jphyscol:1982376>

- Russell, J. J., R. C. Sah, M. J. Tannenbaum, W. E. Cleland, D. G. Ryan and D. G. Stairs. 1971. *Phys. Rev. Lett.* **26**: 46–50.
- Russo, A. 1996. *History of CERN, Volume 3*, J. Krige (editor) (North Holland, Elsevier Science, Amsterdam, 1996), pp. 97–170.
- Russo, A. 1996a. pp. 151–152 in Ref. [Russo 1996].
- Satz, H. and Y. Zarmi 1976. *Lett. Nuovo Cim.* **15**: 421–428.
- Satz, H. 2000. *Rep. Prog. Phys.* **63**: 1511–1574.
- Satz, H. 2013. *Adv. High Energy Phys.* **2013** 242918. <http://inspirehep.net/record/1223872/files/242918.a.pdf>.
- Schwartz, M. 1960. *Phys. Rev. Lett.* **4**: 306–307.
- Segler, S. et al. (CCRS). *Proc. XVII International Conference on High Energy Physics* (London, 1974). J. R. Smith (editor) (Rutherford Laboratory, Chilton, Didcot, UK, 1974), pp. V-41–V-43.
- Shuryak, E. V. 1980. *Phys. Repts.* **61**: 71–158.
- Soltz, R. A., C. DeTar, F. Karsch, S. Mukherjee and P. Vranas. 2015. *Ann. Rev. Nucl. Part. Sci.* **65**: 379–402.
- Tannenbaum, M. J. 1977. p. 598 in Ref. [Cronin 1977].
- Tannenbaum, M. J. 1982. (CCOR) pp. C3-134–C3-139 in Ref. [Repellin 1982] <https://doi.org/10.1051/jphyscol:1982331>
- Tannenbaum, M. J. et al. 1985. (BCMOR) *Proceedings of the Fourth International Conference on Ultra-Relativistic Nucleus-Nucleus Collisions*, Helsinki, Finland, June 17–21, 1984, K. Kajantie (editor) Lecture Notes in Physics 221 (Springer-Verlag, Berlin, Heidelberg, 1985) <https://www.osti.gov/scitech/servlets/purl/6174559>
- Tannenbaum, M. J. 1989. *Int. J. Mod. Phys. A* **4**: 3377–3476.
- Tannenbaum, M. J. 1996. *Heavy Ion Physics* **4**: 139–148.
- Tannenbaum, M. J. 2006. *Rep. Prog. Phys.* **69**: 2005–2059.
- Tannenbaum, M. J. 2008. *Int. J. Mod. Phys. E* **17**: 771–801.
- Tannenbaum, M. J. 2014. *Proceedings of the International School of Subnuclear Physics, ISSP 2014, 52nd Course*, Erice, Sicily, Italy, June 24–July 3, 2014, Antonino Zichichi (editor) The Subnuclear Series: Volume 52 (World Scientific, Singapore, 2017). arXiv:1504.02771.
- Tannenbaum, M. J. 2016. *Eur. Phys. J. H* **41**: 303–325.
- Tavernier, S. P. K. 1987. *Rep. Prog. Phys.* **50**: 1439–1489.
- Thews, R. L., M. Schroedter and J. Rafelski. 2001. *Phys. Rev. C* **63**: 054905.
- van Hees, H., V. Greco and R. Rapp, 2006. *Phys. Rev. C* **73**: 034913.
- Vogt, R., M. Cacciari and P. Nason. 2006. *Nucl. Phys. A* **774**: 661–664.
- Wolf, G. pp. C3-525–C3-568 in Ref. [Repellin 1982] <https://doi.org/10.1051/jphyscol:1982374>
- Yamaguchi, Y. 1966. *Nuovo Cimento* **A43**: 193–199.
- Zichichi, A. Comment in discussion [Piccioni 1966] p. 35.
- Zhao, X. and R. Rapp 2008. *Phys. Lett. B* **664**: 253–257.
- Zweig, G. 2010. *Int. J. Mod. Phys. A* **25**: 3863–3877.